EXPERIMENTAL AND ANALYTICAL INVESTIGATION OF COLD-FORMED STEEL FLOOR TRUSSES UNDER GRAVITY LOADING

A THESIS SUBMITTED TO
THE GRADUATE SCHOOL OF NATURAL AND APPLIED SCIENCES
OF
MIDDLE EAST TECHNICAL UNIVERSITY

BY

CAGAN DIZDAR

IN PARTIAL FULFILLMENT OF THE REQUIREMENTS
FOR
THE DEGREE OF MASTER OF SCIENCE
IN
CIVIL ENGINEERING

JUNE 2017

Approval of the thesis:

EXPERIMENTAL AND ANALYTICAL INVESTIGATION OF COLD-FORMED STEEL FLOOR TRUSSES UNDER GRAVITY LOADING

Submitted by **CAGAN DIZDAR** in partial fulfillment of the requirements for the degree of **Master of Science in Civil Engineering Department, Middle East Technical University** by,

Prof. Dr. Gulbin Dural Unver _____
Dean, Graduate School of **Natural and Applied Sciences**

Prof. Dr. Ismail Ozgur Yaman _____
Head of Department, **Civil Engineering**

Assoc. Prof. Dr. Eray Baran _____
Supervisor**, Civil Engineering Dept., METU**

Examining Committee Members:

Prof. Dr. Cem Topkaya _____
Civil Engineering Dept., METU

Assoc. Prof. Dr. Eray Baran _____
Civil Engineering Dept., METU

Prof. Dr. Afsin Saritas _____
Civil Engineering Dept., METU

Assoc. Prof. Dr. Ozgur Kurc _____
Civil Engineering Dept., METU

Asst. Prof. Dr. Burcu Guldur Erkal _____
Civil Engineering Dept., Hacettepe University

Date: 07.06.2017

I hereby declare that all information in this document has been obtained and presented in accordance with academic rules and ethical conduct. I also declare that, as required by these rules and conduct, I have fully cited and referenced all material and results that are not original to this work.

Name, Last name: Cagan Dizdar

Signature:

ABSTRACT

EXPERIMENTAL AND ANALYTICAL INVESTIGATION OF COLD-FORMED STEEL FLOOR TRUSSES UNDER GRAVITY LOADING

Dizdar, Cagan

M. Sc., Department of Civil Engineering

Supervisor: Assoc. Prof. Dr. Eray Baran

June 2017, 118 pages

Cold-Formed Steel structures are getting increasingly popular in the market with their economic and short construction duration advantages. One of the most common floor system used in CFS buildings utilizes trusses made of CFS members. Despite their increasing use, behavior of CFS floor trusses has been the subject of very limited research. The governing failure mode of these structures under gravity loading is usually local buckling of compression chord elements. Therefore, a reliable design of such structures requires accurate determination of force effects and realistic estimation of CFS member capacities. The current study aims at investigating the validity of analysis assumptions and design techniques currently used for CFS floor trusses. Effect of parameters, such as connection detail at diagonal-chord joints, number of fasteners used at each diagonal-chord connection, CFS member thickness and the presence of OSB sheathing plate were studied as part of the experimental program.

The focus of the study was twofold: truss stiffness and truss load capacity. Truss stiffness was studied in relation to the stiffness of diagonal-chord connections. With the incorporation of joint axial flexibility, the truss stiffness predictions were observed to accurately represent the measured response. In regards to the accurate determination of truss load capacity, both the normal force and bending moment effects on chord members were considered. Experimental and numerical results indicate the presence of significant bending effect on truss chord members. A simple procedure was established in order to quantify this effect and determine the value of chord bending moment. In the proposed procedure maximum bending moment occurred on truss chord members was calculated using imaginary loading, which was determined based on truss midspan deflection. The normal force and bending moment effects on chord members were considered together with the corresponding capacities determined based on the code provisions. Truss load capacities obtained through this procedure were observed to accurately represent the measured capacities.

Keywords: Cold-Formed Steel, CFS Truss, Thin-Walled Member, Screw Connection, Rivet Connection

ÖZ

HAFİF ÇELİK DÖŞEME MAKAS KİRİŞLERİNİN DÜŞEY YÜK ALTINDAKİ DAVRANIŞLARININ DENEYSEL VE ANALİTİK OLARAK İNCELENMESİ

Dizdar, Çağan

Yüksek Lisans, İnşaat Mühendisliği Bölümü

Tez Yöneticisi: Doç. Dr. Eray Baran

Haziran 2017, 118 sayfa

Hafif çelik bina sistemleri ekonomik ve kısa inşaat süresi avantajları ile sektörde tercih sebebi olmaya başlamıştır. Makas kirişler hafif çelik binalarda döşeme sistemleri için yaygın kullanılan elemanlardır. Hafif çelik makasların yaygın kullanımlarına rağmen, bu elemanların davranışlarını inceleyen kısıtlı sayıda çalışma bulunmaktadır. Sistemin düşey yükleme altındaki göçme biçimi çoğunlukla makasların basınç başlığında oluşan yerel burkulmalardır. Bu yüzden bu tip yapıların güvenilir tasarımları yük etkilerinin ve hafif çelik eleman dayanımlarının doğru bir şekilde tahkikini gerektirmektedir. Bu akademik çalışma kapsamında, halihazırda kullanılan analiz varsayımlarının ve tasarım kurallarının döşeme makas kirişleri için geçerliliği incelenmiştir. Deneysel program içerisinde başlık ve çapraz eleman bağlantı detayı,eleman kalınlıkları ve OSB kaplama etkileri, numune değişkenleri olarak incelenmiştir.

Çalışmanın odağı makasların düşey yük altındaki rijitlikleri ve dayanımları olmak üzere iki bölüme ayrılmıştır. Makas rijitliği başlık ve çapraz elemanların bağlantı

detaylarına bağlı olarak incelenmiştir. Birleşim noktalarının esneklikleri ile etkileşimli olarak elde edilen makasların rijitlik tahminleri, ölçülen deneysel verileri isabetli bir şekilde yansıtmıştır. Makasların yük kapasiteleri ile ilgili başlık üzerindeki normal kuvvetler ve eğilme etkileri incelenmiştir. Deneysel ve analitik sonuçlar başlıklar üzerinde moment etkileri olduğunu göstermiştir. Bu moment değerinin hesaplanması için basitleştirilmiş bir prosedür oluşturulmuştur. Bu prosedür orta açıklık sehimi ile elde edilen hayali bir kuvvet aracılığıyla başlık üzerindeki momenti hesaplamaktadır. Başlıklardaki normal kuvvet ve eğilme momentleri ilgili yönetmeliklerde bulunan denklemler ile hesaplanan dayanım değerleri ile incelendiklerinde deneysel veriler ile tutarlılık göstermişlerdir.

Anahtar kelimeler: Hafif Çelik, Hafif Çelik Makaslar, İnce Cidarlı Elemanlar, Perçin Bağlantıları, Vida Bağlantıları

To My Parents…

ACKNOWLEDGEMENTS

First of all, I would like to thank to my supervisor Assoc. Prof. Dr. Eray BARAN for his help and encouragement through my research session. Moreover I need to add my gratitude to my professors Dr. Barıs BINICI and Dr. Cem TOPKAYA who have a great influence on my personal engineering background.

Financial support for this study was provided by METU Scientific Research Project Support Unit (BAP), I hope I used the fund given for research in most productive way. I also would like to thank truss manufacturer EVHANE Steel Construction Company for their generous attitude for my hard requests. Of course I need to thank to all METU Structural Mechanics Laboratory personal for great guidance and help.

In the progress of study, my family always supported me for success and holds my ambition fresh all the time. Especially when I got injured they provide me very important support. Although cause me injured, nevertheless I want to thank my football team “Gaye Arzu”, we shared beautiful moments together and refreshed our minds.

Finally I would like to thank my friends Efe Ozelci, Sinan Ozer, Gokcan Ozakdag, Erkan Istanbulluoglu for their great friendships. They were with me whenever I need any help or enjoy.

This research is also supported by The Scientific and Technological Research Council of Turkey (TUBITAK) under grant number 115M234.

TABLE OF CONTENTS

LIST OF TABLES

TABLES

LIST OF FIGURES

FIGURES

CHAPTER 1

INTRODUCTION

Cold-Formed Steel (CFS) structural systems became preferable on buildings with their economic and construction duration advantages. CFS structures are also considered environmentally friendly due to recyclable feature of steel and other materials usually utilized in CFS construction, as well as producing less waste materials than conventional construction methods. The fact that CFS construction technique is also well suited for off-site construction provides CFS a great potential in terms of saving in construction time. CFS members are obtained mostly by folding of 0.5-4 mm thick sheet metal with a roll forming machine. The members are cut to required lengths and usually assembled with rivets and self-drilling screws, which make transportation problems easier to solve.

Figure 1. CFS Floor Truss System in Steel Building

CFS truss members are essential for designs. They are both compatible with complete CFS building or as shown in Fig. 1 could be used in hybrid designs of hot-rolled steel, reinforced concrete and CFS buildings. The open-web shape of floor trusses permits mechanical equipment transfer, and are comparable to floor joists in terms of structural performance. As a result, floor systems made of CFS trusses have been widely used throughout the world.

1.1 Background

1.1.1 Analytical and Numerical Analysis of Cold-Formed Steel Members

Manufacturing stage of CFS sections are handled with roll-forming machines therefore sections are pre-defined with respect to machine under process. According to compatibility requirements of trusses, designs are mostly standardized with C, U or hat sections. One of the most common section shapes is a lipped C section with intermediate web stiffener as shown in Fig. 2. Lips are acting as edge stiffeners for slender flange elements. Due to relatively small sheet thickness, CFS sections usually possess high local slenderness, which make them susceptible to local instabilities. Hence, flat width to thickness ratios of elements forming CFS cross sections are limited in contemporary design codes [1,2,3]. Stiffeners are usually formed in sections to provide post-buckling strength by stress redistribution and provide extra strength under compression [1].

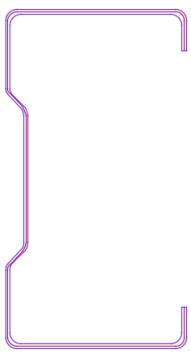

Figure 2. Lipped C Section with Intermediate Web Stiffener

It was reported that code approaches are not fully sufficient on determining local buckling modes in CFS members [4]. As an alternative, Direct Strength Method was included in the appendix of 2012 version of the AISI Specification. This methods was included in the main body of the 2016 version of the AISI S100 Specification [5]. This approach is based on elastic instability capacities of CFS sections, which are generally obtained from analyses utilizing Finite Strip Method. Method provides signature curves of slender section with non-deformed geometries along the length. In Fig. 3 there is an example signature curve drawn for a lipped C section with corresponding buckling mode of various column lengths.

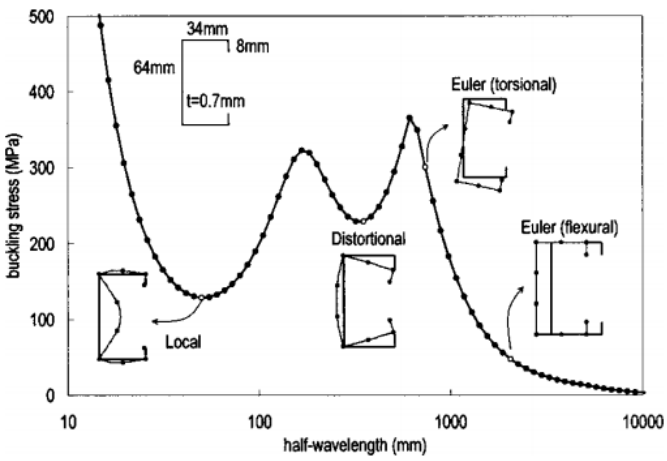

Figure 3. A Sample Signature Curve for Lipped C Section [4]

Due to the fact that the presence of imperfections has a major effect on the behavior of CFS members, non-linear finite element analysis is an essential design tool for such members. However the shape and magnitude of imperfections are another problem for analysis. Schafer and Pekoz [6] presented a study covering probabilistic and comparative results with different imperfection modes and magnitudes. It was reported that finite element models are very effective on determining CFS section capacities but model properties are crucially important on the reliability of results. Another study focuses on experimental and analytical investigation of several lipped C sections under compression loading with different parameters, including member length and dimensions [7]. Analytical model on study took imperfections

from elastic eigenvalue buckling modes and predicts the strength with less than 10% error while accurately capturing the failure modes as shown in Fig. 4.

Figure 4. Comparison of Observed and Predicted Failure Modes [7]

Flexural behavior of C and Z sections was also investigated experimentally and compared with the predictions of both direct strength method and finite element method [8]. For all cases studied, both methods were able to predict flexural capacity with 10% of measured values. Results of direct strength method analysis is presented in Fig. 5.

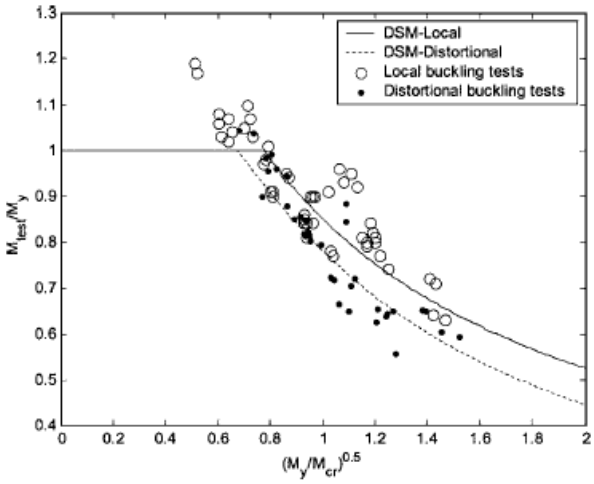

Figure 5. Comparison of Direct Strength Method Prediction with Test Results [8]

1.1.2 Cold-Formed Steel Trusses and Floor Systems

Diagonal-chord connection region of a typical CFS truss is shown in Fig. 6. In this particular connection flange lips in chord members were terminated at the connection region, cross section of diagonal members were reduced at the ends and the connection is provided with a single screw. Different manufacturers prefer to use different details for the chord and diagonal members to form the connection. AISI S214-12 North American Standard for Cold-Formed Steel Framing—Truss Design provides guidance for analysis as well as geometrical limitations for the diagonal-chord connection region. Chord members are required to be modeled as continuous and web members should be pin connected to the chords. The standards also allows the use of full member cross section as opposed to effective section for serviceability checks. In terms of eccentricity at the diagonal-chord connections, the standard allows the use of both the multiple and single node analysis. Truss models created based on the multiple and single node approaches are shown in Fig. 8. AISI S214-12 also states that when screws are used to provide the connection between diagonal and chord members of C-shaped cross section, a minimum of four screws should be provided at each connection. Even though the minimum number of fasteners is explicitly specified in the related standard, manufacturers do not always satisfy this criteria and in many cases a single or two fasteners (screw or rivet) are used to form the diagonal-chord connections in CFS trusses.

Figure 6. Re-Folded Truss Connection Example

In thin-walled members behavior of rivets and screws have an important effect on general system behavior. Previously, studies investigated load transfer of specific connectors on thin-walled plates [9]. Their effect on general behavior was presented with a truss test. In Fig. 7 local deformations are shown. These local deformations affected truss behavior more than member stiffness.

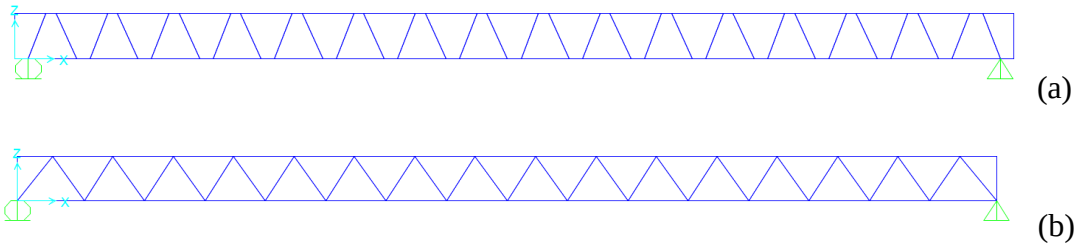

Figure 7. (a) Multi Nodes and (b) Single Node Model

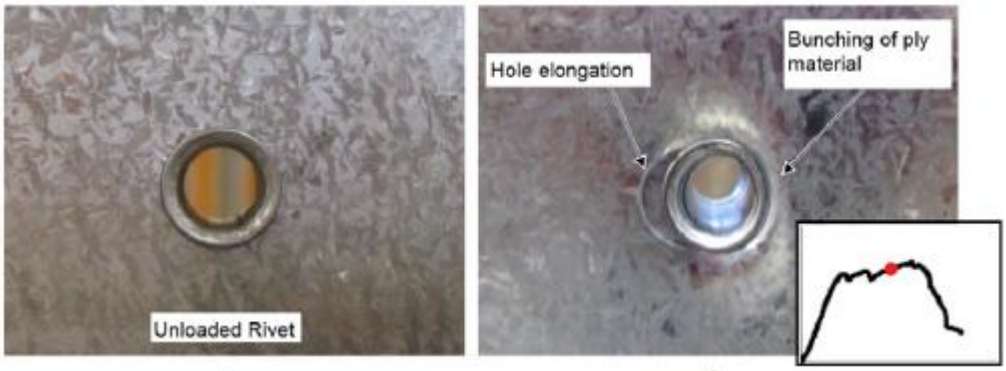

Figure 8. Rivet Behavior on Truss [9]

In 2006, a study covered experimental program of full scale CFS roof trusses by Wood and Dawe [10]. Results of that experimental study indicated that the dominant failure modes of trusses under flexural loading are the local buckling of compression chords and connection failures. No serviceability problem of trusses was not stated.

In 2008, a study was conducted to observe the effect of particular type of connection called mechanical clinching on CFS trusses by Pedreschi, R., Sinha, B. [11]. The study maintained the general attidute to expected CFS truss failures as local buckling while investigating adequacy of connection strength.

In 2012, an experimental study was handled on wide CFS truss by Mohammad, S., Tahir, M. M., Tan, C. S., and Shek, P. N [12] . In that study non-dominant failures

were observed along the loading process. In the conclusion of study every member of truss is indicated with their slenderness.

In 2006, an experimental study was handled to investigate floor systems consist of CFS joists rather than trusses by Lakkavalli, B. S., Liu, Y. [13] . They mostly investigated the shear transfer mechanisms between concrete deck and joist with mainly four different types of enhancement and their identical parameters. Failures of test specimens were initialized with transverse cracks in concrete then followed with tension yielding of joists.

In 2007, a detailed study was conducted by Xu, L., Tangorra, F. [14] about vibration behavior of a floor system consists of CFS C joists and OSB sheating. Several parameters such as joist end-support conditions, bond of OSB sheating, screw patterns and span lengths were taken into account while observing their effects on vibration and displacement of whole system. Study presented natural frequencies and damping of systems correspondingly with parameters.

1.2 Aim of the Research

Review of the limited literature on CFS trusses shows that the governing failure mode of these structures under gravity loading is usually local buckling of compression chord elements. Therefore, a reliable design of such structures requires accurate determination of force effects and realistic estimation of CFS member capacities. The current study aims at investigating the validity of analysis assumptions and design techniques currently used for cold formed steel floor trusses. Effect of parameters, such as connection detail at diagonal-chord joints, number of fasteners used at each diagonal-chord connection, CFS member thickness and the presence of OSB sheathing plate were studied as part of the experimental program.

The focus of the experimental program was twofold: truss stiffness and truss load capacity. Truss stiffness was studied in relation to the stiffness of diagonal-chord connections. With the incorporation of joint flexibility, the truss stiffness predictions were observed to accurately represent the measured response. Capacity of trusses was investigated with pure compression limit of chord member. Section was tested under different lip conditions and buckling lengths. However, no clear relation could

be established between the axial compression capacity of individual members and the axial force level in truss chord member at the time of failure. Finally, some truss configurations were further studied in an attempt to reveal the extent to which the presence of bending moment, in addition to axial compression, influences the capacity of chord members and hence the truss capacity.

1.3 Organization of Thesis

The thesis is divided into six chapters. Following this introduction chapter, details of load testing performed on truss specimens are presented in Chapter 2. Results of the experiments are discussed in regards to the effect of different test parameters.

Chapter 3 focuses on the analysis of truss stiffness. Truss response obtained from linear elastic structural analysis with axially rigid connection assumption is presented and discrepancy between the predicted and measured truss stiffness is demonstrated. Testing program conducted to determine the axial stiffness of screw connection typically used between diagonal and chord members in trusses is explained. Finally, analysis results incorporating the connection axial flexibility are discussed.

Methods used in an attempt to accurately determine the compression capacity of truss chord members are discussed in Chapter 4. Results of compression tests performed on CFS sections are presented in comparison with the predictions of analytical and numerical methods.

Chapter 5 covers the studies conducted in order to quantify the bending effect on truss chord members. Verification of finite element analysis results with the measured strain profiles obtained on truss chords is provided. A simple analysis procedure is presented to determine the magnitude of chord moment is presented and the accuracy of this procedure is demonstrated.

Chapter 6 includes conclusions reached during the course of this study.

CHAPTER 2

TRUSS LOAD TESTS

2.1 Truss Specimens

A segment of truss specimens tested in the study is given in Fig. 9. Trusses with 300 mm overall depth and 6 m length were chosen to be representative of floor trusses frequently used in CFS structures in Turkey. The top and bottom chords, as well as the diagonal members were made of the lipped channel CFS section ("C" section) shown in Fig. 10. As will be mentioned in the following sections, three different CFS member thickness of 0.8 mm, 1.2 mm, and 1.5 mm were used in test specimens. As illustrated in Fig. 9, typically 60 mm and 80 mm of eccentricity exists between two rivets at locations where the diagonal members are connected to the top and bottom chords, respectively. A clear length of 300 mm exists between two connection regions in the top chord.

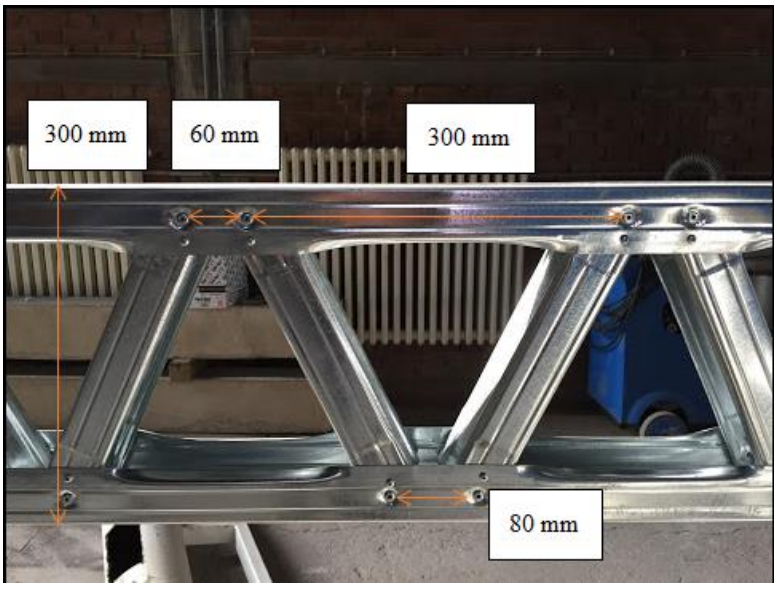

Figure 9. Geometric Details of Truss Specimens

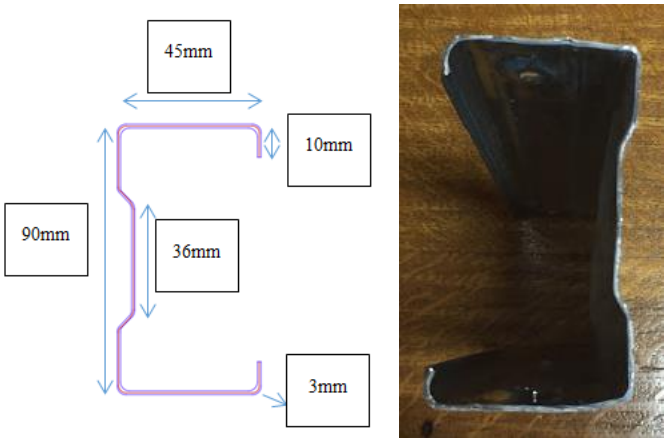

Figure 10. Section Highlight of Dimensions and Imperfection Example

Connection between the diagonal and chord members was provided with rivets and screws shown in Fig. 11. In manufacturing stage rivet holes were punched by roll-forming machine and 4.8 mm diameter blind rivets were used in these holes. In majority of specimens, screws were used to provide connection between the diagonal and chord members, in addition to rivets. These screws were driven with electric hand drills. The screws used in trusses are #6 (3.5 mm diameter) standard screws with minimum length of 25 millimeters. Only one specimen was configured with #12 (6.3 mm diameter) screw size.

Figure 11. Screw and Rivet used in Truss Specimens

Table 1 summarizes the major details for all truss specimens tested. As shown, 24 truss specimens were tested in total as part of the experimental study. The major test parameters were the CFS section thickness and connection detail between the diagonal and chord members. Naming of truss specimens is configured with notation of CFS Section Thickness_Number of Rivets + Number of Screws_Presence of Absence of OSB Plate (Yes – No) _ (RCC – SG – NDL – SS) where RCC stands for Reinforced Compression Chord, SG stands for strain gauge instrumented, NDL stands for Non-Deformed Lip and SS stands for short span specimen. Discussion about these different construction details used in truss specimens is provided in the following parts.

Table 1. List of All Truss Tests

Specimen	Thickness (mm)	Material Group	Connection Property	OSB Sheating	Ultimate Vertical Force (kN)	Failure Vertical Displacement(mm)	Initial Stiffness (kN/mm)	Failure Type
0.8_1+1_N	0.8	Group 1	Rivet +1 Screw	-	5.7	40.4	0.16	ICR
0.8_1+3_N	0.8	Group 1	Rivet + 3 Screw	-	5.9	35.4	0.21	VCR
0.8_PL_N	0.8	Group 1	Plate	-	7.1	36.3	0.22	ACR
0.8_1+3_N_RCC	0.8	Group 2	Rivet + 3 Screw	-	10.7	74.6	0.23	ACR
0.8_1+1_N_SG	0.8	Group 2	Rivet +1 Screw	-	5.1	30.1	0.20	VCR
0.8_1+3_N_SG	0.8	Group 2	Rivet + 3 Screw	-	5.3	24.2	0.23	ICR
1.2-0.8_1+2_N	1.2 - 0.8	Group 1	Rivet +2 Screw	-	10.7	75.3	0.21	ICR
1.5-0.8_1+3_N_SG	1.5 - 0.8	Group 2	Rivet + 3 Screw	-	12.8	121.8	0.26	TSY
0.8_1+3_Y	0.8	Group 1	Rivet + 3 Screw	YES	8.7	51.2	0.21	ACR
0.8_PL_Y	0.8	Group 1	Plate	YES	10.6	54.3	0.24	ACR
0.8_1+3_D	0.8	Group 1	Rivet + 3 Screw	DENSE	12.5	84.2	0.21	ICR
1.2_1+0_N	1.2	Group 1	Only Rivet	-	6.8	72.9	0.17	RSO
1.2_0+1_N	1.2	Group 1	Single #12 Screw	-	11.9	113.9	0.13	ICR
1.2_1+1_N	1.2	Group 1	Rivet +1 Screw	-	11.5	62.8	0.24	VCR
1.2_1+2_N	1.2	Group 1	Rivet +2 Screw	-	13.6	57.4	0.30	ULP
1.2_1+3_N	1.2	Group 1	Rivet + 3 Screw	-	12.7	49.2	0.32	ULP
1.2_PL_N	1.2	Group 1	Plate	-	13.1	45.3	0.34	ACR
1.2_1+1_N _NDL	1.2	Group 2	Rivet +1 Screw	-	11.9	70.4	0.25	ACR
1.2_1+3_N _NDL	1.2	Group 2	Rivet + 3 Screw	-	12.6	52.5	0.31	ACR
1.2_1+2_Y	1.2	Group 1	Rivet + 2 Screw	YES	16.1	70.9	0.30	ICR
1.2_1+3_Y	1.2	Group 1	Rivet + 3 Screw	YES	14.2	50.88	0.33	VCR
1.2_PL_Y	1.2	Group 1	Plate	YES	18.5	67.8	0.36	ICR
1.2_1+3_Y _NDL	1.2	Group 2	Rivet + 3 Screw	YES	15.6	63.3	0.33	VCR
1.2_1+3_N _SS	1.2	Group 2	Rivet + 3 Screw	-	24.8	31.8	0.99	VCR

ICR : Top Chord Buckling Inside Connection Region

VCR : Top Chord Buckling In Vicinity of Connection Region

ACR : Top Chord Buckling Away from Connection Region

ULP : Top Chord Buckling Under Loading Point

TCY : Tension Chord Yielding

RSO : Rivet Shear Off

In order to reflect the common construction practice used for CFS floor systems, some of the truss specimens were tested with a 600 mm wide oriented strand board (OSB) plate attached to the web of the top chord along the entire truss length as shown in Fig 12. For this purpose, 11 mm thick OSB plates were used together with #8 (4.8 mm diameter) screws. Attachment of OSB onto truss upper chord was made with 150 mm spacing except one specimen (Specimen 0.8_1+3_D) to study the

possible influence of screw layout. In this specimen spacing of screws was reduced to 30 mm.

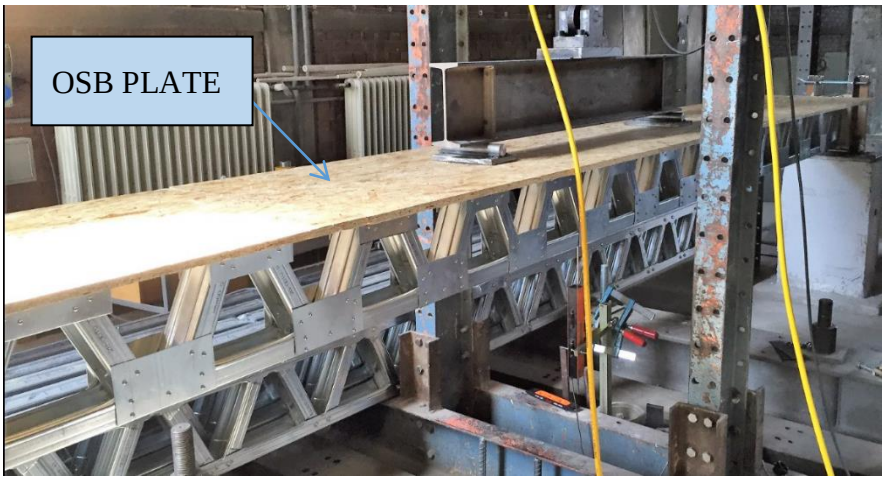

Figure 12. Placement of OSB Sheathing on Specimens

The three connection details used at the ends of diagonal members in truss specimens are shown in Fig. 13. The detail in Fig. 13(a) is the one that is widely used in the industry with different number of fasteners. The detail in Fig. 13(b) was developed in an attempt to limit the relative rotation between the diagonal members and the chords. In order to eliminate the negative effect of the chord lip termination, which is required to insert the ends of diagonal members inside the chord members in the original detail in Fig. 13(a), the detail in Fig. 13(c) was developed and used in some of the truss specimens. Specimens having this detail are indicated as “NDL” in Table 1. In Specimen 08_1+3_N_MS, the top chord member was formed by three CFS sections as shown in Fig. 14. In this detail the compression chord member was reinforced in an attempt to improve the load capacity of truss specimen.

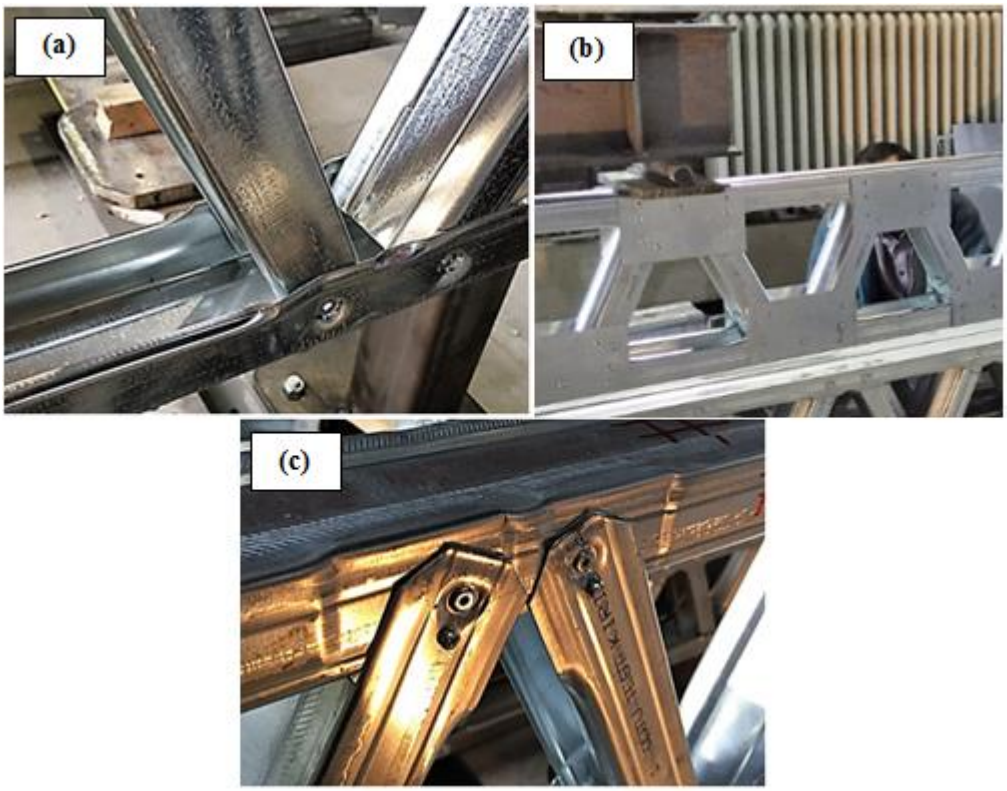

Figure 13. Connection details used in truss specimens: (a) diagonal end is placed inside chord; (b) diagonal end is placed inside chord and cover plates is attached; (c) diagonal flanges are attached outside of chord

Figure 14. Reinforced Compression Chord

Coupon samples were extracted from steel sheets that the CFS members used in truss specimens were manufactured and these samples were tested as shown in Fig. 15 to obtain the yield and ultimate strength values. Results of these coupon tests are

presented in Table 2. Because steel sheet rolls were changed twice while manufacturing of the CFS members, two groups of materials exist in study. The material group that each truss specimen belongs to is indicated in Table 1. The yield strength values were measured to be 396, 409 MPa, and the ultimate strength values were measured to be 468, 470 MPa, respectively for sheet thickness of 0.8 mm, 1.2 mm for Group-1. For Group-2 the yield strength values were measured to be 353, 452, 421 MPa, and the ultimate strength values were measured to be 409, 513, 541 MPa, respectively for sheet thickness of 0.8 mm, 1.2 mm, 1.5 mm. As evident in the table, the supplier provided steel grades usually stay on conservative side with the measured strength values being higher than the specified values.

The chord and diagonal members were roll-formed and assembled together by a local producer and the assembled truss specimens were transported to the Middle East Technical University Structural Mechanics Laboratory, where load tests were performed.

Table 2. Coupon Test Results

#	Nominal Thickness (mm)	Actual Thickness (mm)	F_y (MPa)	F_u (MPa)	Steel Grade Stated by Provider
GROUP #1					
1	1.2	1.26	409	470	S350
2	0.8	0.84	396	468	S280
GROUP #2					
1	1.5	1.43	421	541	S350
2	1.2	1.16	452	513	
3	0.8	0.78	353	409	S280

Figure 15. Coupon Tests of Sheet Material

2.2 Test Setup

Truss specimens were subjected to four-point bending tests using the test setup shown in Fig. 16. Loading was applied at two points 555 mm spaced out from mid-span with a clear span between two roller supports of 5810 mm. Location of the loading points were selected to coincide with the connection between diagonal members and the top chord. Similarly, the supports at two ends of trusses were located at the connection between diagonal members and the bottom chord. An IPN200 section steel beam was used to distribute applied vertical force from the hydraulic piston to the loading points. After realizing local buckling of top chord member directly underneath the loading point in some of the specimens, top chord members in the following specimens were reinforced by attaching steel plates on both flanges at these locations, as shown in Fig. 17.

Lateral supports made of steel tube sections were used at each support and also at two other locations along the shear spans. Because no significant lateral deformation was observed in early tested specimens, the two intermediate lateral supports were eliminated in specimens tested at later stages of the study. Lateral supports consisted of wooden blocks placed against steel supports at both sides of truss specimens, as shown in Fig. 18. In order to minimize the unintended restraint that may develop at lateral support locations, teflon sheets were placed between the specimen and wooden blocks.

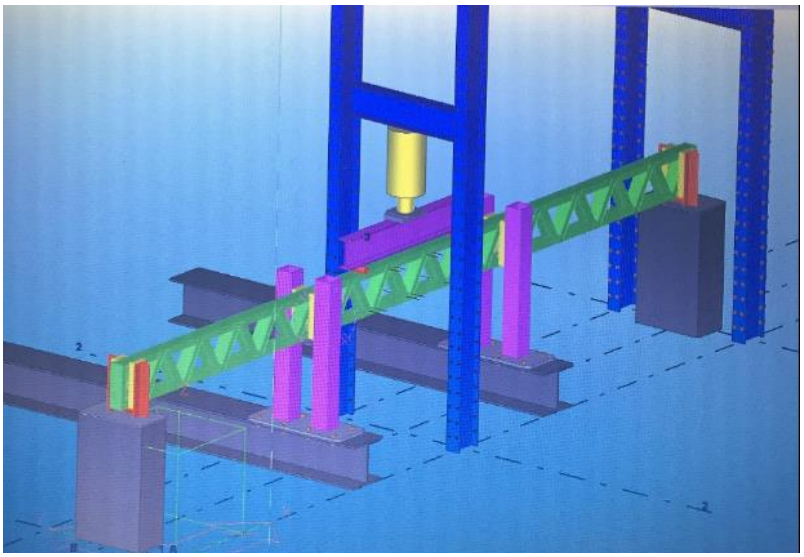

Figure 16. Solid Model of Truss Test Setup

Figure 17. Reinforcement of Top Chord Member at Loading Point

Figure 18. Lateral Supports used at Truss Ends

Instruments that were used in experiments included a load cell to measure the load applied by hydraulic piston, linear variable displacement transducers (LVDTs) to measure the vertical displacement at midspan section and lateral displacements at intermediate lateral support locations, and strain gages to monitor strains at several locations in top and bottom chord members. Figure 19 shows the loading points and the LVDTs used on specimens.

Figure 19. Positions of LVDTs

Truss specimens were tested under monotonically increasing vertical displacement loading until the failure of specimen, which in majority of specimens was in the form of local-distortional buckling of top chord member.

2.3 Results from Truss Load Tests

Measured response of all truss specimens in terms of load capacity, deflection at load capacity, and service stiffness is summarized in Table 1. The reported load capacity values represent the maximum value of the load measured by the load cell attached at the end of the hydraulic piston. The service stiffness values were determined by considering the load and deflection values at the service point, which was taken as the point corresponding to 60% of the load capacity of each specimen. The observed failure mode for each specimen is also indicated in the table.

The load capacity and service stiffness values shown in Table 1 are presented in graphical form, respectively in Figs. 20 and 21. Specimens 1.2_1+3_N_SS and 0.8_1+3_N_RCC are excluded in the graphs in Figs. 20 and 21, becausebtheir geometric properties from others make their capacity and stiffness incomparable. In these graphs, the truss specimens are arranged in six groups as: (1) 0.8 mm CFS section thickness, (2) 0.8 mm CFS section thickness with OSB plate attached to the web of the top chord, (3) 0.8 mm CFS section thickness for bottom chord and diagonal members but 1.2 mm or 1.5 mm CFS section thickness for top chord member, (4) 1.2 mm CFS section thickness and connection between diagonal and chord members provided by a single fastener, (5) 1.2 mm CFS section thickness with OSB plate attached to the web of the top chord, and (6) 1.2 mm CFS section thickness. Figure 20 shows general trends among load capacities for these six groups of specimens. Truss specimens made of 1.2 mm thick CFS members had almost twice the load capacity of those made of 0.8 mm thick members. Presence of OSB plate also resulted in a significant increase in load capacity for both 0.8 mm and 1.2 mm CFS section thickness. Another important observation valid in Fig. 21 is that truss specimens with a single fastener used to connect diagonal members to top and bottom chord members had significantly smaller load capacities than the companion trusses where these connections were formed with two or more fasteners. Different

than the pattern observed in load capacities, no apparent difference was noted in observed failure modes for these six groups of specimens.

The relation among the six groups of specimens in terms of truss service stiffness is similar to the load capacity, as evident in Fig. 20. Increasing the CFS member thickness from 0.8 mm to 1.2 mm and attaching OSB plate at web of top chord member resulted in notable increase in service stiffness of truss specimens. Connecting the diagonal members to the top and bottom chords with single fastener, as opposed to providing two or more fasteners for these connections, significantly reduced the service stiffness of truss specimens.

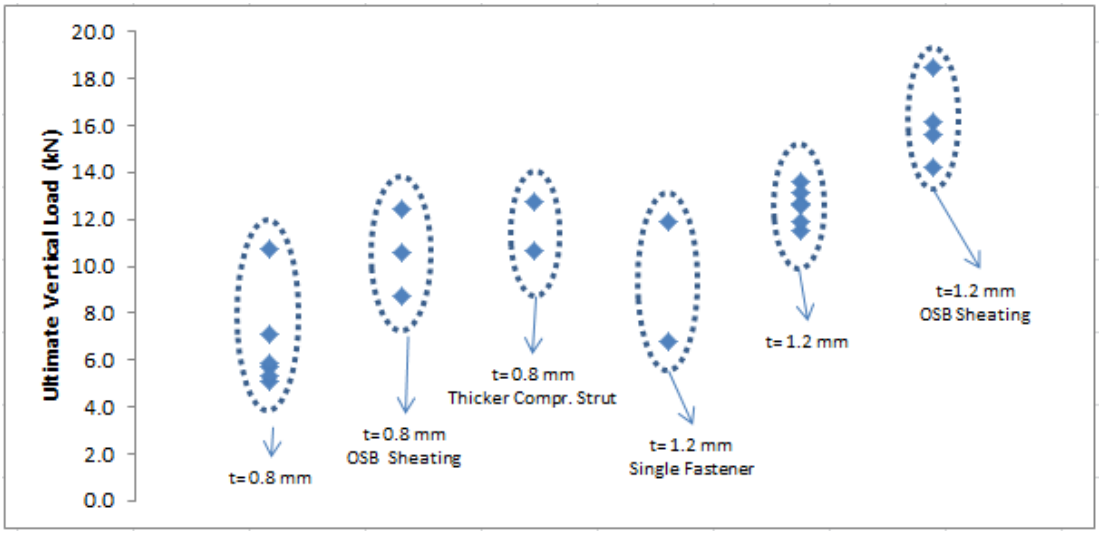

Figure 20. Measured Load Capacity of Truss Specimens

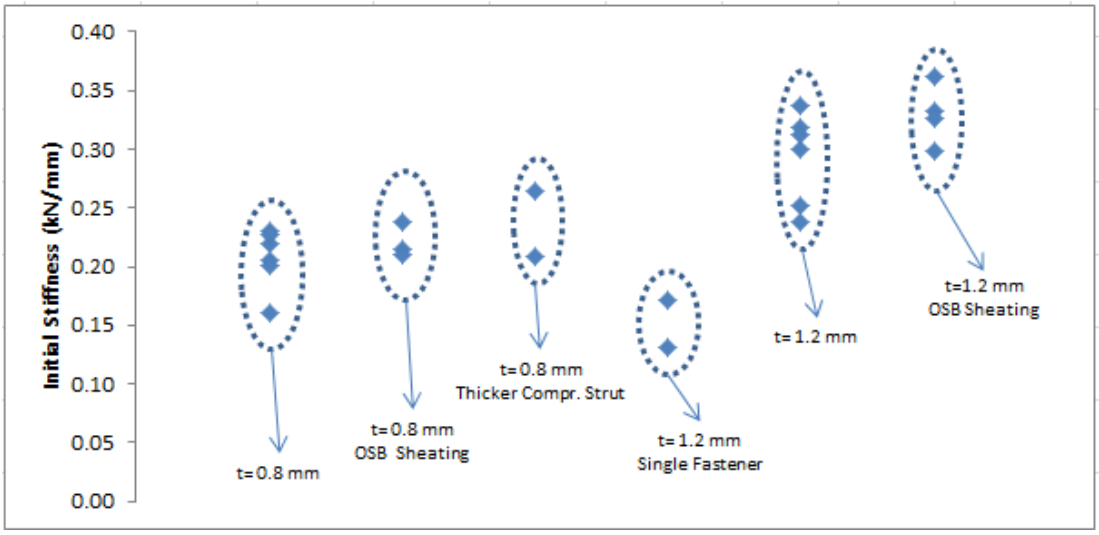

Figure 21. Measured Service Stiffness of Truss Specimens

2.3.1 Observed Failure Modes

Among all 24 truss specimens tested, yielding of bottom chord occurred in one specimen (1.5-0.8_1+3_N_ML) and shear failure of rivets connecting diagonal members to chords occurred in another specimen (1.2_1+0_N), while the failure mode for the remaining specimens was local buckling of top chord member. As shown in Fig. 22 local buckling of top chord member occurred either within the short length between the ends of two diagonal members, termed as "inside connection region", in the vicinity of the connection region, or in the unsupported length between two connection regions. No direct correlation was observed between the location of top chord buckling and the test parameters used, such as CFS section thickness, connection detail, and presence of OSB plate. Imperfection that exists on top chord CFS member is believed to have a significant influence on the location of top chord local buckling.

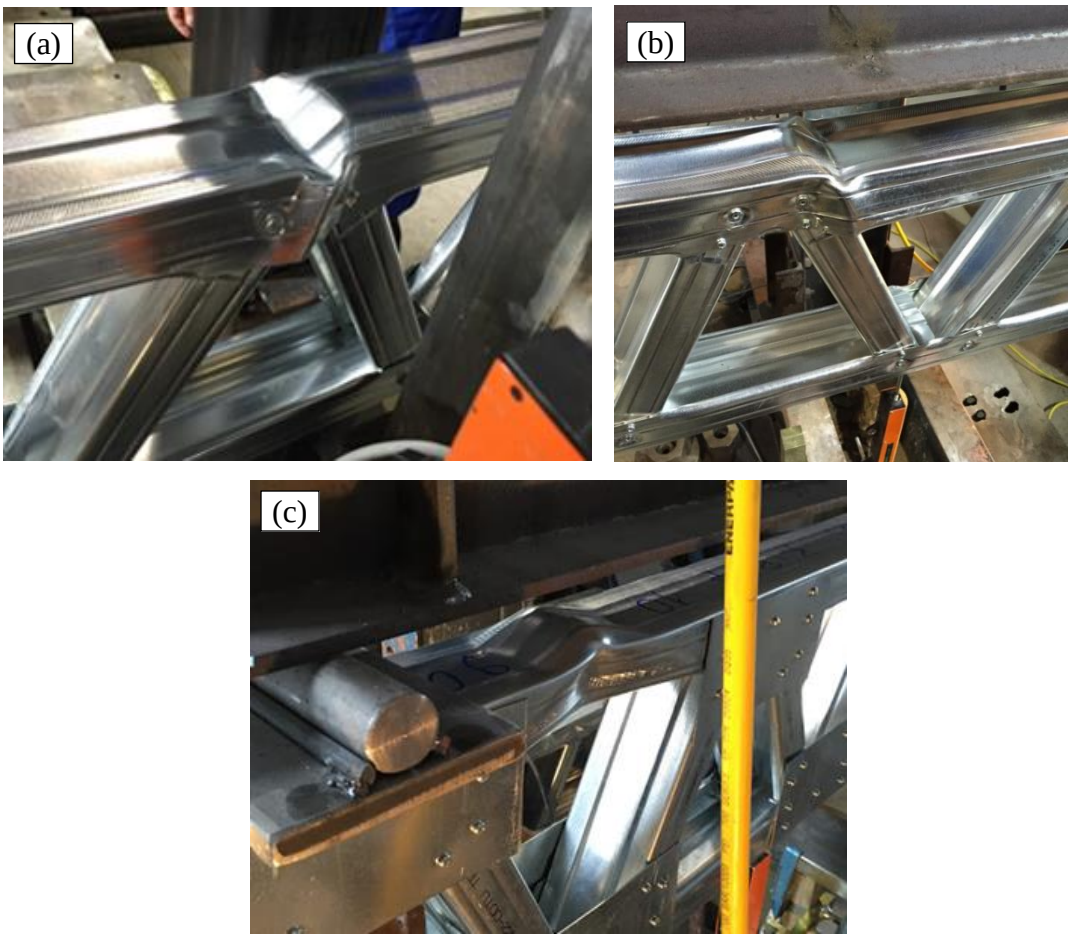

Figure 22. Buckling modes of top chord member observed in specimens: (a) inside connection region; (b) in the vicinity of connection region; (c) away from connection region

2.3.2 Effect of Fastener Type

Specimen 1.2_1+0_N had a single rivet used to connect each diagonal member end to the chord members, while in specimen 1.2_0+1_N a single #12 screw (6.3 mm diameter) was used for this purpose. These two truss specimens behaved somewhat differently from other specimens with their low stiffness. The reason for such low stiffness is insufficient rotational restraint of single fastener on chord and web connections. Failure mode for 1.2_1+0_N specimen was rivet shear off while specimen 1.2_0+1_N showed a local buckling failure mode in top chord member. Load-displacement graph of both specimens is given in Fig. 23.

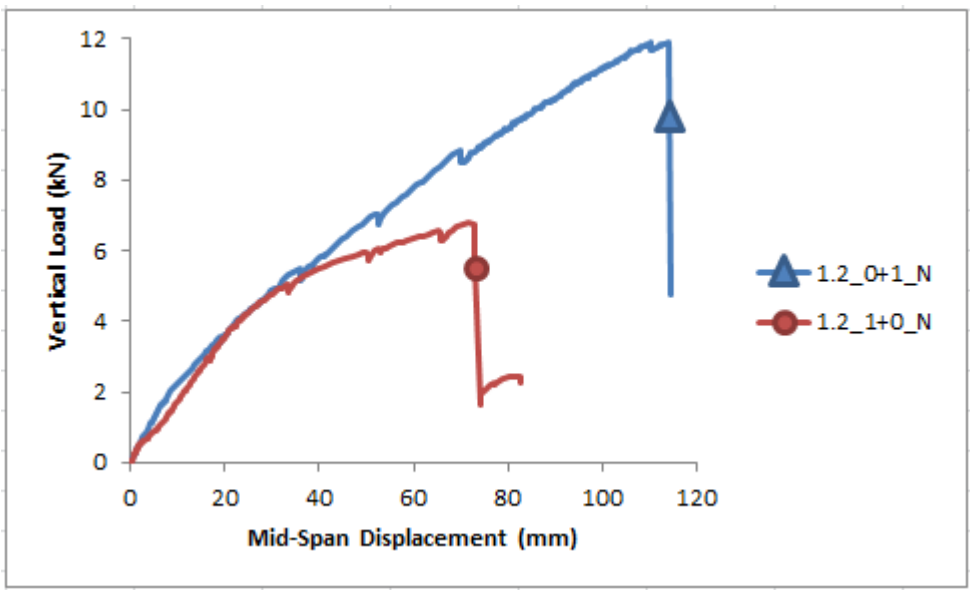

Figure 23. Load-Displacement Graph of Specimens with Single Stiffener

For specimen 1.2_1+0_N, measured maximum load and displacement were 6.8 kN and 72.9 millimeters, respectively. The location that rivet failure was observed during load testing of specimen is indicated in Fig. 24 and 25. After shear off limit of specimen, a hinge behavior was occurred in the failure location and an excessive displacement was obtained as shown in Fig. 26.

Figure 24. Rivet Shear-Off Failure Location

Figure 25. Rivet Shear-Off Failure of Specimen 1.2_1+0_N

Figure 26. Deformed State of Specimen 1.2_1+0_N

Specimen 1.2_0+1_N was configured with single #12 screw (6.3 millimeter diameter) assembled to rivet holes. Connection strength became adequate for shear force transfer onto web chords with this implementation and failure mode changed as compression chord failure. Even though the load capacity has increased compared to specimen 1.2_1+0_N due to elimination of fastener failure, the service stiffness was not affected from replacing each connector rivet by a screw. Specimen 1.2_0+1_N

reached ultimate strength in 11.9 kN vertical force, at that instant measured displacement was 113.9 mm. Buckling on top chord was observed outside of constant moment zone, inside connection region shown in Figs. 27 and 28.

Figure 27. Failure Mode of Specimen 1.2_0+1_N

Figure 28. Failure Location of Specimen 1.2_0+1_N

2.3.3 Effect of Number of Fasteners

AISI S214 specification requires a minimum of four screws for each diagonal-chord connection [2]. It is stated in the specification that this requirement is based on experience with no other reasoning provided. Validity of this requirement and the effect of the number of fasteners at diagonal-chord connectors on the overall truss response were investigated by testing truss specimens including one, two, or three connector screws provided in addition to a rivet. Screws were attached on truss members as shown in Fig. 29.

Figure 29. Use of Rivet and Screws at Diagonal-Chord Connections

Relation among the load-displacement response of specimens with different number of connector screws is presented in Figs. 30 and 31, respectively for 1.2 mm and 0.8 mm CFS section thickness.

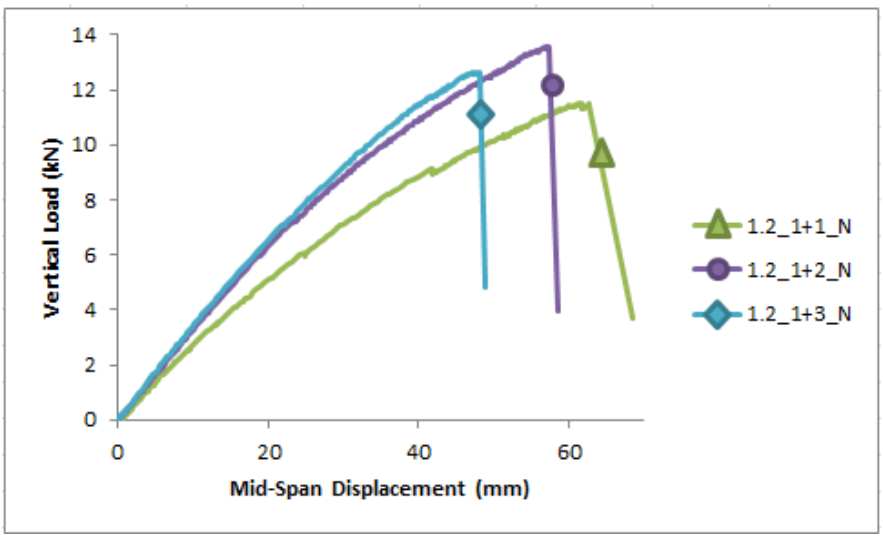

Figure 30. Effect of Number of Fasteners on Load-Displacement Response for 1.2 mm Section Thickness

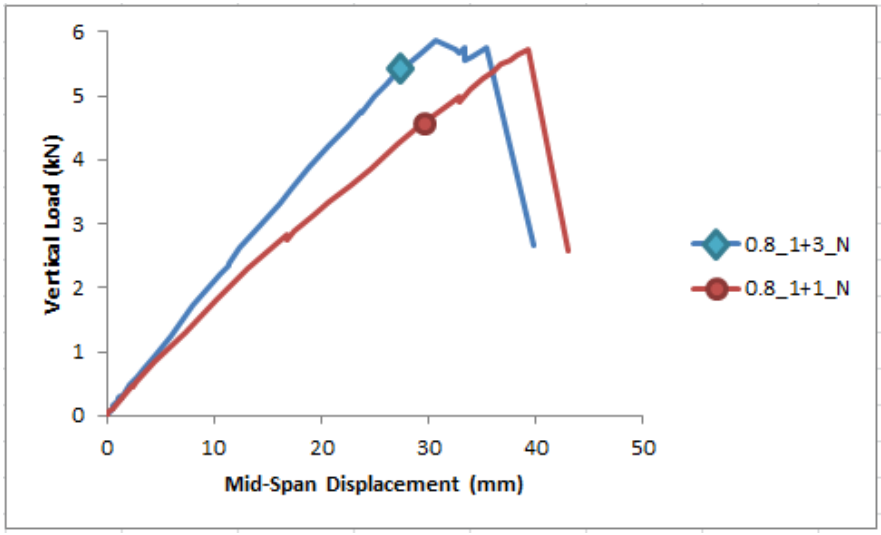

Figure 31. Effect of Number of Fasteners on Load-Displacement Response for 0.8 mm Section Thickness

The specimens presented in Fig. 30 were made of 1.2 mm thick steel sheet and tested without OSB plates attached on top chord members. The only difference between these three specimens was the number of screws used to connect the diagonal members to chord members. Specimen 1.2_1+1_N has a single connection screw in addition to a rivet, specimen 1.2_1+2_N has two additional screws, and specimen 1.2_1+3_N has three additional screws at each diagonal-chord connection. The compression chord member in all of these three specimens underwent buckling as indicated in Fig. 30. The effect of increasing number of connection screws is generally in the form of an increase in load capacity and stiffness of truss specimens. Providing two additional screws instead of one resulted in 18% increase in load capacity and 25% increase in service stiffness. The fact that a similar trend doesn't exists between the cases of two and three additional screws could be related with the failure mode of specimens 1.2_1+2_N and 1.2_1+3_N. In these specimens, compression chord buckling occurred under one of the loading points, as indicated in Fig. 32. The localized effect of loading points could be the reason for specimen 1.2_1+3_N having lower load capacity than specimen 1.2_1+2_N. In order to eliminate such local effect of loading, reinforcing plates were attached on flanges of compression chord directly under loading points in the following tests.

Effect of the number of connection screws on truss behavior for CFS section thickness of 0.8 mm is shown on the plots given in Fig. 31. Providing three additional screws instead of one increased the truss service stiffness by 31% without a major change in load capacity and failure mode (Fig. 33).

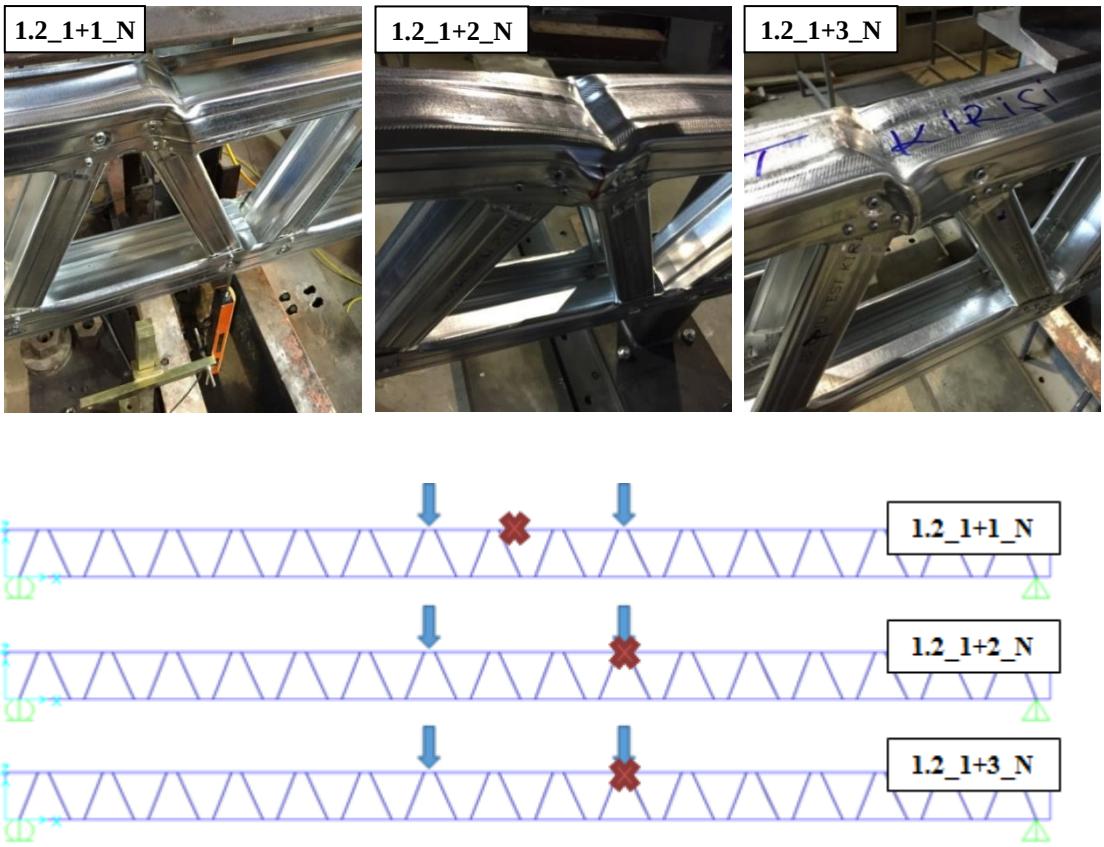

Figure 32. Pattern and Location of Buckling in Specimens 1.2_1+1_N, 1.2_1+2_N, 1.2_1+3_N

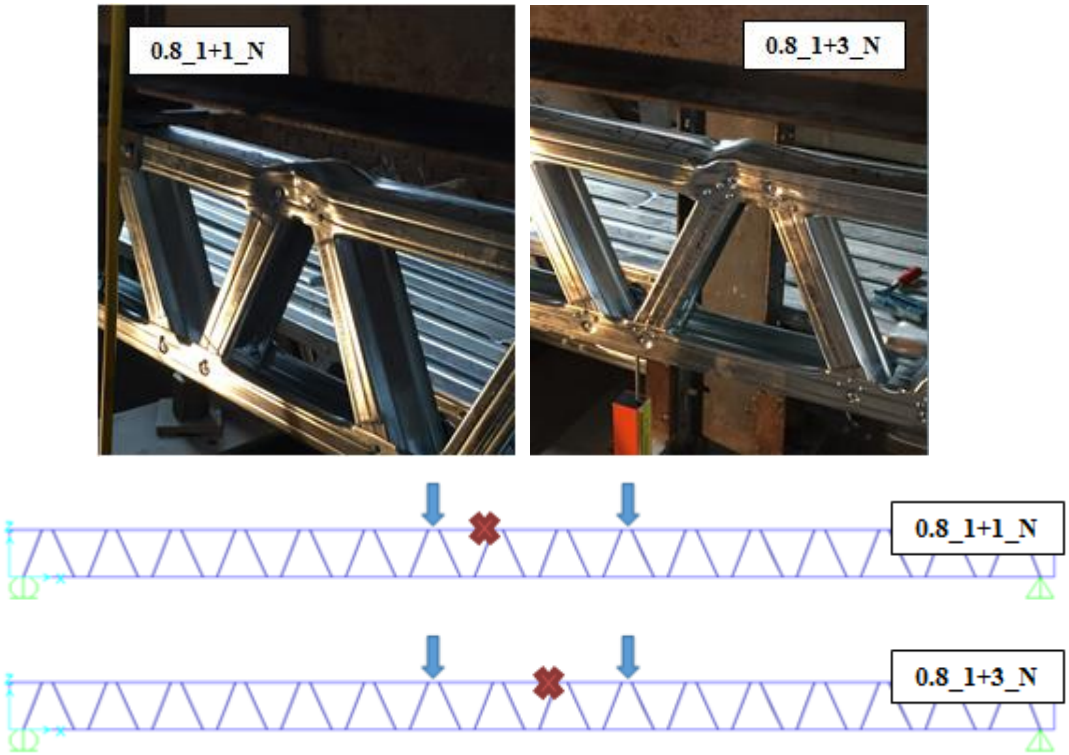

Figure 33. Pattern and Location of Buckling in Specimens 0.8_1+1_N, 0.8_1+3_N

2.3.4 Effect of Using Two Different CFS Member Thicknesses

When difference in tension and compression capacity of CFS members is considered, designing all of truss members from same thickness becomes uneconomical. Moreover, if tension capacity of lower chord member is kept below the compression capacity of upper chord member a ductile failure behavior would be expected. In order to investigate this design approach hybrid trusses were tested in two specimens.

In Specimen 1.2-0.8_1+2_N the upper chord member was obtained from Group 1 – 1.2 mm thick material, while the rest of truss members were obtained from Group 1 – 0.8 mm thick material. Connection of web members and chord members was configured with single rivet and two additional screws.

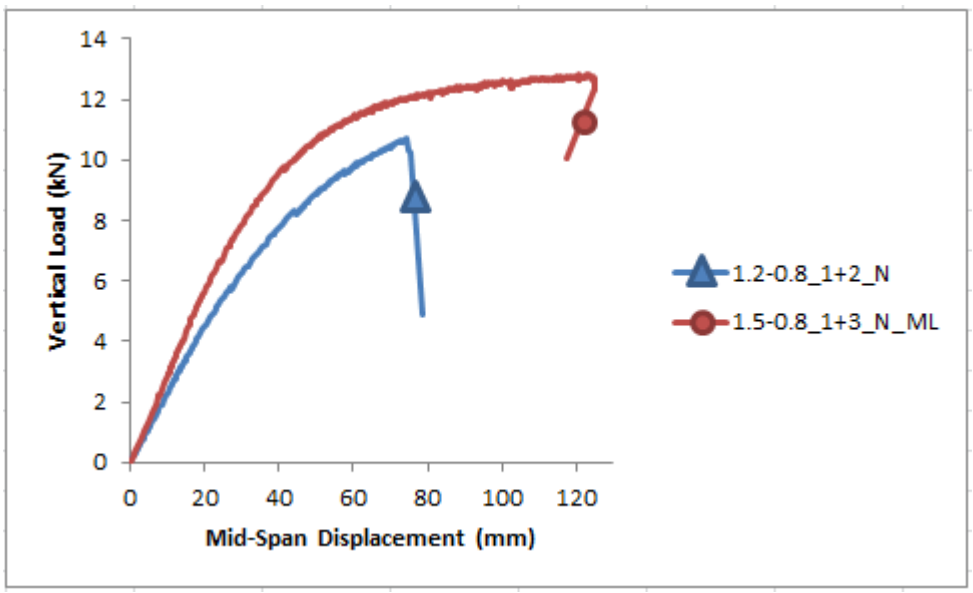

Figure 34. Load-Displacement Graph of Specimens 1.2-0.8_1+2_N and 1.5-0.8_1+3_N

Specimen 1.2-0.8_1+2_N failed due to buckling of compression chord and didn't exhibit a ductile behavior as expected. Load-displacement response of the specimen is shown in Fig 34. Location of failure is indicated in Fig. 35. Initial calculations performed according to AISI [5] Chapter 5 indicated compression chord to have a higher strength than the yielding capacity of lower chord. However, compression chord member underwent buckling during load testing as shown in Fig. 36. Truss failed under 10.7 kN of vertical loading,. Stiffness of hybrid truss reduced in 30% amount when compared with 1.2_1+2_N truss specimen. Load deformation response of specimens 1.2_1+2_N and 1.2-0.8_1+2_N is given in Fig. 37.

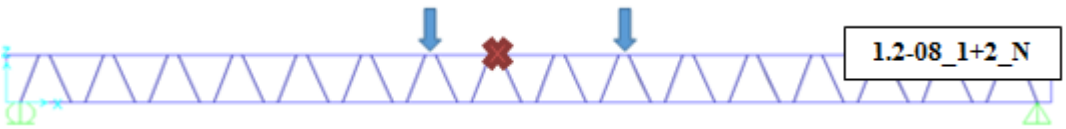

Figure 35. Failure Location Specimen 1.2-0.8_1+2_N

Figure 36. Failure Mode of Specimen 1.2-0.8_1+2_N

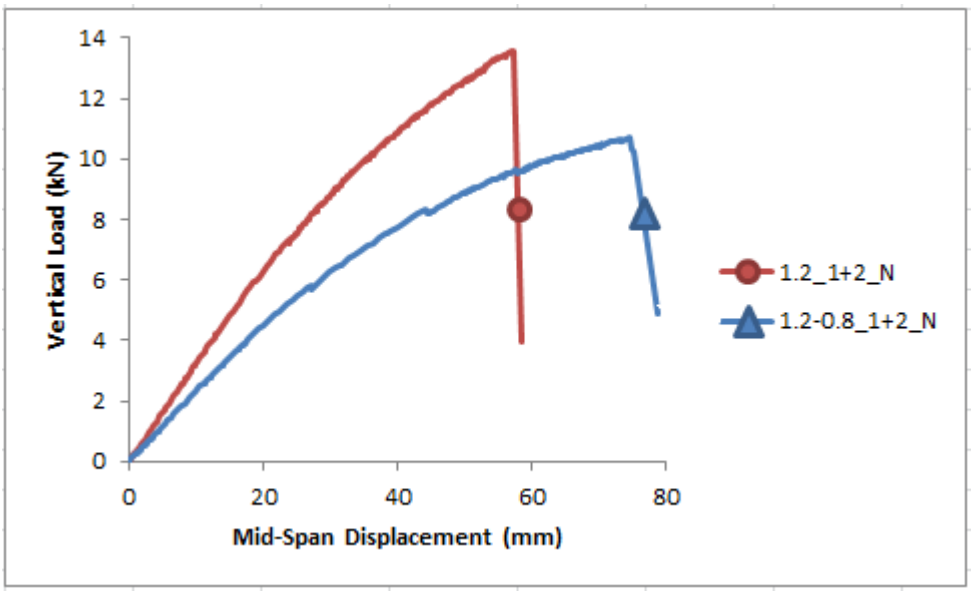

Figure 37. Load Displacement Graph of 1.2_1+2_N and 1.2-0.8_1+2_N

Upper chord member of specimen 1.5-0.8_1+3_N_SG was obtained from Group 2 – 1.5 mm thick material and the rest of truss members were obtained from Group 2 – 0.8 mm thick material. Connection of web members and chord members was configured with single rivet and three additional screws. Different than specimen 1.2-0.8_1+2_N, this specimen failed due yielding of tension chord member with no buckling observed on compression chord member. From this perspective, the hybrid design approach was adopted successfully for this specimen. As evident in Fig. 34,

using 1.5 mm CFS member thickness for compression chord and 0.8 mm thickness for all other members resulted in a ductile behavior. Another observation valid in this figure is that by increasing the thickness of compression chord member from 1.2 mm to 1.5 mm while keeping the thickness of other members at 0.8 mm resulted in a major increase both in stiffness and load capacity of truss.

2.3.5 Effect of Connection Cover Plate

In an attempt to reduce the deformation at diagonal-chord connections, cover plates shown in Fig. 38 were used to cover the connection region in four specimens. These plates were in sizes of 188 x 100 mm and were attached to trusses with nine screws as shown in Fig. 38. Comparison of the load-deflection response of truss specimens utilizing such connection cover plates with the companion specimens is provided in the plots given in Fig. 39. The diagonal-chord connection in companion specimens was achieved through a rivet and three additional screws. As evident in these plots, forming the diagonal-chord connections with a rivet and a cover plate instead of a rivet and three screws resulted in a slight increase in truss stiffness and load capacity. This result is valid for both 0.8 mm and 1.2 mm CFS member thickness. The effect of connection cover plates seems to be more pronounced in specimens tested with an OSB plate attached on top chord member as compared to those tested without an OSB plate.

Figure 38. Attachment of Connection Cover Plate

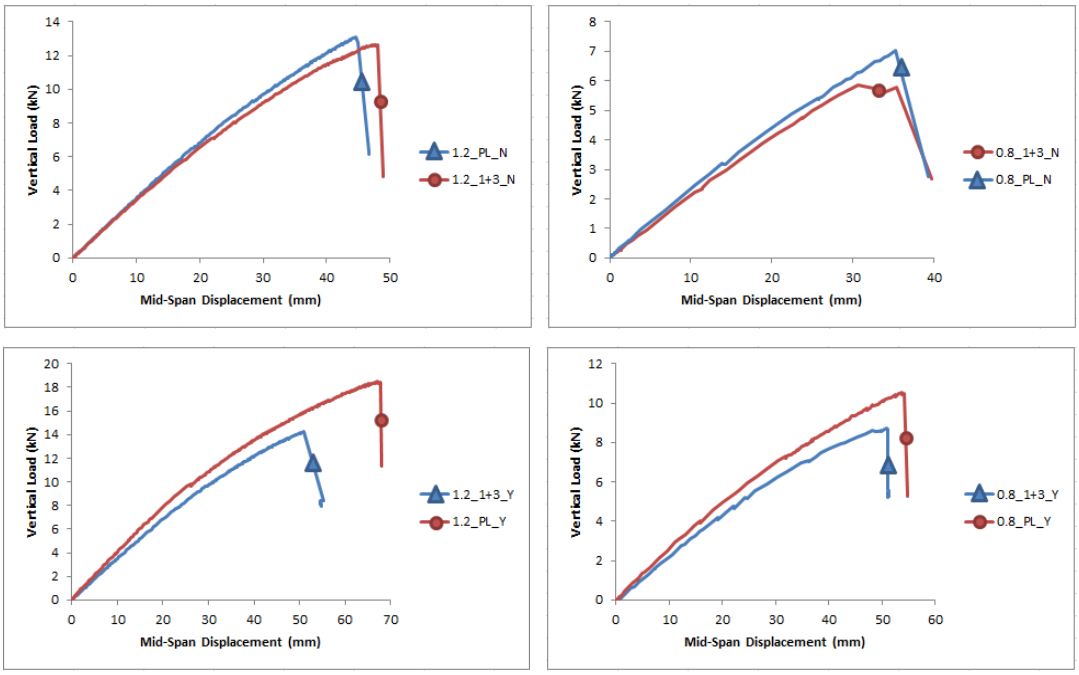

Figure 39. Effect of Connection Cover Plate on Load-Displacement Response

In specimens with connection cover plates, failure was due to buckling of compression chord, irrespective of the CFS member thickness and the presence or absence of OSB plate. Photographs showing the buckling failure regions in these

specimens are given in Fig. 40, with the failure locations indicated in Fig. 41. It is interesting to note that in specimen 1.2_PL_Y the presence of connection plate was not able to prevent the buckling of compression chord member within the connection region. In fact, the connection cover plate also underwent buckling together with the chord member in this specimen.

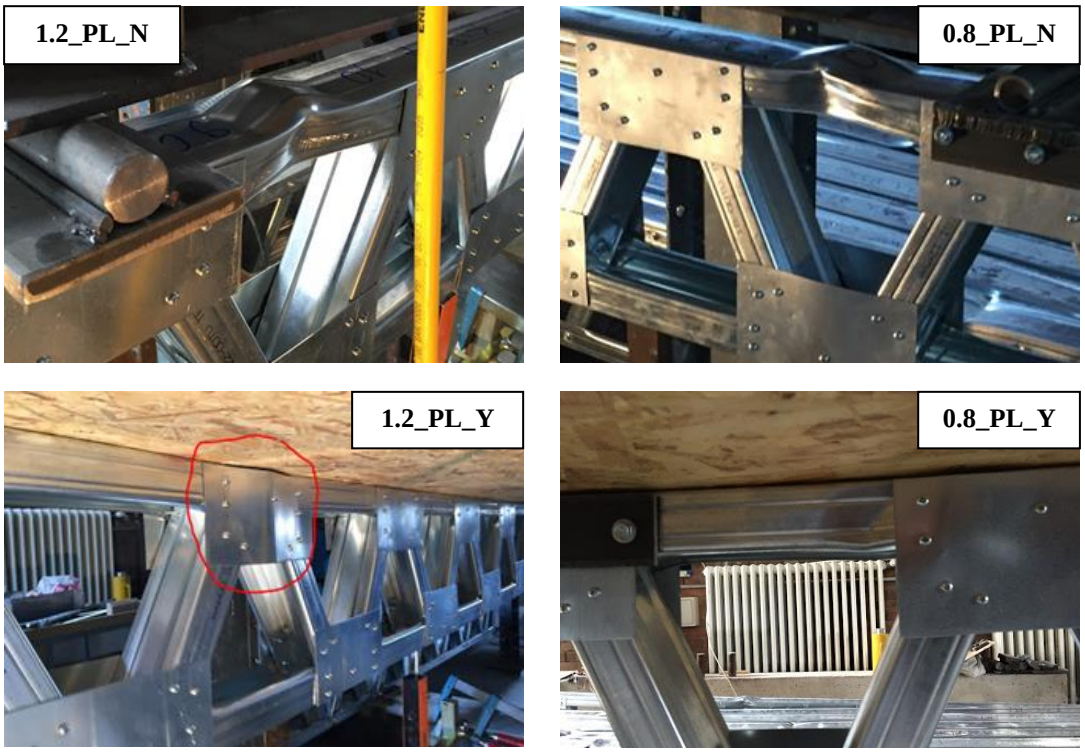

Figure 40. Failure Mode of Specimens with Connection Cover Plate

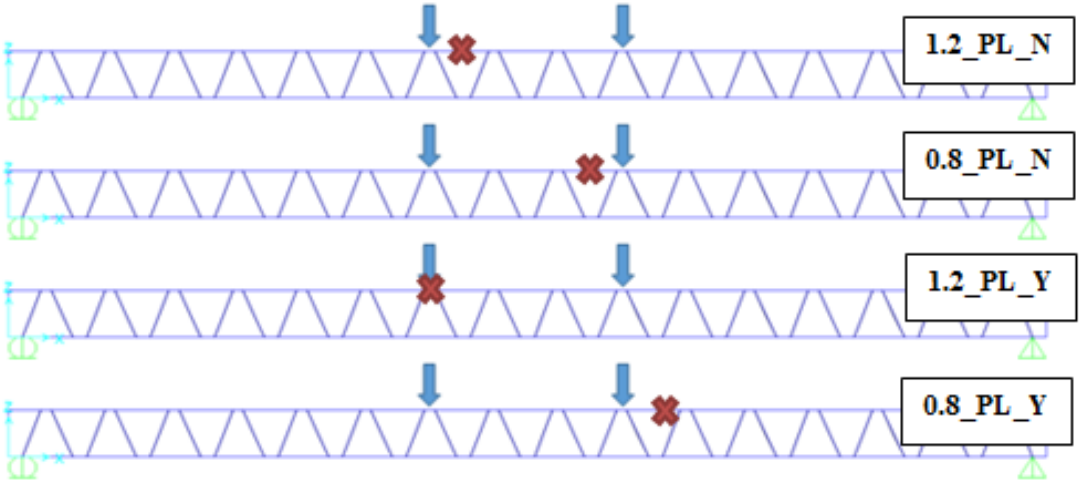

Figure 41. Failure Locations in Specimens with Connection Cover Plate

2.3.6 Effect of CFS Member Thickness

Some of the truss specimens were tested with 0.8 mm CFS member thickness. In these tests, the diagonal-chord connections were formed by rivet + 1 screw, rivet + 3 screws, and connection cover plate. Load-deflection response of these trusses is compared in Fig. 42 with that of companion trusses with 1.2 mm CFS member thickness. Irrespective of the CFS section thickness, all truss specimens presented in Fig. 42 exhibited compression chord buckling. Photographs showing the buckling failure regions in specimens with 0.8 mm CFS member thickness are given in Fig. 43, with the corresponding failure locations indicated in Fig. 44.

For all three diagonal-chord connection details studied, increasing the CFS member thickness from 0.8 mm to 1.2 mm significantly improved the truss behavior by increasing both the stiffness and the load capacity. The increase in service stiffness is between 50% and 55%, and the increase in load capacity is between 100% and 115%. This trend was not affected by the presence or absence of OSB plate attached on compression chord member.

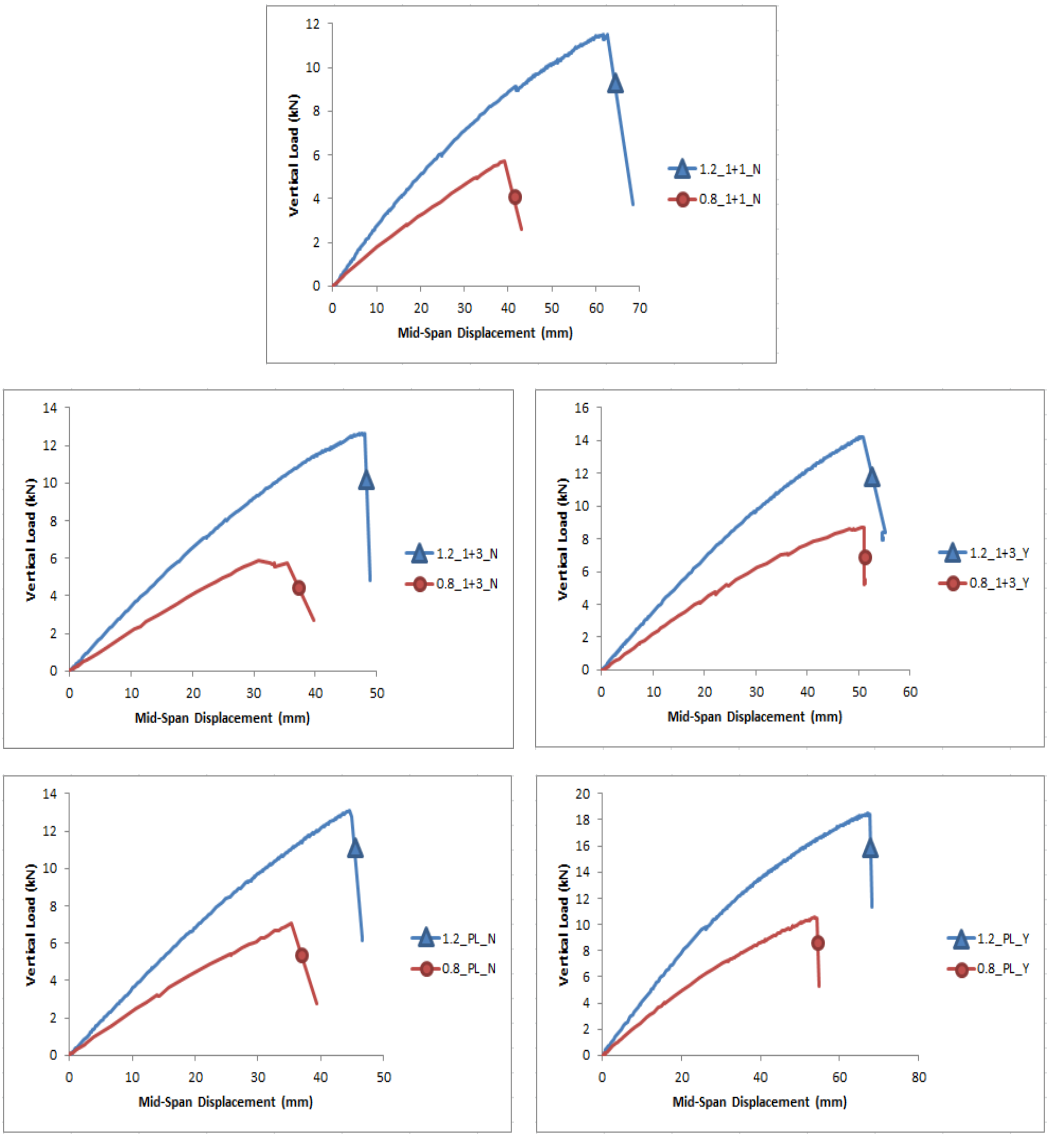

Figure 42. Effect of Section Thickness on Load-Displacement Response

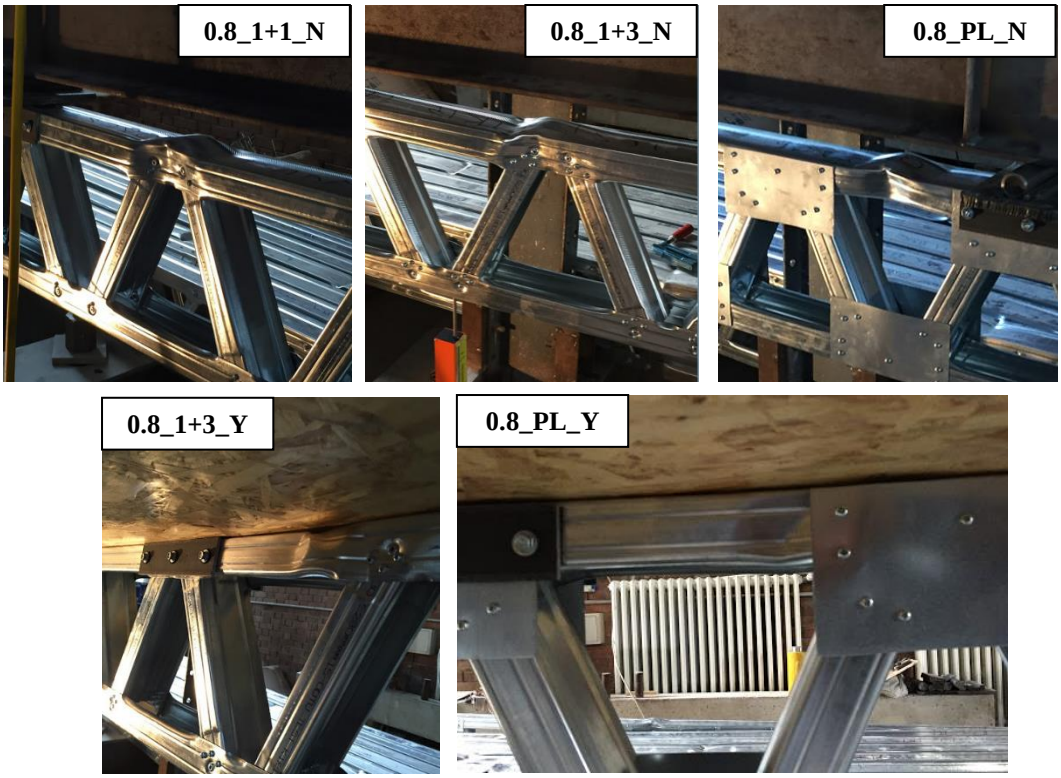

Figure 43. Failure Mode of Specimens with 0.8 mm CFS Section Thickness

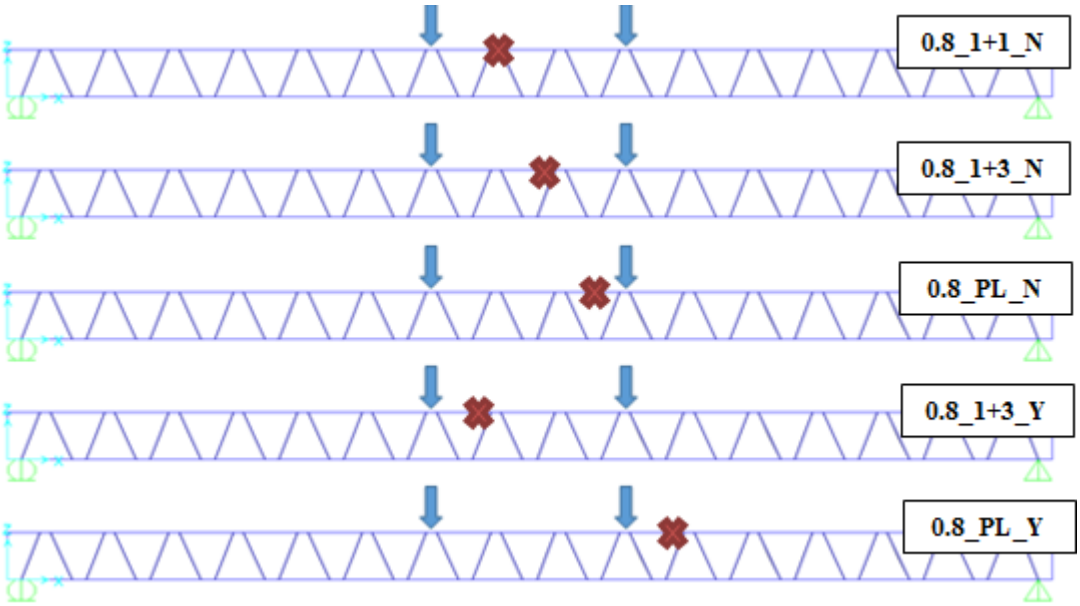

Figure 44. Failure Locations in Specimens with 0.8 mm CFS Section Thickness

2.3.7 Effect of the Presence of OSB Plate

In one of the methods that is commonly used in CFS construction to form the floor system, OSB plates are placed on CFS trusses and attached to web of top chord members using screws. The OSB plates attached on web of top chord member through screws that are spaced at certain distance will provide bracing for this member and increase the axial load capacity. In order to investigate such beneficial effect, some of the truss specimens were tested with 600 mm wide 11 mm thick OSB plates attached on web of top chord members. Load-deflection response of these specimens is compared to that of companion specimens tested without OSB plates in Figs. 45 and 46, respectively for CFS section thickness of 1.2 mm and 0.8 mm.

Failure of truss specimens was due to bucking of compression chord member even with the presence of OSB plates. Presence of OSB plates, however, improved the truss response by delaying the buckling of compression chord and hence increasing the truss load capacity. The improvement in truss load capacity with the presence of OSB plates was a function of CFS section thickness and the diagonal-chord connection detail. For trusses with 1.2 mm CFS section thickness and OSB plates connected to web of top chord member at 150 mm spacing, the increase in load capacity was between 12% and 24% when diagonal-chord connection plates were not used. A 41% increase in load capacity was obtained when the diagonal-chord connection was formed by connection plates.

Considering that OSB plates delay the buckling of compression chord and a CFS section with 0.8 mm thickness is more susceptible to buckling than the one with 1.2 mm thickness, the improvement of truss behavior with the presence of OSB plates is expected to be more significant for CFS section thickness of 0.8 mm as compared to 1.2 mm. A comparison of plots given in Figs. 45 and 46 reveals such a trend. For trusses with 0.8 mm CFS section thickness and OSB plates connected to web of top chord member at 150 mm spacing, the increase in load capacity was 47% for the case of three connector screws. A more significant improvement in truss capacity was obtained when the spacing of screws connecting the OSB plate to top chord member

was reduced to 30 mm. In this case, the increase in truss load capacity was 112% as compared to the case with no OSB plate.

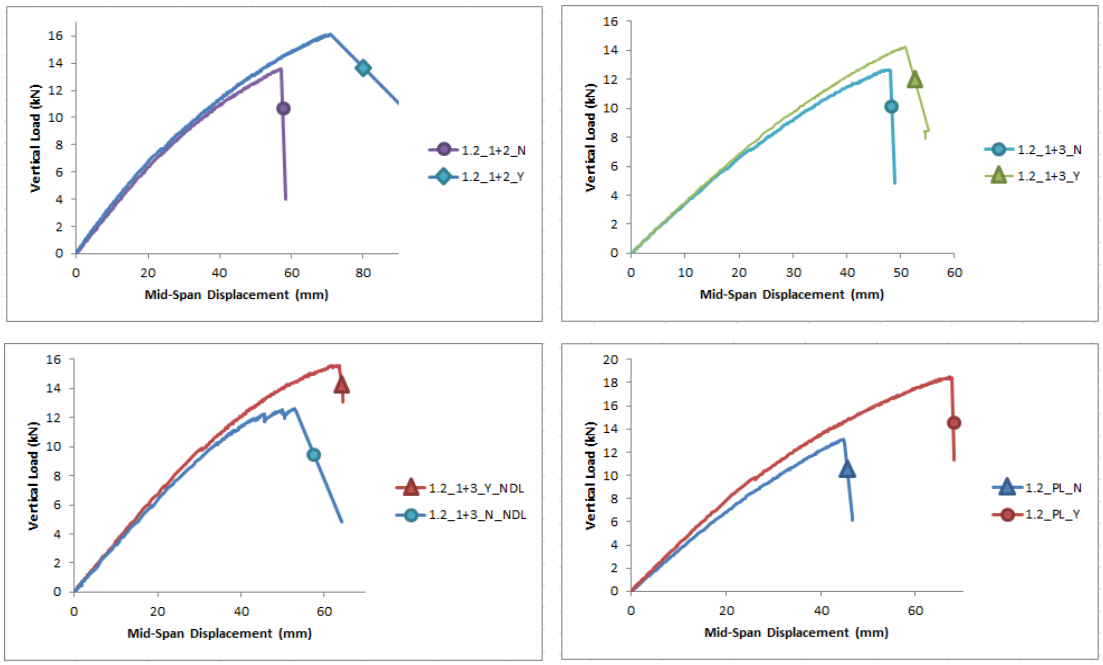

Figure 45. Effect of the Presence of OSB Plate on Load-Displacement Response (1.2 mm CFS Section Thickness)

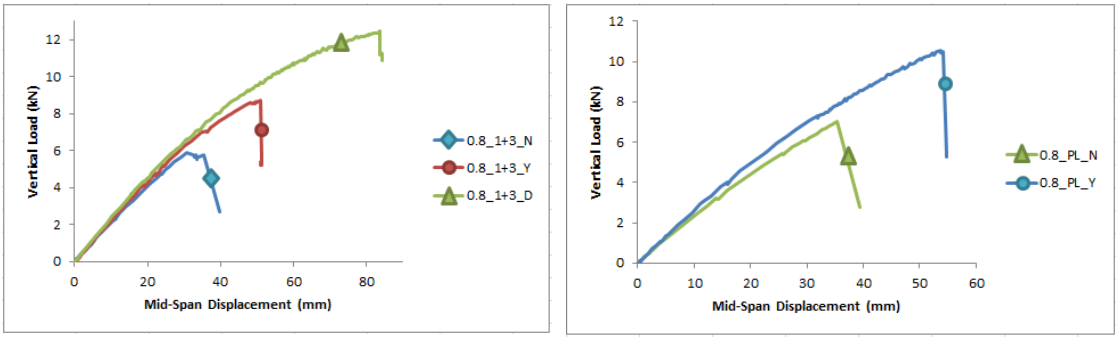

Figure 46. Effect of the Presence of OSB Plate on Load-Displacement Response (0.8 mm CFS Section Thickness)

2.3.8 Effect of Chord Member Lip Condition

As mentioned earlier, the connection detail shown in Fig. 47 was tested in some of the truss specimens in an attempt to eliminate the negative effect of the chord lip termination, which is required to insert the ends of diagonal members inside the chord members in the original connection detail. Three truss specimens with 1.2 mm CFS section thickness were tested with this new connection detail.

Figure 47. Connection Detail with Continuous Chord Lips (Specimen 1.2_1+1_N_NDL)

As mentioned in previous parts, local buckling of the compression chord member within the short length between the ends of two diagonal members occurred in many of the truss specimens. It was believed that this type of buckling was caused by the lack of sufficient restraint against buckling due to termination of the flange lips locally in the connection region. Having the flange lips continuous without any termination was considered to solve such local buckling problem within the connection region and improve the truss behavior. The compression chord buckling modes observed in these specimens are shown in the photographs given in Fig. 48. Buckling of compression chord within the connection region was eliminated by not terminating the chord lip. The compression chord buckling occurred either in the vicinity of the connection region or away from the connection region. However, as evident in the plots presented in Fig. 49, no major difference occurred in the load-

deflection response of truss specimens with continuous lip when compared to those of the companion specimens with terminated chord lip. The largest increase in truss load capacity was 10% with almost no change in the stiffness.

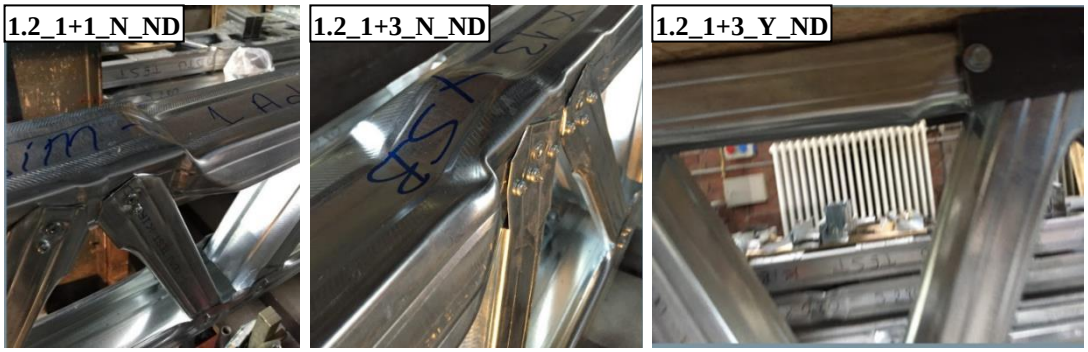

Figure 48. Failure Mode of Specimens with Continuous Chord Lip

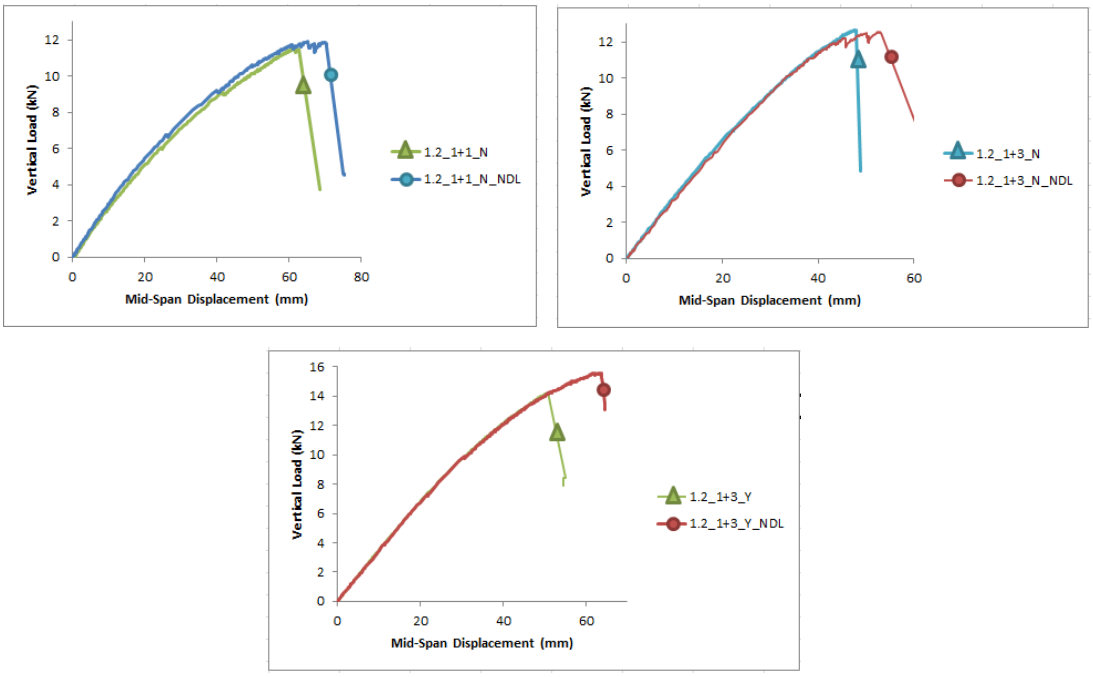

Figure 49. Effect of Chord Member Lip Condition on Load-Displacement Response

2.3.9 Effect of Reinforcing Compression Chord Member

Another detail used in test specimens to improve the truss load capacity was to provide CFS channel section members on either sides of compression chord, as illustrated in Fig. 50. The reinforcing members were attached on either side of compression chord by 5.5 mm diameter screws spaced at 150 mm. Only one specimen was tested with this detail and the experimentally determined load-deflection response is given in Fig. 51. Reinforcement of the compression chord member resulted in a significant improvement in truss response. Compared to the companion specimen with conventional compression chord the increase in load capacity was 81%. The improvement in truss response was obtained through delaying of compression chord buckling due to the existence of reinforcing members. Failure of the specimen with reinforced compression chord was due to local buckling of the compression chord as well as the reinforcing members, as shown in Fig. 52.

It should be mentioned that the diagonal pattern in specimen 0.8_1+3_N_RCC was slightly different than that of other truss specimens. In this specimen 36 diagonal members were used, as opposed to 34 diagonal members used in other specimens. This geometry difference also resulted in a slight change in the moment arm used during load testing. The moment arm used for specimen 0.8_1+3_N_RCC was 2535 mm, which is 180 mm longer than the moment arm used for testing of other specimens.

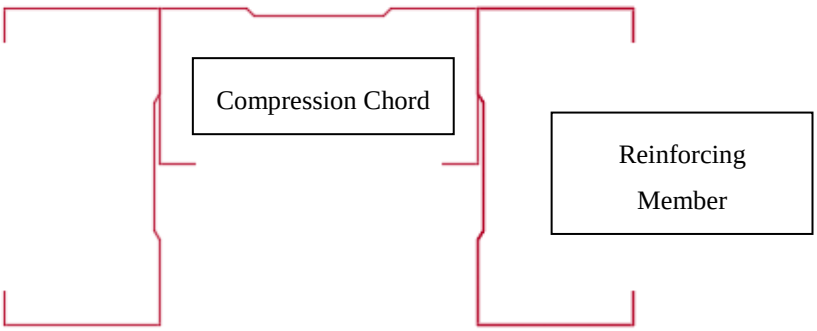

Figure 50. Reinforced Compression Chord Section View

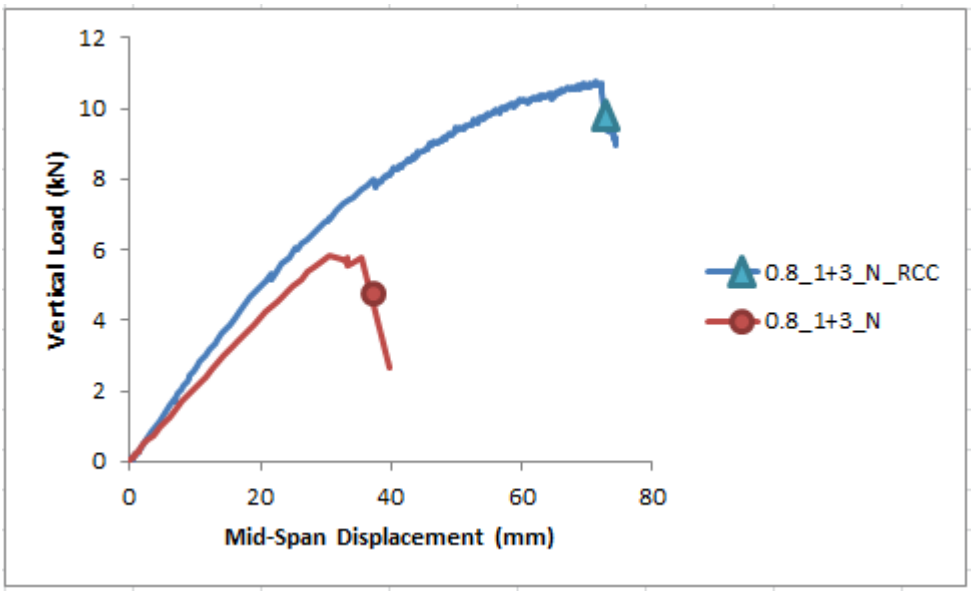

Figure 51. Effect of Reinforcing Compression Chord Member on Load-Displacement Response

Figure 52. Failure Mode of Specimen with Reinforced Compression Chord

2.3.10 Test of Shorter Span Truss

One of common property of all test specimens was a clear span length of 5820 mm. However it was thought that second order effects due to excessive vertical deflection of truss specimens may have influenced the behavior and reduced the load capacity of specimens. In order to investigate this issue, a specimen with a clear span length of 3780 mm was tested. Measured load-deflection response of this shorter specimen is shown in Fig. 53. Similar to the other specimens, failure of this specimen was due to local buckling of compression chord as shown in Fig. 54. The specimen failed at a load of 24.8 kN, and this level of load corresponds to a 59.2 kN axial force in the compression chord member. This level of force is only 10% higher than the average of seven tests made with 1.2 mm thick section thickness. Thus, results point out that second order effects due to excessive vertical deformation has a negligible effect on the ultimate capacity.

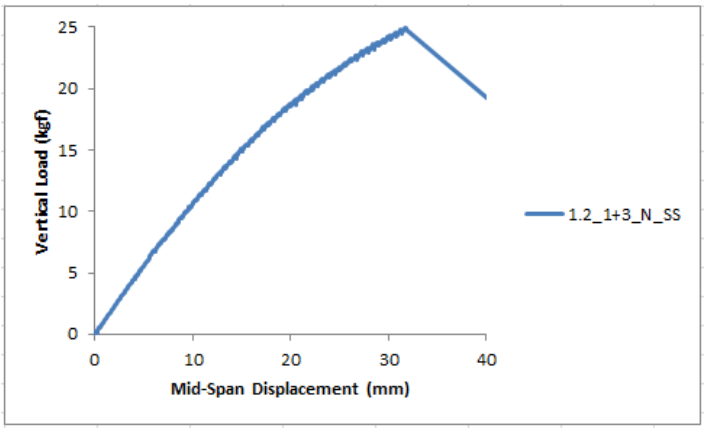

Figure 53. Load-Displacement Graph of Specimen 1.2_1+3_N_SS

Figure 54. Failure Mode of Specimen 1.2_1+3_N_SS

2.4 Discussion of Process and Results

Details of tested specimens were given in Section 2.3 and a chart summarizing the test results is provided in Table 1. In the end of experimental studies on trusses, several important points are inferred.

First of all, truss tests were initialized with mid-span lateral supports however after third test according to instrumentally collected data, it was noticed that truss geometry provides adequate stability therefore lateral supports became unnecessary and were removed from setup. In the test of the first specimen it was understood that shear capacity of the rivets was critical on failure limit. This result opened the vision of modifications to connections. Then test session of screw installed trusses were applied, results are given briefly. Preparation of screw installed trusses had taken a long time, for this reason in order to help reduce man-hour cost of trusses, connection was tested with single big screw rather than rivets. We met the problem of serviceability in that trial. One step further data collection was prolonged with different material thicknesses.

Another point that experimental study focused on was the OSB Sheating of trusses. That was important for the investigation of the floor trusses in a more complete manner because the floor trusses are commonly used in this format. The sheeting improved stiffness and strength values in significant amounts. Details were given in the previous section. Also installation spacing effect was tested with single specimen.

With purpose to leave no suspicion if geometric non-linear effects are dominant or not, on calculating load capacity of trusses, one shorter span truss was also tested. Results did not orient study into focusing non- linear effects.

Reliability of design methods is criticized and several modifications are offered in the following sections. Determining vertical deflection would be the first topic on analytical studies. A new test setup which concentrates on the connection of trusses will be introduced. Then the load capacity of the truss will be investigated on member scale approach.

Truss tests results were served into World Structural Engineering literature, therefore material yield and ultimate limits were also provided in Table 2. These material properties were also taken into account on analytical studies in following chapters.

CHAPTER 3

ANALYSIS OF TRUSS STIFFNESS

Service stiffness obtained from a linear structural analysis with axially rigid connection assumption was observed to overpredict the experimentally obtained stiffness values of truss specimens. In order to overcome such disagreement in the predicted and measured stiffness flexibility of joints between diagonal and chord members was included in the analyses. Additional tension tests were conducted on riveted and screwed connections in order to obtain the connection stiffness when different number of fasteners are used. Experimental and numerical studies conducted in order to investigate the flexural stiffness of truss specimens are explained in this chapter.

3.1 Linear Elastic Structural Analysis of Trusses

Trusses were modeled with respect to the Structural Analysis Section of AISI S214-12 Truss Design Specifications [2] using the computer program SAP2000 v18 [15]. Effective area concept was excluded in these models. For each truss specimen, two models were analyzed: single-node connection case and two-node connection case. In the single-node connection case, two diagonal members at each joint shared a single node. In this case, the eccentricity existing in the truss specimens between the ends of two diagonal members at each diagonal-chord connection was not taken into consideration. In the two-node connection models, each diagonal member had its own node and the location of these nodes coincided with the physical location of rivets connecting each end of diagonal members to chord members in truss specimens. Undeformed and deformed shapes of both models are given respectively

in Figs. 54 and 55. To investigate the shorter span truss test, one more two-node connection model was created as shown in Fig. 57.

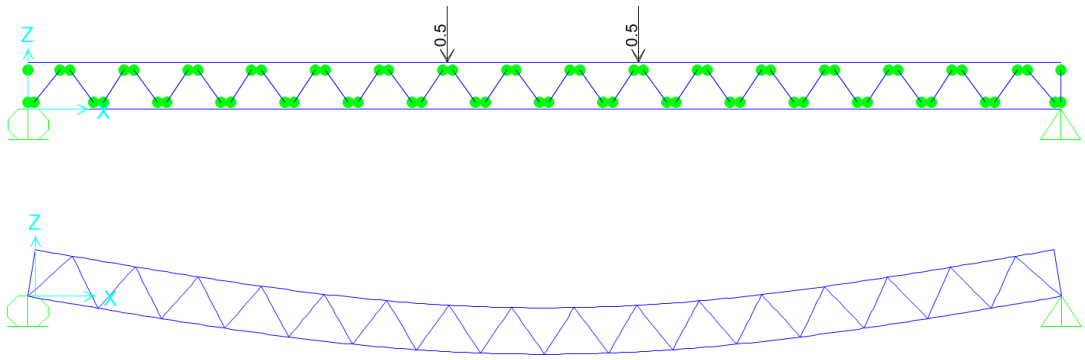

Figure 55. Analysis Model with Single-Noded Connections

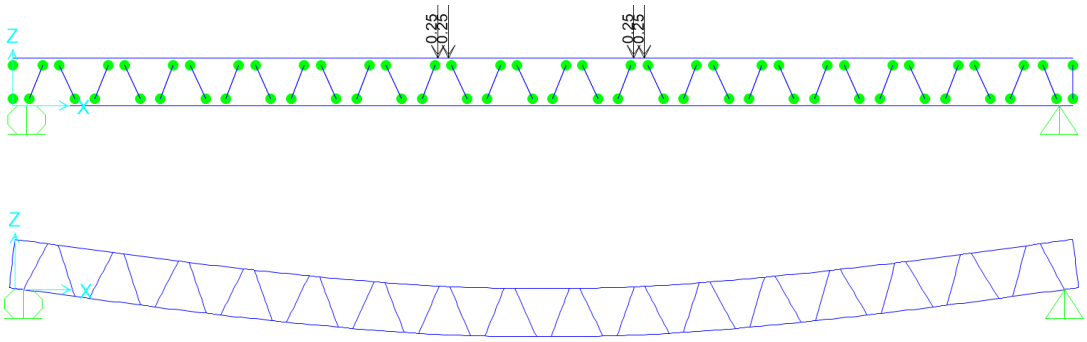

Figure 56. Analysis Model with Two-Noded Connections

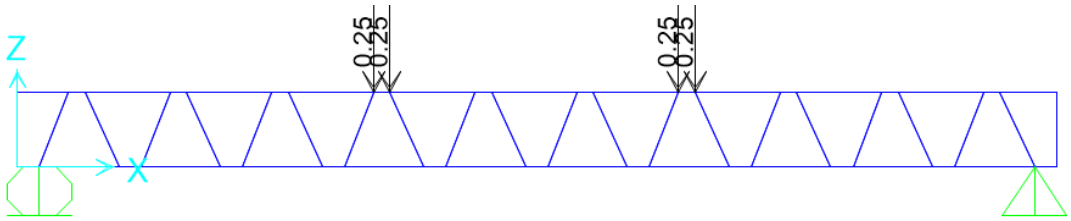

Figure 57. Short Span Analysis Model with Two-Noded Connections

Top and bottom chord members in models were defined as continuous members and moment releases were assigned at the ends of diagonal members. Sections were defined for two nominal thickness values with an elastic modulus of 210 GPa. Section geometries were defined with nominal dimensions of 90 mm height, 45 mm

flange width, and 10 mm lip length. The web stiffener existing on the section used in test specimens was not included in models. Truss depth in models was assigned as 270.2 mm, which corresponds to the distance between the centroids of top and bottom chord members. Loading was applied by defining nodal forces.

3.2 Results From Linear Elastic Analysis Models

The load-displacement responses of test specimens obtained from the linear elastic models explained in the previous section are plotted together with the experimentally obtained response in Figs. 58-60. These figures respectively show the results for 1.2 mm CFS section thickness, 0.8 mm section thickness, and short span specimen. Each plot includes analysis results for both the single-node and two-node connection models.

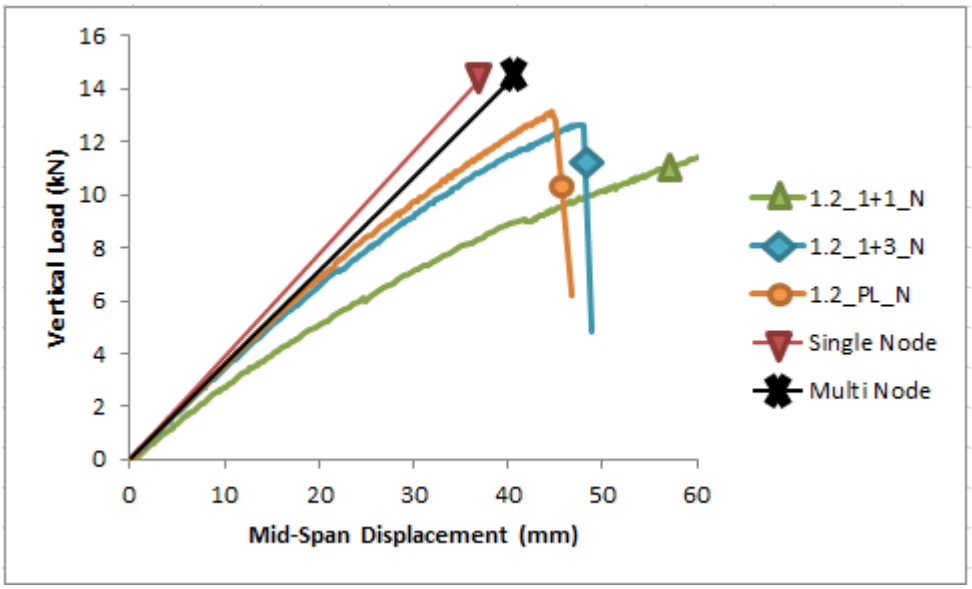

Figure 58. Load –Displacement Data Comparison of Truss Tests and Analyses of 1.2 mm Section Thickness

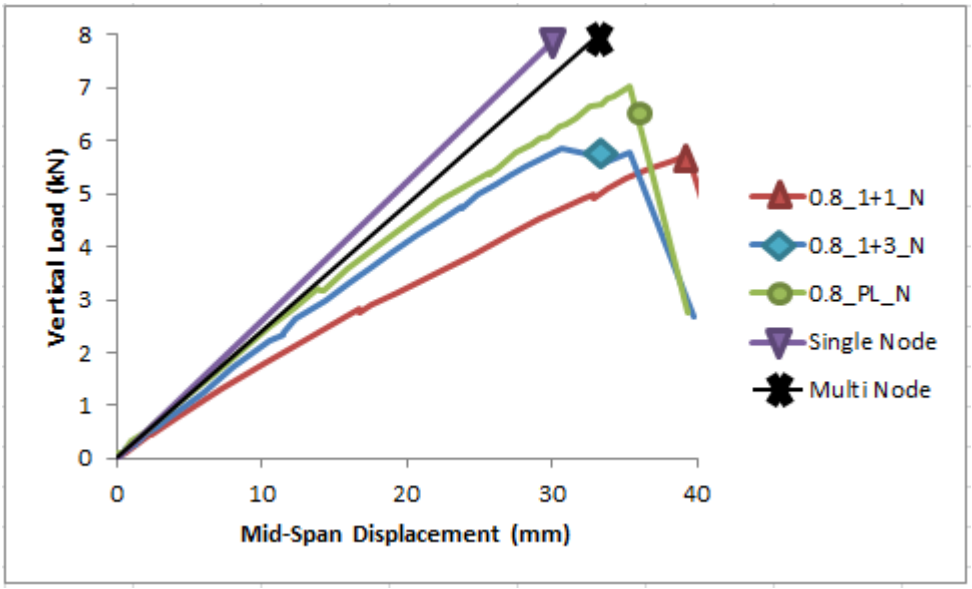

Figure 59. Load –Displacement Data Comparison of Truss Tests and Analyses of 0.8mm Section Thickness

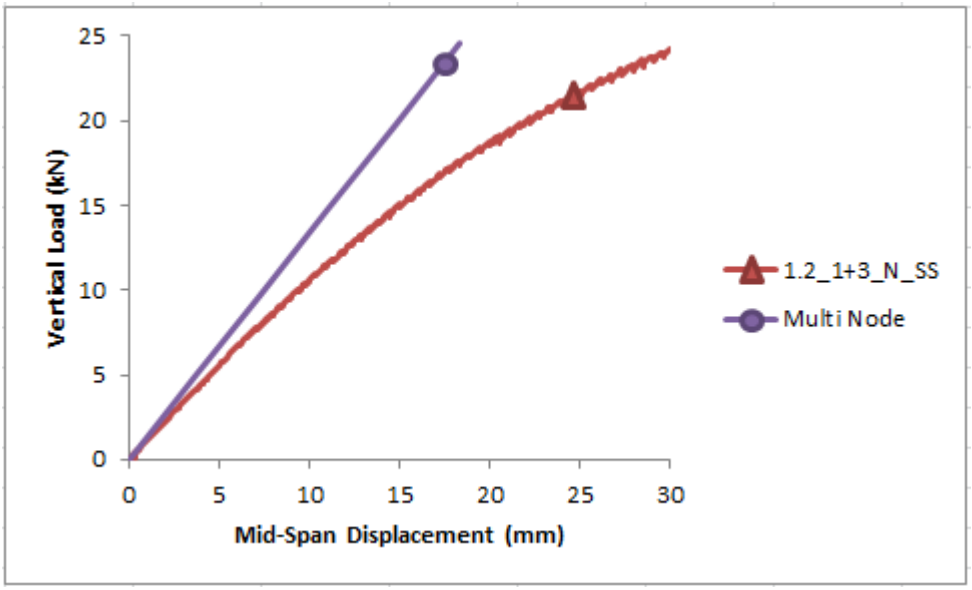

Figure 60. Load –Displacement Data Comparison of Short Span Truss Test and Analysis

As it is clearly seen from the plots, both the single-node and two-node connection models have large error rates on predicting the truss service stiffness. Another fact that is noticed on these charts is that, trusses which have connections with fewer fasteners give higher error rates. Error between the predicted and experimentally

determined deflection values at ultimate load capacity of truss specimens are listed numerically in Table 3.

Table 3. Comparison of Analysis and Test Results

Specimen #	Thickness (mm)	Connection Property	Ultimate Vertical Force (kN)	Failure Vertical Displacement (mm)	Multi-Node Analysis Displacement (mm)	Error Rate (%)	Single-Node Analysis Displacement (mm)	Error Rate (%)
1.2_1+1_N	1.2	Rivet +1 Screw	11.5	62.8	32.3	48.5	29.7	52.7
1.2_1+3_N	1.2	Rivet +3 Screw	12.7	49.2	35.5	27.9	32.6	33.7
1.2_PL_N	1.2	Plate	13.1	45.3	36.9	18.7	33.9	25.2
0.8_1+1_N	0.8	Rivet +1 Screw	5.7	40.4	23.8	41.1	21.9	45.7
0.8_1+3_N	0.8	Rivet +3 Screw	5.9	35.4	24.4	31.0	22.5	36.4
0.8_PL_N	0.8	Plate	7.1	36.3	29.3	19.3	27.0	25.6
1.2_1+3_N_SS	1.2	Rivet +3 Screw	24.8	31.8	18.5	41.9	-	-

Disagreement between the numerically predicted and experimentally determined deflections is also valid at service load level. This discrepancy is presented in Table 4. The service load level was assumed to be % 60 of ultimate load capacity of each truss specimen.

Table 4. Comparison of Analysis and Test Results at Service Load Condition

Specimen #	Thickness (mm)	Connection Property	%60 of Ultimate Force (kN)	Displacement Under %60 Capacity (mm)	Multi-Node Analysis Displacement (mm)	Error Rate (%)	Single-Node Analysis Displacement (mm)	Error Rate (%)
1.2_1+1_N	1.2	Rivet +1 Screw	6.9	29.0	19.4	33.1	17.8	38.5
1.2_1+3_N	1.2	Rivet +3 Screw	7.6	23.7	21.3	10.2	19.6	17.4
1.2_PL_N	1.2	Plate	7.9	23.5	22.1	5.9	20.3	13.4
0.8_1+1_N	0.8	Rivet +1 Screw	3.4	20.8	14.3	31.3	13.2	36.7
0.8_1+3_N	0.8	Rivet +3 Screw	3.5	17.4	14.7	15.8	13.5	22.4
0.8_PL_N	0.8	Plate	4.3	19.3	17.6	8.9	16.2	16.1
1.2_1+3_N_SS	1.2	Rivet +3 Screw	14.9	15.1	11.1	26.6	-	-

Comparison of the numerically predicted response obtained from linear elastic models with the experimentally determined load-deflection behavior of truss specimens tested with OSB plates connected to web of top chord member is given in Figs. 61 and 62. Error in predicted and measured displacement for these specimens at

maximum load capacity and service load level is presented respectively in Tables 5 and 6. It should be mentioned that even though these specimens were tested with OSB plates placed on top of truss specimens, the analyses were performed considering the CFS trusses alone without OSB plates.

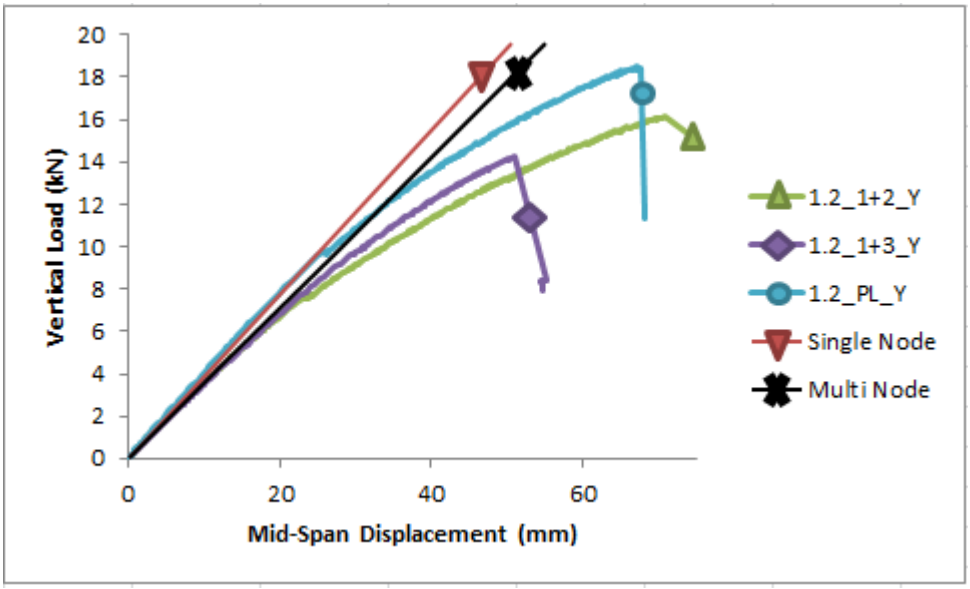

Figure 61. Load –Displacement Data Comparison of OSB Sheathed Truss Tests and Analyses of 1.2 mm Section Thickness

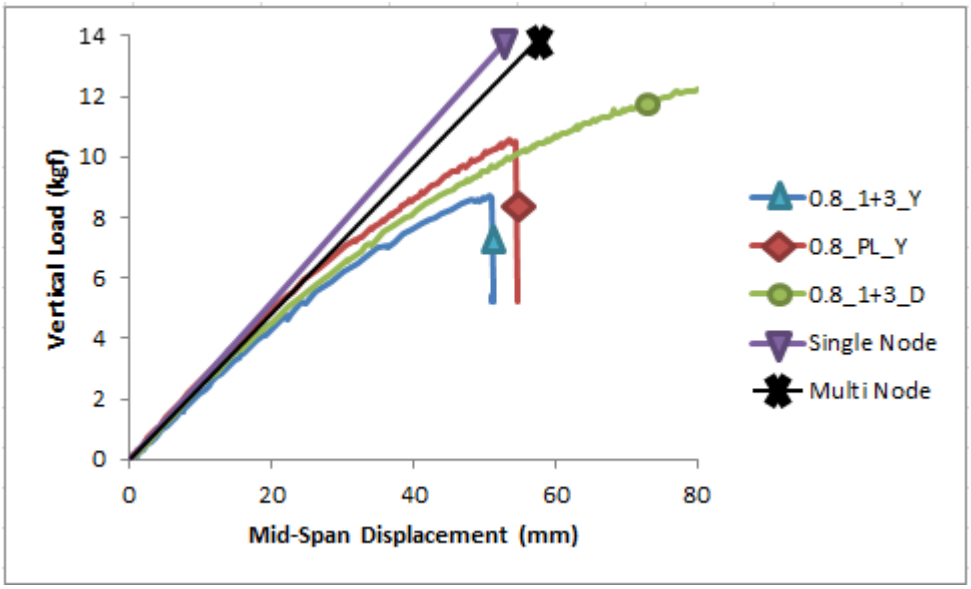

Figure 62. Load –Displacement Data Comparison of OSB Sheathed Truss Tests and Analyses of 0.8 mm Section Thickness

Table 5. Comparison of Analysis and Test Results at Ultimate Load Condition

Specimen #	Thickness (mm)	Connection Property	OSB Sheating	Ultimate Vertical Force (kN)	Failure Vertical Displacement (mm)	Multi-Node Analysis Displacement (mm)	Error Rate (%)	Single-Node Analysis Displacement (mm)	Error Rate (%)
1.2_1+2_Y	1.2	Rivet +2 Screw	YES	16.1	70.9	45.2	36.2	41.6	41.3
1.2_1+3_Y	1.2	Rivet +3 Screw	YES	14.2	50.9	39.9	21.6	36.7	27.9
1.2_PL_Y	1.2	Plate	YES	18.5	67.8	51.8	23.5	47.7	29.7
0.8_1+3_Y	0.8	Rivet +3 Screw	YES	8.7	51.2	36.2	29.3	33.4	34.8
0.8_PL_Y	0.8	Plate	YES	10.6	54.3	44.0	19.0	40.5	25.4
0.8_1+3_D	0.8	Rivet +3 Screw	DENSE	12.5	84.2	51.7	38.6	47.6	43.4

Table 6. Comparison of Analysis and Test Results at Service Load Condition

Specimen #	Thickness (mm)	Connection Property	OSB Sheating	%60 of Ultimate Force (kN)	Displacement Under %60 Capacity (mm)	Multi-Node Analysis Displacement (mm)	Error Rate (%)	Single-Node Analysis Displacement (mm)	Error Rate (%)
1.2_1+2_Y	1.2	Rivet +2 Screw	YES	9.66	32.6	27.2	16.5	25.0	23.2
1.2_1+3_Y	1.2	Rivet +3 Screw	YES	8.52	25.7	23.9	6.9	22.0	14.4
1.2_PL_Y	1.2	Plate	YES	1130	30.9	31.1	0.6	28.6	7.5
0.8_1+3_Y	0.8	Rivet +3 Screw	YES	535	24.3	21.8	10.4	20.1	17.4
0.8_PL_Y	0.8	Plate	YES	650	26.5	26.5	0.2	24.4	8.0
0.8_1+3_D	0.8	Rivet +3 Screw	DENSE	760	35.4	30.9	12.6	28.5	19.5

Results presented in plots and tables indicate that stiffness obtained from the linear elastic models agrees well with the service stiffness of truss specimens tested with OSB plates attached to the web of top chord member. The level of agreement is better when two-node connection approach is adopted as opposed to the single-node connection approach. However, when the ultimate load level is considered, instead of the service load level, the linear elastic models overpredict the stiffness of truss specimens even with the presence of OSB plates.

3.3 Effects of Connection Flexibility on Truss Stiffness

When the experimentally determined stiffness of trusses were analyzed, it was noticed that connection type has a major effect on truss stiffness. Shear effects of connections were also mentioned earlier by other researchers [9]. Therefore, axial flexibility of connection between diagonal and chord members were reflected in

SAP2000 models as explained in following sections. Shear tests were conducted on connection specimens in order to determine the connection flexibility with different number of fasteners.

3.4 Connection Test Setup

Test setup was basically prepared as a tension test of two plates connected by various connectors. All base metals were cut from plates which were obtained from Group 1 materials (Table 2). Rivets and screws used for tests were taken from the same manufacturer with trusses. Loading was applied on plates with an electric motor and was measured with a load cell connected right onto the motor piston. Relative displacement of the two plates was measured by an extensometer as given in Fig. 63.

Figure 63. Extensometer Location of Connection Tests

Design considerations of connection test specimens include the details of truss connections. When truss connection detail is observed edge distances were specified and on connector specimens these edge distances were nominally satisfied. Theses distances are provided in Fig. 64.

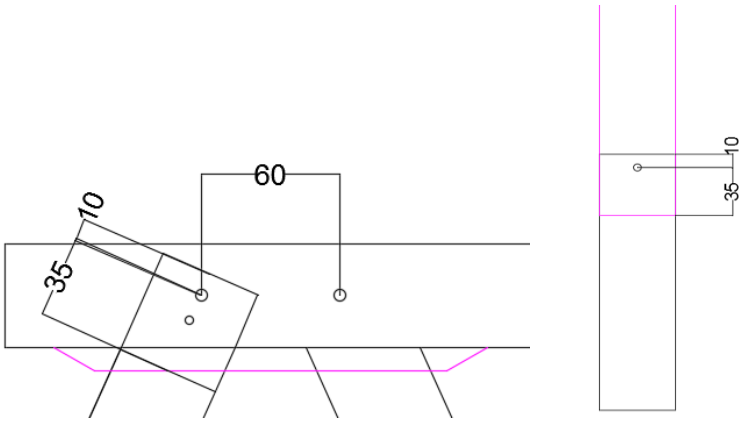

Figure 64. Edge Distance Details of Truss and Connection Specimens

Initially, test specimens were prepared considering the number of fasteners used to connect each flange of diagonal member to chord members. These cases included a single rivet and 1, 2, or 3 additional screws. Then, the measured stiffness of these connections was multiplied by two in order to obtain the total connection stiffness at each diagonal member end. However, it was observed that the connection stiffness determined this way overestimated the actual connection stiffness due to the effect of group action of fasteners in truss specimens [16]. Therefore, new connection specimens were prepared with the number of fasteners equal to the total number of fasteners present at both flanges of diagonal members in truss specimens. The number and layout of rivets and screws in connection specimens are shown in Fig. 65. Specimens were named according to the properties of Base Plate Thickness_Number of Rivets+Number of Screws.

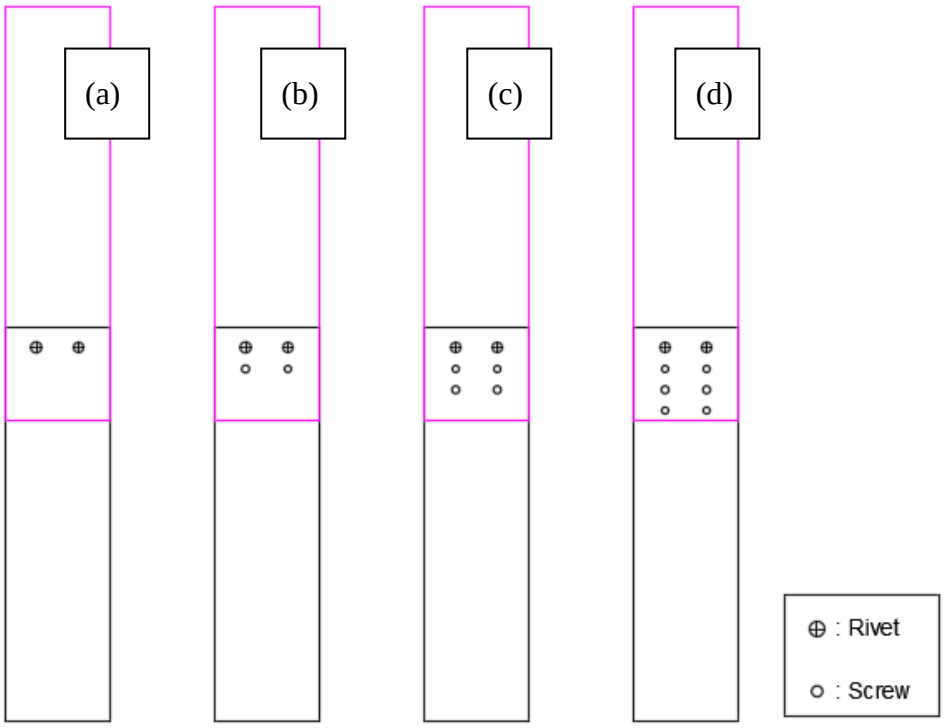

Figure 65. Connection Test Specimens (a) 1.2_2+0, (b) 1.2_2+2, (c) 1.2_2+4, (d) 1.2_2+6

3.5 Connection Test Results

While applying loading to the connection specimens, deformation of the connecting plates and the fasteners were noticeable. The recorded data supports that bearing is initially occurred in holes and this is represented by a relatively stiffer load-deformation behavior. After tilting deformation of screws and rivets begun stiffness of the system was observed to decrease immediately. The parameters that had the most significant effect of the response of the connection are discussed in following sections.

3.5.1 Fastener Group Effect on Connection Specimens

As mentioned earlier, the connection test specimens were initially prepared considering the number of fasteners used to connect each flange of diagonal member to chord members. The idea was to multiply the stiffness measured from these tests by two in order to obtain the stiffness of each diagonal end connection. However, it

was later realized that this approach overlooks the group action effect of fasteners. The effect of group action among the fasteners is illustrated in Fig. 66. As evident, multiplying the results of specimen 1.2_1+1 by two resulted in gross overestimation of the connection stiffness and load capacity. The actual response of the connection at each end of diagonal members is represented by specimen 1.2_2+2.

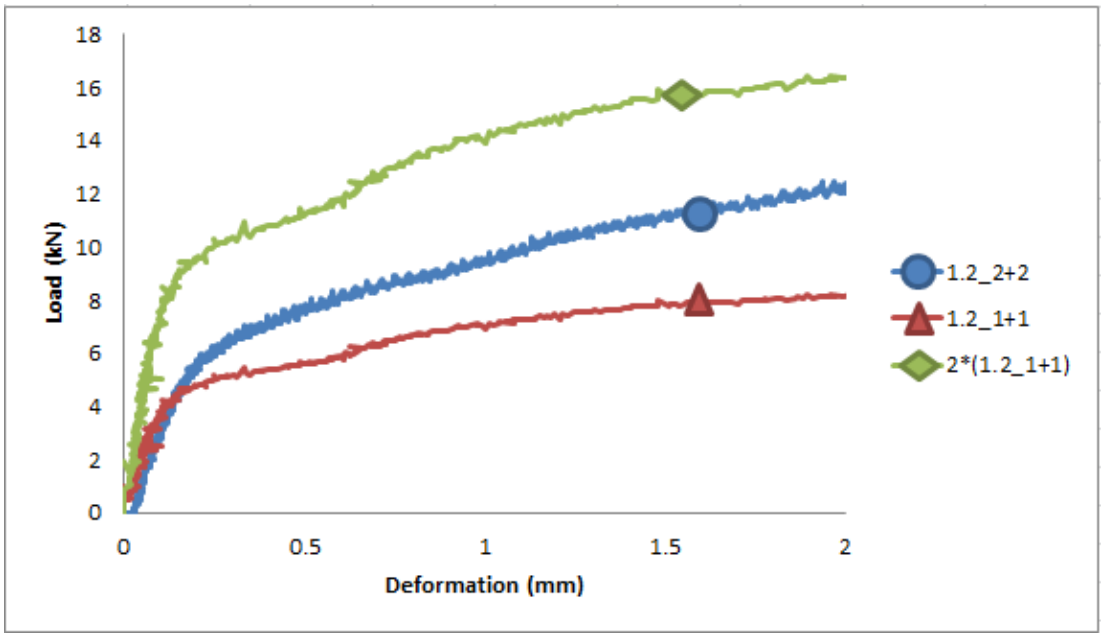

Figure 66. Load –Displacement Data of Specimens 1.2_1+1 and 1.2_2+2

3.5.2 Effect of Plate Thickness

Plate thickness of connected parts was determined to have a significant effect on connection behavior. The plot in Fig. 67 compares the load-deformation response of the connection with two rivets and six screws for the cases of 0.8 mm and 1.2 mm plate thickness. As evident, with the same number of fasteners a stiffer and stronger connection is obtained between 1.2 mm thick plates as opposed to 0.8 mm plates.

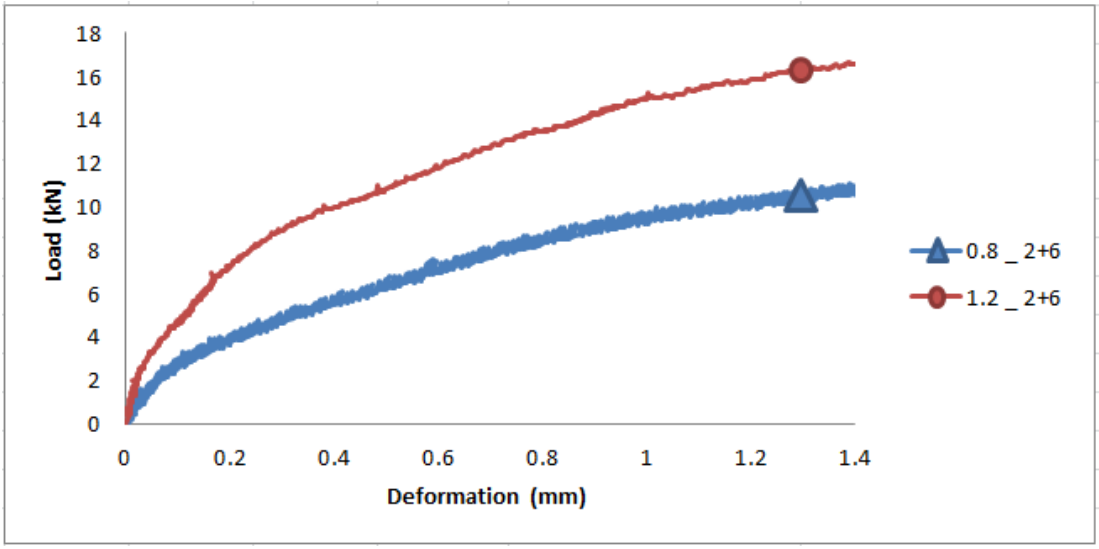

Figure 67. Load –Displacement Data of Specimens 1.2_2+6 and 0.8_2+6

3.5.3 Connection Response with Different Number of Fasteners

Load-deformation response of connection specimens with different number of fasteners is shown in Figs. 68-71. In these four specimens the connected parts had 1.2 mm plate thickness. All four specimens included two rivets and zero, two, four, or six screws. Increase in connection load capacity with increasing number of connection screws is evident in the plots. The maximum load capacities were 5.1 kN, 13.5 kN, 16.2 kN, and 19.7 kN, respectively when zero, two, four, and six screws were used in the connection in addition to two rivets. These values indicate that a significant part of the connection load capacity is provided by screws rather than rivets.

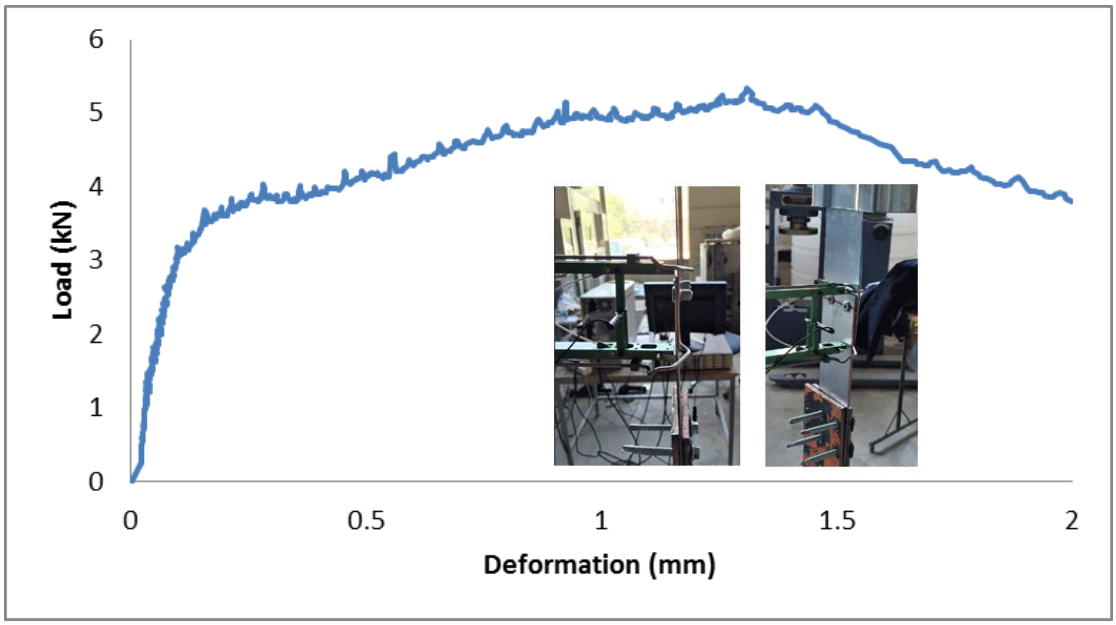

Figure 68. Load –Displacement Data of 1.2_2+0

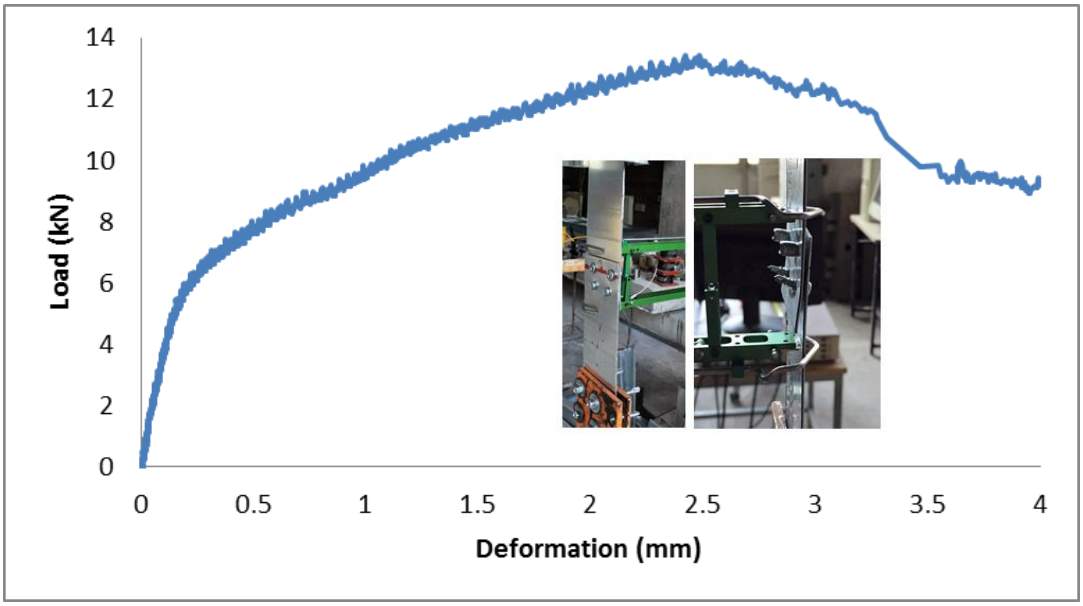

Figure 69. Load –Displacement Data of 1.2_2+2

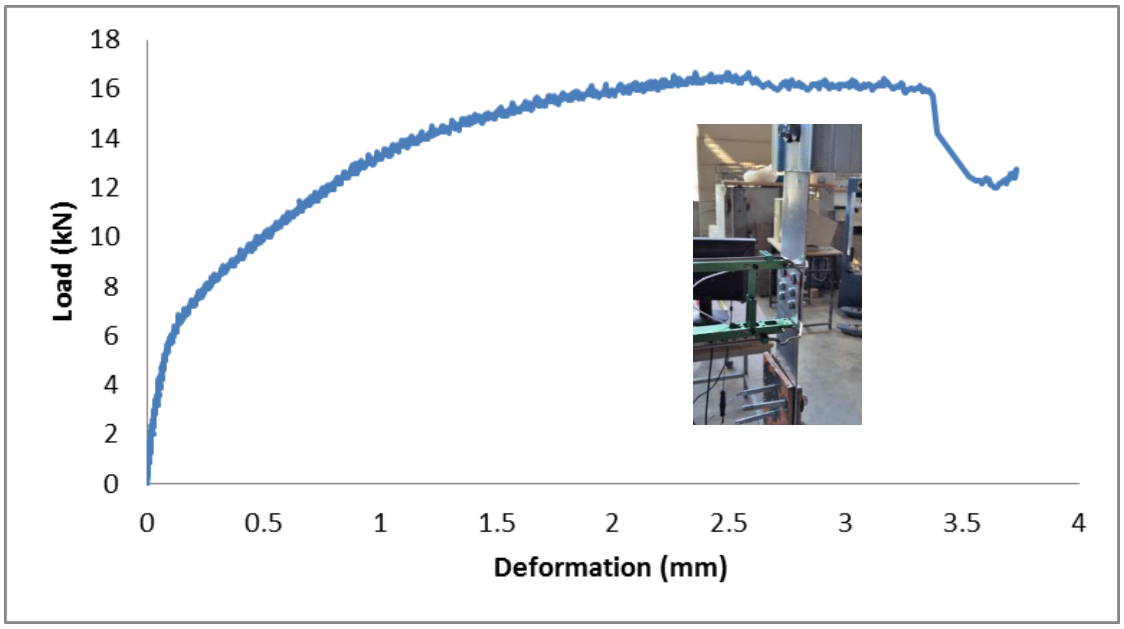

Figure 70. Load –Displacement Data of 1.2_2+4

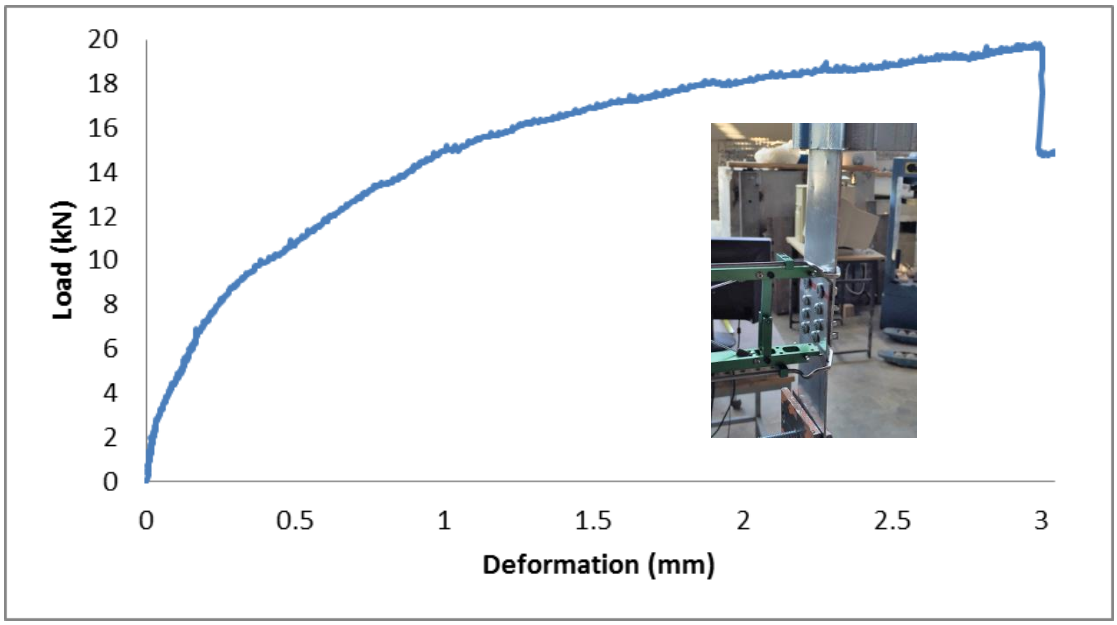

Figure 71. Load –Displacement Data of 1.2_2+6

3.6 Analytical Studies on Connectors

3.6.1 Analytical Expressions of Experimentally Recorded Data

In order to include the connection flexibility in structural analysis of trusses, the measured load-deformation response of connectors with different configurations was represented by mathematical expressions. The analytical expression used for curve fitting procedure has the form of $A\Delta * \left(1 - e^{-\frac{1}{B\Delta}}\right) = F$. The values of coefficients A and B for each connection configuration are provided in Table 7. The table also provides the corresponding coefficient of determination values. Comparison of the analytical expression predictions with the measured load-deformation response is provided in Fig. 72.

Table 7. Analytical Expressions of Experimental Data

Specimen	Analytical Expression	Coeff. Of Determination(R^2)
1.2_2+0	49.05Δ(1-exp(-1/10Δ))	0.95
1.2_2+2	34.34Δ(1-exp(-1/3Δ))	0.98
1.2_2+4	44.15Δ(1-exp(-1/2.8Δ))	0.95
1.2_2+6	41.20Δ(1-exp(-1/2.5Δ))	0.97

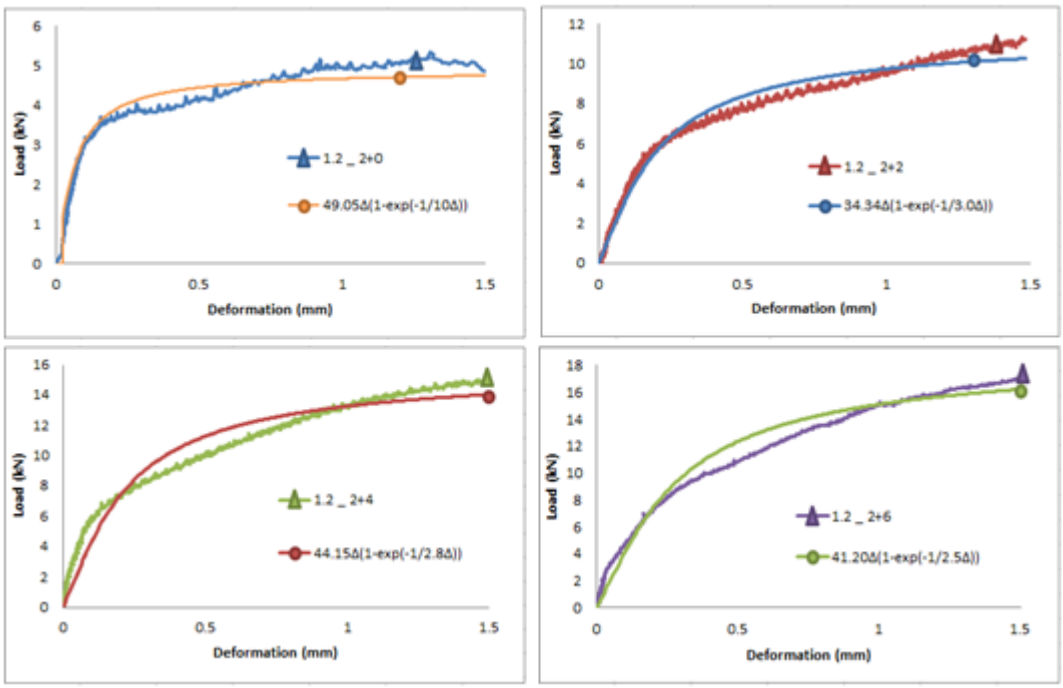

Figure 72. Relation Between Analytical Expression and Measured Connection Response

3.6.2 Modeling of Trusses Including Connection Flexibility

As introduced in previous sections, the accuracy of the conventional linear elastic models with axially rigid member connections was relatively poor in predicting truss stiffness. Modified models included the axial flexibility provided by rivets and screws at diagonal-chord member connections. Modeling of this phenomenon was achieved by using linear axial springs defined at both ends of diagonal members. In this approach, diagonal member ends were connected to chord members with moment releases, therefore any rotational restraint that may be present at the connection was neglected.

The procedure used for modeling trusses with connection screws included the following steps:

Step 1: The maximum vertical load resisted by each truss specimen during load tests was applied on the simple analysis model that included axially rigid diagonal-chord connections.

Step 2: The maximum axial force in diagonal members was recorded.

Step 3: The spring stiffness values were determined for the corresponding connector configuration by simply calculating the secant stiffness of the analytical expressions provided in Table 7 considering five different load levels. These load levels were taken as 100, 80, 60, 40 and 20% of the maximum diagonal axial force determined in the previous step.

Step 4: For each connection configuration analyses were repeated five times using five different spring stiffness values determined in the previous step.

3.6.3 Results of Analyses including Connection Flexibility

The linear load-deflection response obtained from the model including connection flexibility using the method explained in previous section is shown in Fig. 79 for truss 1.2_1+0_N. Stiffness determined from connection configuration 1.2_2+0 was used in this model. As mentioned earlier, each model was analyzed five times, by first applying a vertical load equal to the maximum vertical load resisted by the truss

specimen during load tests and reducing this load by 20% each time. The maximum diagonal member force and the corresponding connection stiffness used in the analyses are indicated in Table 8. The deflection values corresponding to the L/360 and L/240 limits, which are usually used for serviceability check of beams, are also indicated on the graph given in Fig. 73.

Comparison of the measured and predicted truss load-deflection response in Fig. 73 indicates that determining the connection stiffness considering the diagonal member axial force corresponding to 60% of the measured truss load capacity results in the best representation of truss elastic stiffness. Even though there is some level of difference between the measured and predicted truss stiffness, the improvement in the prediction is valid when the stiffness of the flexible connection model is compared with the response obtained based on axially rigid connection assumption.

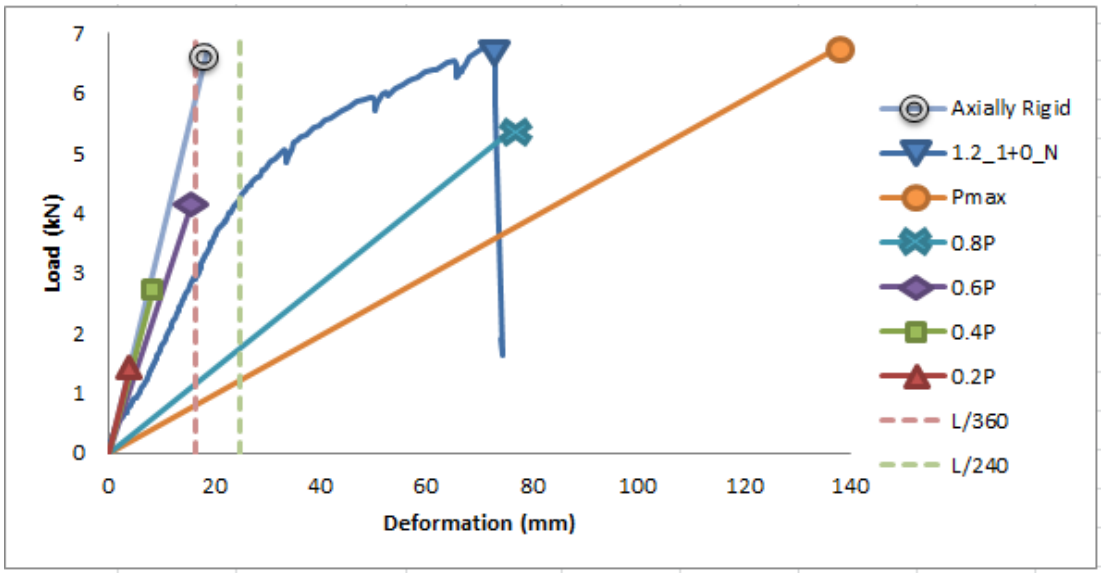

Figure 73. Measured and Predicted Response for Truss with Single-Fastener Connections

Table 8. Analysis Steps used for Truss 1.2_2+0

Step	Vertical Load (kN)	Force on Web Member (kN)	Spring Constant (kN/mm)
100%	6.8	6.0	2
80%	5.4	4.8	3
60%	4.1	3.6	24
40%	2.7	2.4	40
20%	1.4	1.2	48

Results of analyses for trusses 1.2_1+1_N and 1.2_1+1_N_NDL including connection flexibility are provided in Fig. 74 with the maximum diagonal member force and the corresponding connection stiffness values presented in Table 9. Connection configuration 1.2_2+2 was used in these analyses. The analysis results accurately predict the measured service stiffness of these trusses when the connection stiffness is determined based on a diagonal member axial force corresponding to 60% of the measured truss load capacity.

Table 9. Analysis Steps used for Truss 1.2_2+2

Step	Vertical Load (kN)	Force on Web Member (kN)	Spring Constant (kN/mm)
100%	11.5	10.3	7
80%	9.2	8.2	17
60%	6.9	6.2	26
40%	4.6	4.1	32
20%	2.3	2.1	34

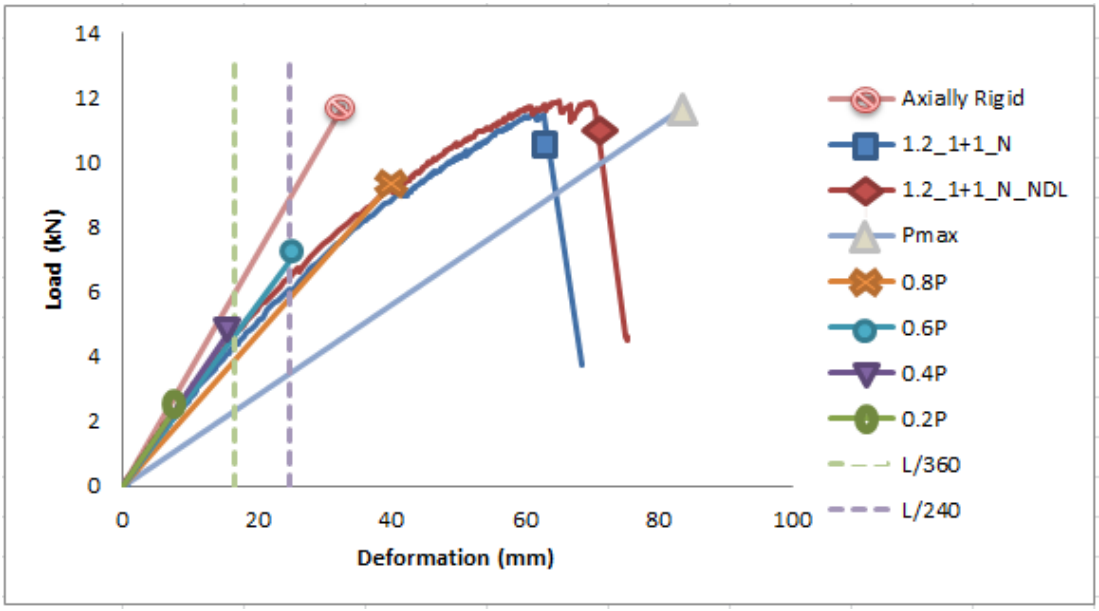

Figure 74. Measured and Predicted Response for Trusses with Two-Fastener Connections

Comparison of the measured truss behavior with the predicted elastic response including the connection flexibility is provided in Figs. 75 and 76, respectively for connection configurations of 1.2_2+4 and 1.2_2+6. The connection stiffness values used in these analyses are given in Tables 10 and 11. Consistent with the previous results, an accurate estimate of truss service stiffness is obtained by determining the connection stiffness based on a diagonal member axial force corresponding to 60% of the measured truss load capacity.

Table 10. Analysis Steps used for Truss 1.2_2+4

Step	Vertical Load (kN)	Force on Web Member (kN)	Spring Constant (kN/mm)
100%	13.6	12.0	20
80%	10.8	9.6	30
60%	8.2	7.2	37
40%	5.4	4.8	42
20%	2.7	2.4	44

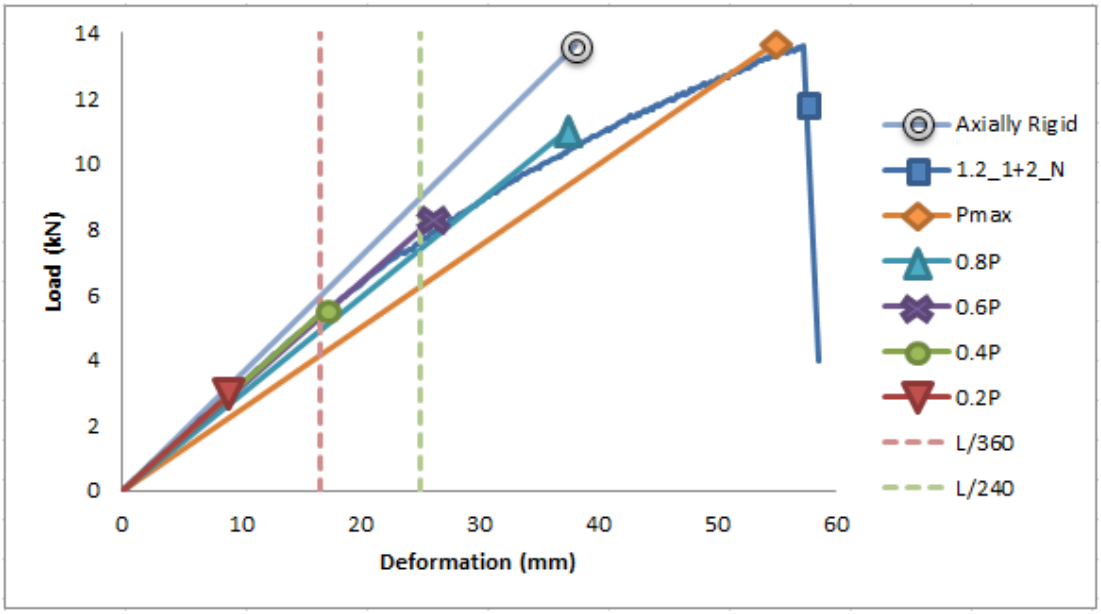

Figure 75. Measured and Predicted Response for Truss with Three-Fastener Connections

Table 11. Analysis Steps used for Truss 1.2_2+6

Step	Vertical Load (kN)	Force on Web Member (kN)	Spring Constant (kN/mm)
100%	12.7	11.2	23
80%	10.2	8.9	31
60%	7.6	6.7	37
40%	5.1	4.5	40
20%	2.5	2.2	41

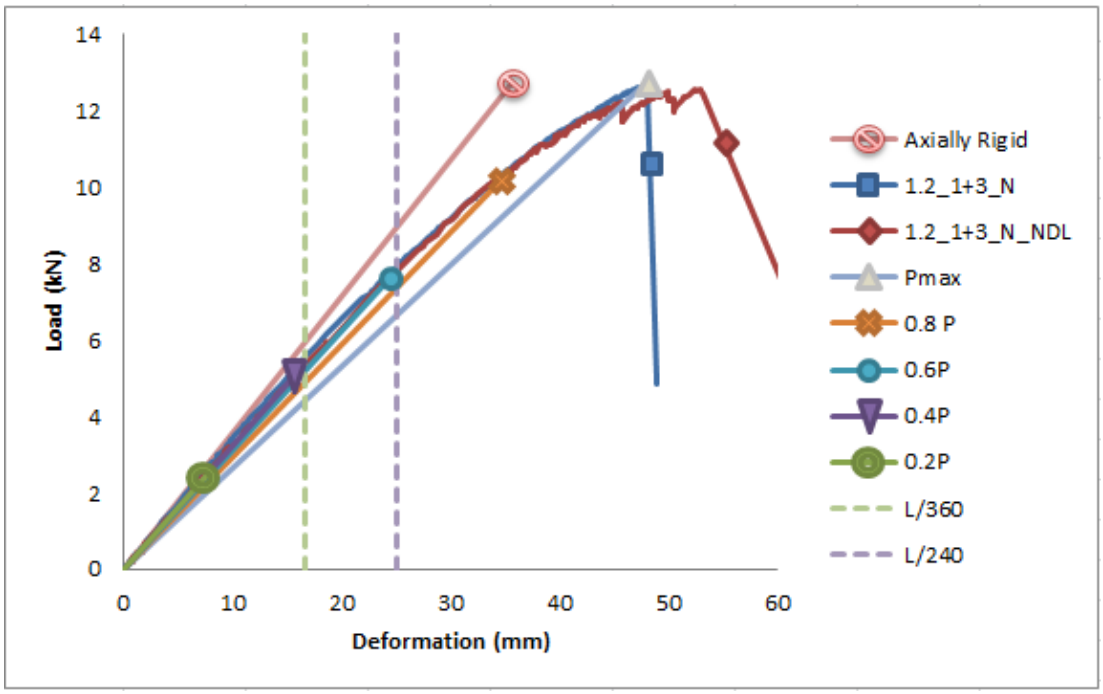

Figure 76. Measured and Predicted Response for Truss with Four-Fastener Connections

The predicted elastic response reflecting the connection flexibility and presented in Figs. 73-76 indicate that for models with fewer connection fasteners, the overall truss stiffness is affected significantly by the connection stiffness used at diagonal member ends. When the number of fasteners used at diagonal-chord connections is increased, effect of the axial stiffness of these connections on the overall flexural stiffness of trusses is observed to reduce.

3.7 Discussion of Procedure and Results

Thin-walled members and structures have identical tenderness on joints. From past experiences rigid and semi-rigid connections of structural steel design was an issue that all designers were familiar with, however in thin members transition of connection was also noted as an important issue. When connections were tested, it is understood that the behavior is divided into two parts. First part is stiffer and continues until tilting of the connector starts.

In the study, four types of connection systems were tested and the data was adapted as a mathematical formula expression. However any relation of thickness, screw size could not be managed with these expressions. This may be selected as a future study topic to investigate these factors and configuring a universal data expression for all types of structures.

In the end linear elastic analysis were modified with spring constant and reliability has increased in a great amount. After study, it is strongly recommended that the designers take this connector effects seriously.

CHAPTER 4

COMPRESSION CAPACITY OF TRUSS CHORDS

Capacity of trusses was limited with compression capacity of upper chord in most of the cases. Because the load capacity of compression chord has a major effect of the behavior of truss, the CFS section used in the truss specimens was further studied under concentric compressive force. An experimental approach was adopted to determine the chord section capacity on member scale. Moreover, there are several numerical methods that can be used to identify the compressive response of CFS sections, as introduced in the background chapter. In this chapter these methods are explained in more detail.

4.1 Pure Compression Tests

Eight different specimens were designed to determine compression capacity of CFS lipped C section. All specimens were obtained from 1.2 mm thick Group 1 material (Table 2). Five of the specimens had lengths ranging from 100 mm to 300 mm with 50 mm increments. Maximum length was extended until 300 mm in order to represent the largest unrestraint chord length existing in truss specimens. The cross section used in this group of specimens had lips continuous along the entire specimen length, and therefore these specimens were named as ‘Standard’. A photograph of the 300 mm long standard specimen is shown in Fig. 77.

Figure 77. Standard CFS Section

In order to reflect the lip condition existed in truss specimens, the specimen called 'Partially Un-Lipped' was designed. In this specimen, the lips at the flange tips were straightened at diagonal member connection locations, as shown in Fig. 78 (a). Lastly, two specimens were designed without lips. In one of these specimens, the lips were straightened continuously along the enter specimen length, and this specimen was named as 'Refold Un-Lipped' shown in Fig 78 (b). In the other specimen, the lips were cut and this specimen was named as 'Removed Lips' shown in Fig. 78 (c). The purpose of using these different lip details in compression test specimens was to investigate the extent to which different lip conditions has an influence on the buckling mode and compression capacity of the CFS section used in truss specimens.

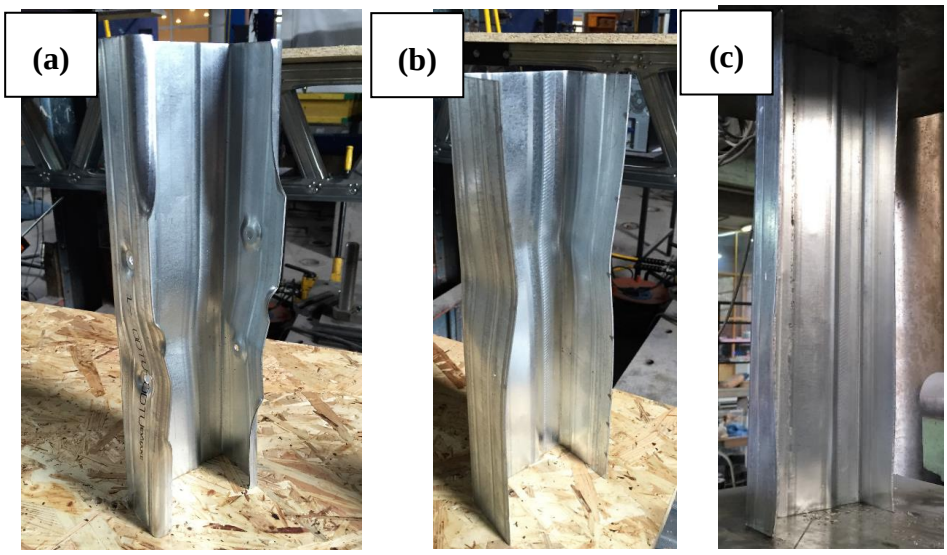

Figure 78. Deformed Shapes of (a) 'Partially Un-Lipped' , (b) 'Re-Fold Unlipped' and (c) 'Removed Lips' Specimens

Tests were carried out with 100 kN capacity hydraulic testing machine. Test setup is shown in Fig 79. The ends of the specimens were meticulously arranged in order to have a uniform and concentric transfer of compression from the testing machine to the specimen. Two specimens were tested for each combination of specimen length and lip condition, except for 150 mm long Standard lip condition.

Figure 79. Compression Test Setup

Test results are provided in Table 12. As expected, 'Standard' sections capacity values decreased with the increase of length. Partially eliminating the flange lips has shown a great amount of effect on compression resistance. 'Partially Un-Lipped' member was observed to have 33% less resistance than 'Standard' member in same length. This specimen represents the lip condition existed in truss test specimens. Therefore, it could be concluded that termination of flange lips at diagonal member connection locations has a significant negative effect on the compression load capacity of truss chord members. The reduction in compression load capacity with respect to the standard case is also valid for the other two lip conditions studied.

Table 12. Results of Pure Compression Capacity Tests

Specimen Type	Length (cm)	Test1		Test2		Average	
		Force (kN)	Stress (MPa)	Force (kN)	Stress (MPa)	Force (kN)	Stress (MPa)
Standart	10	81.9	363	83.4	370	82.6	366
Standart	15	-	-	80.9	359	80.9	359
Standart	20	80.4	357	81.4	361	80.9	359
Standart	25	72.1	320	79.0	350	75.5	335
Standart	30	66.7	296	69.7	309	68.2	302
Partially Un-Lipped	30	43.2	191	48.1	213	45.6	202
Re-Fold Un-lipped	30	45.1	200	54.0	239	49.5	220
Removed Lips	30	45.6	202	46.1	204	45.9	203

Deformed shape of specimens are illustrated in Fig. 80. Two types of buckling modes observed are (1) local buckling near one end of specimen and (2) distortional buckling near midlength of specimen. Specimens with 100, 150 and 200 mm length were observed to have local buckling near one end, while 250 and 300 mm long specimens underwent distortional buckling near midlength, as illustrated in Fig. 81.

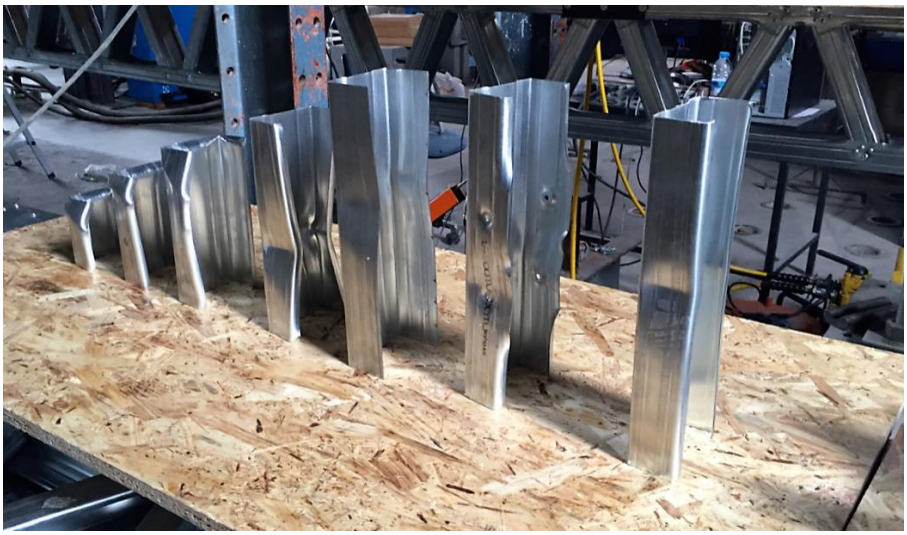

Figure 80. Deformed Shapes of Compression Specimens

Figure 81. Distortional Buckling of Standard Section

4.2 Direct Strength Method

Direct Strength Method is a specific tool for determining the capacity of thin-walled members. This method is included in an appendix in the Specification for Design of Cold-Formed Steel [1]. Method is used with analysis results of Finite Strip Method. Elastic buckling capacity determined from Finite Strip Analysis (P_{crd}) is used in Direct Strength Method to determine the member capacity. Figure 82 shows the

procedure provided in AISI Appendix 1 Section 1.2.1.3 [5] to determine the distortional buckling capacity.

1.2.1.3 Distortional Buckling

1.2.1.3.1 Columns Without Holes

The *nominal axial strength* [*resistance*], P_{nd}, for *distortional buckling* shall be calculated in accordance with the following:

(a) For $\lambda_d \leq 0.561$

$$P_{nd} = P_y \qquad (Eq.\ 1.2.1\text{-}10)$$

(b) For $\lambda_d > 0.561$

$$P_{nd} = \left(1 - 0.25\left(\frac{P_{crd}}{P_y}\right)^{0.6}\right)\left(\frac{P_{crd}}{P_y}\right)^{0.6} P_y \qquad (Eq.\ 1.2.1\text{-}11)$$

where

$$\lambda_d = \sqrt{P_y / P_{crd}} \qquad (Eq.\ 1.2.1\text{-}12)$$

where

P_y = Member yield strength as given in Eq. 1.2.1-4

P_{crd} = Critical elastic column *distortional buckling load* determined by analysis in accordance with Section 1.1.2

P_y = Member yield strength

$$= A_g F_y \qquad (Eq.\ 1.2.1\text{-}4)$$

A_g = *Gross area* of cross-section

F_y = *Yield stress*

Figure 82. Distortional Buckling Resistance Determination Procedure [5]

In this thesis study CUFSM software was used to conduct FSM analysis. CUFSM V.4.05 program was developed and introduced by Li and Schafer [17] in 2010. Direct Strength Method became popular with higher accuracy on determination of distortional buckling strength against the conventional method existing in the main part of the Specification [1].

The CFS section used in the truss specimens was modeled in CUFSM using 55 nodes as shown in Fig. 83. The member had a length of 300 mm with simply supported boundary conditions. It is worth to note that the continuous lip case was studied in CUFSM program, as partial termination of flange lips cannot be reflected due to the geometric constraints. The elastic modulus and shear modulus values in the analysis were taken as 210 GPa and 78 GPa, respectively. By the nature of elastic analysis the

yield strength of material was not involved in FSM stage. A unit compressive load of 1 kN was applied on the section. The outputs of the FSM analysis are the elastic load capacity and deformed shape corresponding to the first buckling mode.

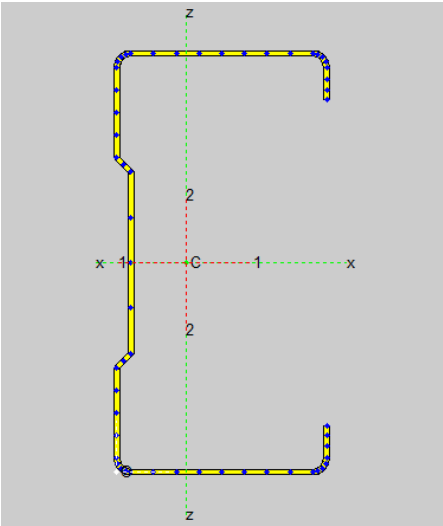

Figure 83. Model of Standart Section

After analysis was conducted for the particular section of study, results obtained are given in Fig. 84. Deformed shape seems to be very similar with the experimentally obtained deformed shape given in Fig. 81. The elastic buckling capacity was determined as 67.44 kN.

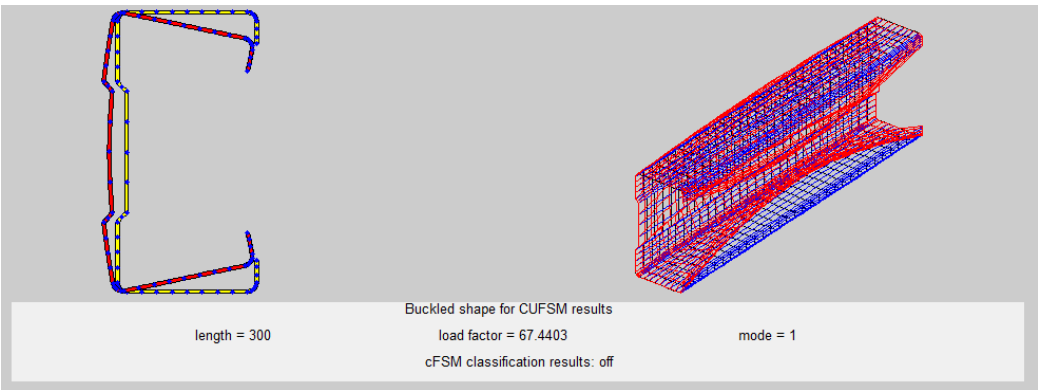

Figure 84. FSM Analysis Results from CUFSM Software

Using the elastic buckling capacity determined from the FSM analysis and going through the procedure provided in AISI Appendix 1 Section 1.2.1.3 [5], the distortional buckling resistance of the CFS section used in the truss specimens was determined to be 62.3 kN. The calculation steps are given below. The yield strength F_y was taken from Table 2 – 1.2 mm thick Group 1 material as 410 MPa.

$$\lambda = \sqrt{\left(\frac{97.2}{67.44}\right)} = 1.2 > 0.561\ ;$$

$$P = \left[1 - 0.25\left(\frac{67.44}{97.2}\right)^{0.6}\right]\left(\frac{67.44}{97.2}\right)^{0.6} * 97.2 = 62.3\ kN;$$

In the end, for selected significant section of study Direct Strength Method was resulted in a distortional buckling resistance of 62.3 kN. Pure compression tests were resulted in an average value of 68.2 kN.

4.3 Finite Element Analysis

Finite element analysis of a 300 mm long CFS section was also conducted in order to numerically determine the compression capacity. Nonlinear analysis was conducted in ANSYS software using SHELL181 4-node isoparametric quadrilateral thin-shell elements [18]. The model consisted of 2562 nodes and the cross section of the member was formed with 42 nodes, as shown in Fig. 85. Boundary conditions were defined such that all the nodes at one end were restraint against displacement in all directions while at the other end displacement of the nodes were restraint in out of plane directions and displacement loading was applied in normal direction.

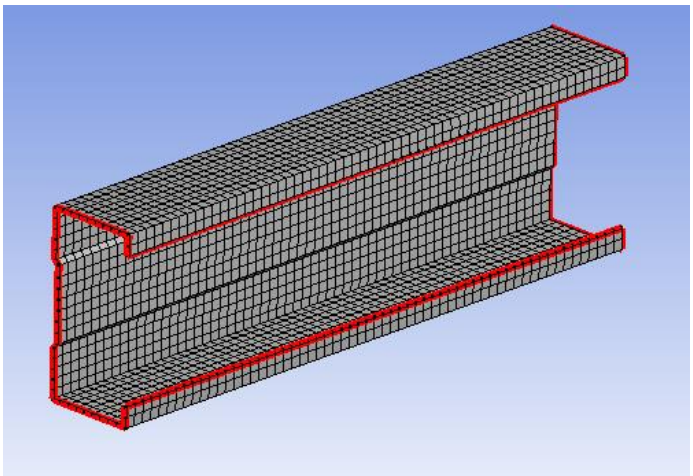

Figure 85. Finite Element Model

Imperfection of model was obtained by eigenvalue buckling analysis of elastic model. Various recommendations are available in literature in regards to the modeling of initial imperfections in cold-formed steel members. When the CFS sections used in truss specimens were investigated, it was noticed that the level of imperfections changes significantly with the steel sheet thickness of sections. Moreover, in study of Aghoury, Hanna and Amoush [19] the effect of global imperfection modes and residual stresses were found to be very low. Therefore, in order to preserve the simplicity of analysis, first buckling mode of model, which corresponds with distortional buckling shape given in Fig. 86, was taken as initial shape. In elastic buckling analysis the strength of CFS member was found as 83.8 kN.

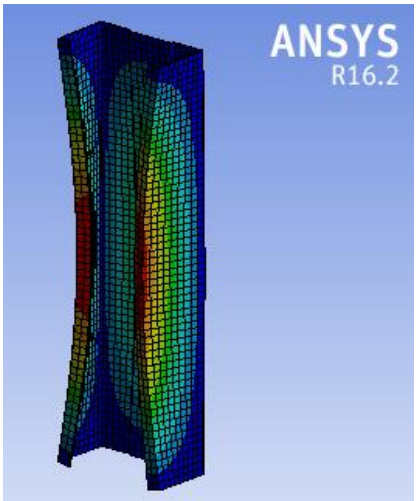

Figure 86. Eigenvalue Analysis 1st Mode Deformed Shape

After the definitions of geometric nonlinearities were completed, material nonlinearities were adopted with bilinear isotropic model. The material model shown in Fig. 87 was used with yield strength of 410 MPa.

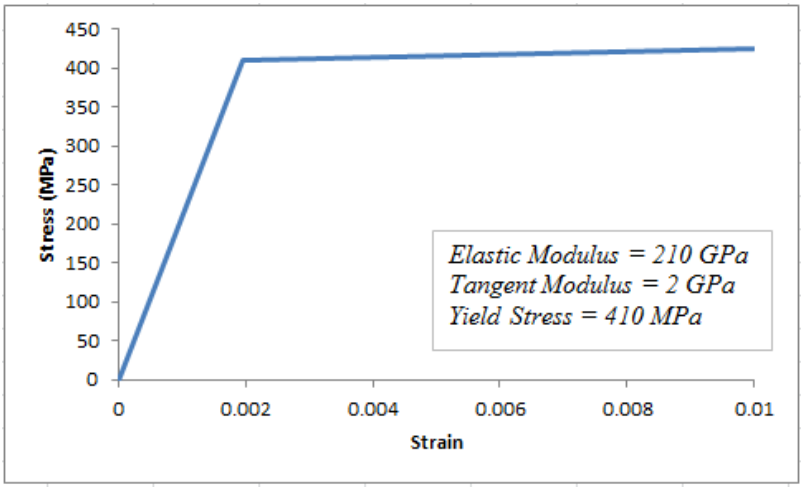

Figure 87. Bilinear Isotropic Material Model

The non-linear Finite Element Analysis resulted in a compression load capacity of 68.2 kN. Error rate of analysis with respect to experimental result is less than 0.1%. The eigenvalue analysis and nonlinear analysis results are plotted below in Fig. 88. Buckled shape obtained from the finite element analysis is given in Fig. 89. This deformation shape agrees well with the experimentally observed buckling shape given in Fig. 81.

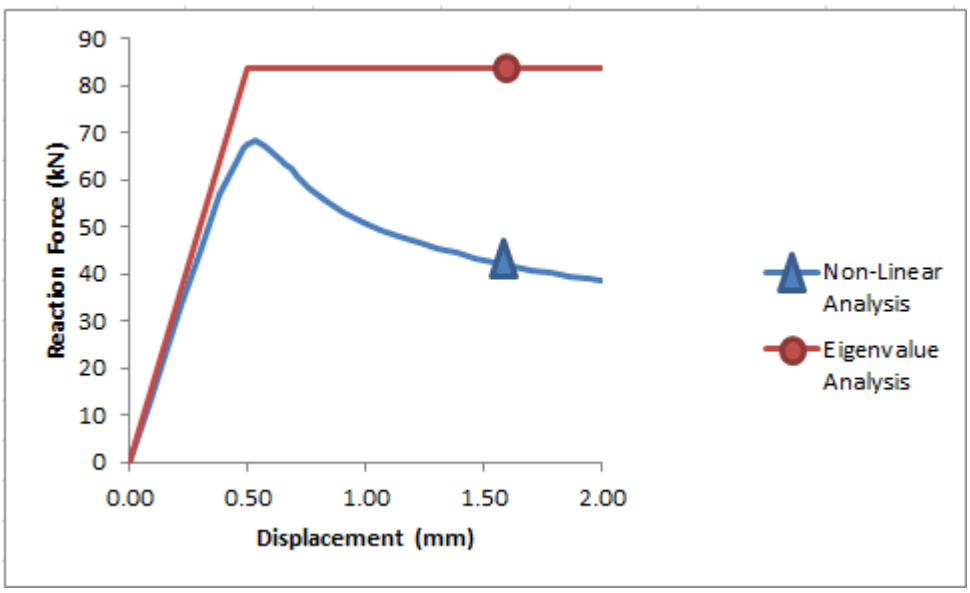

Figure 88. FE Analysis Results

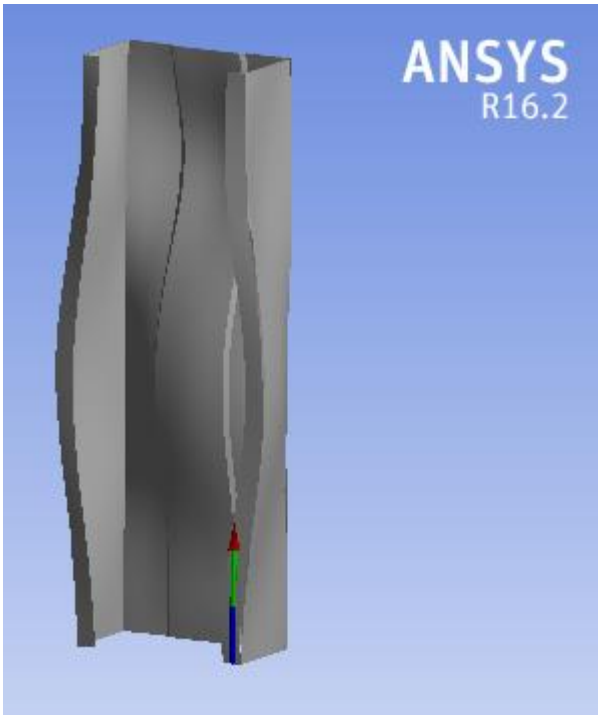

Figure 89. Buckled Shape of Nonlinear Analysis

A comparison of the predicted axial load capacity of a 300 mm long CFS section from direct strength method and finite element analysis with the measured capacity is provided in Table 13.

Table 13. Comparison of Measured and Numerically Predicted Axial Load Capacities

	Compression Test	Direct Strength Method	Finite Element Analysis
Axial Load Capacity (kN)	68.2	62.3	68.2

4.4 Truss Chord Resistance

After evaluation of analytical design tools, study re-focused on truss specimens again. Previous experimental data on compression chord axial force at the failure of truss specimens was determined and compared with the results of pure compression tests. Table 13 provides such a comparison. The comparison is provided for the cases of continuous flange lips (Standard case) and lips terminated at diagonal member connection locations (Partially-Unlipped case). As evident, the axial force in the compression chord member at the time of truss failure remains between the measured axial load capacity of Standard and Partially-Unlipped cases for all truss specimens shown in Table 14. In an attempt to have the predicted compressive load capacity of the CFS section better represent the axial force in the compression chord member at the time of truss failure, a loading eccentricity was introduced and the finite strip analyses were repeated. These analyses are explained in the following section.

Table 14. Data Comparison of Trusses and Columns

Specimen #	Thickness (mm)	Truss Property	Max Vertical Load (kN)	Chord Compression Force (kN)	P/Pn	
					Standart	Partially-Unlipped
1.2_1+1_N	1.2	Rivet +1 Screw	11.5	50.2	0.73	1.09
1.2_1+2_N	1.2	Rivet +2 Screw	13.6	59.2	0.86	1.28
1.2_0+1_N	1.2	Single #12 Screw	11.9	51.9	0.75	1.13
1.2-0.8_1+2_N	1.2 - 0.8	Rivet +2 Screw	10.7	46.6	0.68	1.01
1.2_1+3_N	1.2	Rivet + 3 Screw	12.7	55.1	0.80	1.20
1.2_PL_N	1.2	Plate	13.1	57.3	0.83	1.24
1.2_1+1_N_NDL	1.2	Rivet +1 Screw	11.9	51.9	0.75	1.13
1.2_1+3_N_NDL	1.2	Rivet + 3 Screw	12.6	54.9	0.79	1.19
1.2_1+3_N_SS	1.2	Rivet + 3 Screw	24.8	59.1	0.86	1.28
				MEAN :	0.78	1.17

4.5 Finite Strip Analysis of Eccentric Loading

From the nature of buckling phenomenon singly-symmetric sections has to be studied in detail under eccentric loading. Design interaction equations in Specifications [1], [2], [3] were basically presented as the summation of axial and flexural stresses or loads divided by resistance corresponds on the section designed. These equations provide a control of whether design loads stay lower than resistance load or stress. All stresses or loads due to different force effects are summed up separately by assuming their corresponding limits.

In the C shaped section shown in Fig. 90, if the eccentricity of the axial force is increased, the stress on lips and flange tips would decrease. Therefore, critical distortional buckling stress is supposed to be increased by this fact, making the yield stress critical in section on web part.

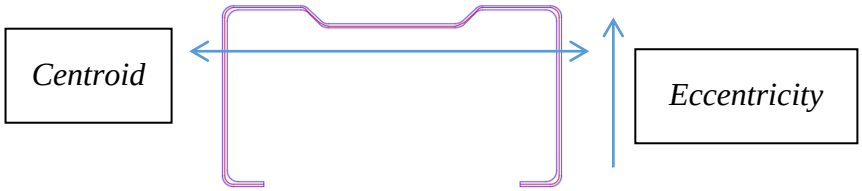

Figure 90. Cross-Section Centroid and Eccentricity Direction

A parametric study was conducted on 1.2 mm and 0.8 mm thick C sections with continuous lips. Elastic buckling resistance of section for different eccentricity levels were calculated with Finite Strip Method. In the different eccentric loading conditions maximum stress calculated on web element of section was compared with material yield limit.

1.2 mm thick section was modeled in CUFSM v.4.05 [17] with unit (1 kN) load in different eccentricity levels. Stress gradient of section was calculated with CUFSM software. An example stress distribution is shown in Fig. 91. The model is analyzed with different eccentricity values starting from zero and increased to 10 mm. For

each eccentricity value, the axial load causing the initiation of yielding in the member was determined. These yield load values were then compared with the elastic distortional buckling loads obtained from FSM. All analysis results are provided in Table 15.

As provided in Table 14 starting from the eccentricity value of 4 mm, the critical limit state changes from distortional buckling to yielding. Section capacity has to be taken as the yield capacity for eccentricities exceeding this value. This behavior is also explained in the plots shown in Fig. 92. Each graph includes two plots; one showing the variation of buckling capacity with the member length, termed as elastic signature curve, and another one showing the values of yield capacity. The points of interest in these plots are the points corresponding to a half wave length of 300 mm, which is the length of chord segments between diagonal member connection locations in truss specimens. For zero eccentricity case distortional buckling capacity at 300 mm half wave length remains below the yield capacity, while for the case of 6 mm eccentricity the critical limit state becomes yielding.

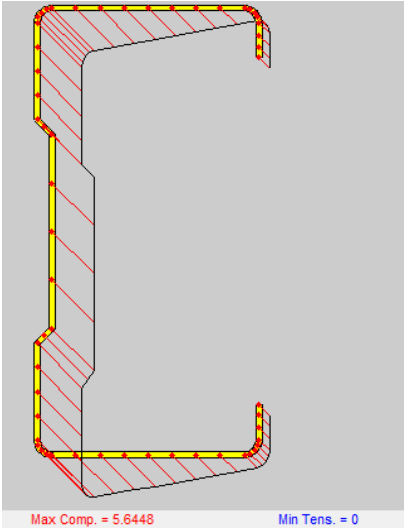

Figure 91. Stress Gradient of Section under 6 mm Eccentric Unit Load

Table 15. FSM Results of 1.2 mm Thick Section Eccentric Loading

Eccentricity	Max. Compression Stress on Unit Load (MPa)	Yield Load (kN)	Elastic Buckling Load (kN)	MODE
0	4.23	96.93	67.44	BUCKLE
1	4.46	91.93	70.80	BUCKLE
2	4.7	87.23	74.10	BUCKLE
4	5.17	79.30	80.70	WEB YIELD
6	5.65	72.57	86.97	WEB YIELD
8	6.12	66.99	91.66	WEB YIELD
10	6.59	62.22	94.49	WEB YIELD

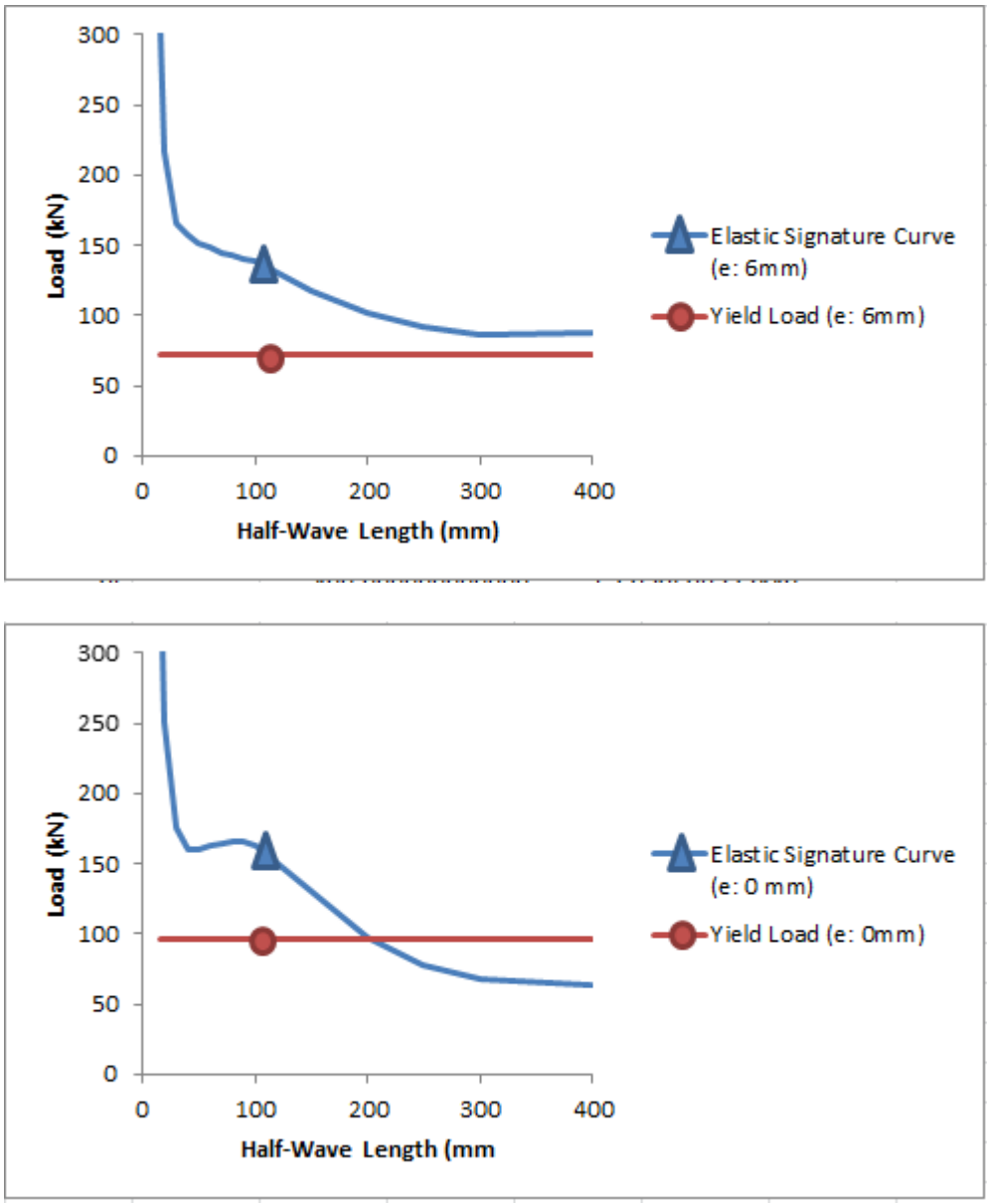

Figure 92. Representation of Yielding and Buckling Failure Modes (1.2 mm CFS Thickness)

The procedure explained above was repeated for 0.8 mm section thickness. The yield strength values was taken as 395 MPa, which was the value measured from coupon tests. In the analyses eccentricity level was increased up to 6 mm. Different from the case of 1.2 mm section thickness the failure mode did not change at 4 mm eccentricity value. As indicated in Table 16 for all eccentricity values studied buckling limit state controlled over yielding. The yield capacity and signature curve at 6 mm eccentricity are compared in Fig. 93.

Table 16. FSM Results of 0.8 mm Thick Section Eccentric Loading

Eccentricity	Max. Compression Stress on Unit Load (MPa)	Elastic Buckling Load (kN)	Yield Load (kN)	MODE
0	6.34	33.77	62.32	BUCKLE
1	6.69	35.07	59.02	BUCKLE
2	7.05	36.30	56.05	BUCKLE
4	7.76	38.31	50.92	BUCKLE
5	8.11	39.20	48.69	BUCKLE
6	8.47	39.70	46.65	BUCKLE

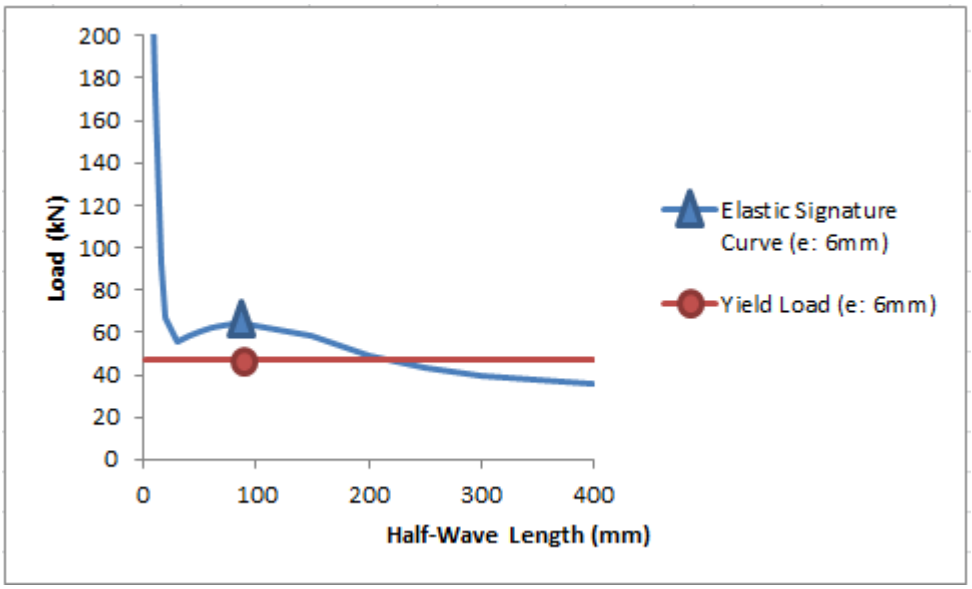

Figure 93. Representation of Yielding and Buckling Failure Modes (0.8 mm CFS Thickness)

CHAPTER 5

BENDING EFFECT ON TRUSS CHORDS

Until this stage, the study included several truss tests and separate member compression tests. However strength of truss tests could not be correlated with pure compression strengths of same CFS members. Therefore, the investigation has focused on the effect of eccentric axial force on capacity of truss compression chord member. Within this context, a numerical study utilizing finite element model of truss specimens and an experimental study including load testing of three additional truss specimens instrumented with strain gages, namely 0.8_1+1_N_SG, 0.8_1+3_N_SG, and 1.5-0.8_1+3_N_SG, were performed. The purpose of these studies was to verify the eccentric axial force hypothesis and determine the magnitude of bending effect on compression chord member of trusses. Results of these studies are reported in this chapter.

5.1 Numerical Study

5.1.1 Truss Model

Trusses used in test specimens 0.8_1+1_N_SG, 0.8_1+3_N_SG and 1.5-0.8_1+3_N_SG were modeled in ANSYS Workbench [18] software platform as shown in Fig. 94. Elastic material behavior was used in model. Chord members were modeled with 4-node quadrilateral elements (SHELL 181) and diagonal members were modeled with 2-node linear beam elements (BEAM188). In order to imply connection displacements into general behavior, area of web elements were reduced

in adequate amount to obtain resultant stiffness. These adopted cross section areas were found with actual test results.

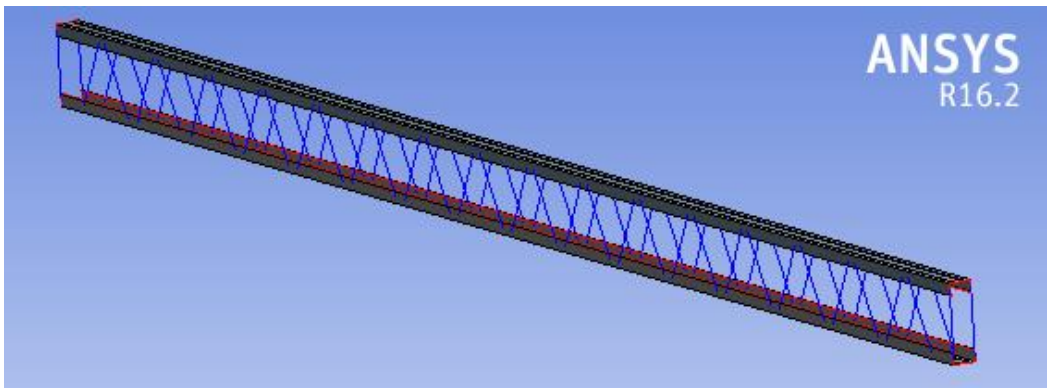

Figure 94. Finite Element Model of Truss

Beam elements representing the diagonal members were connected to the chord members through a single node as shown in Fig. 95.

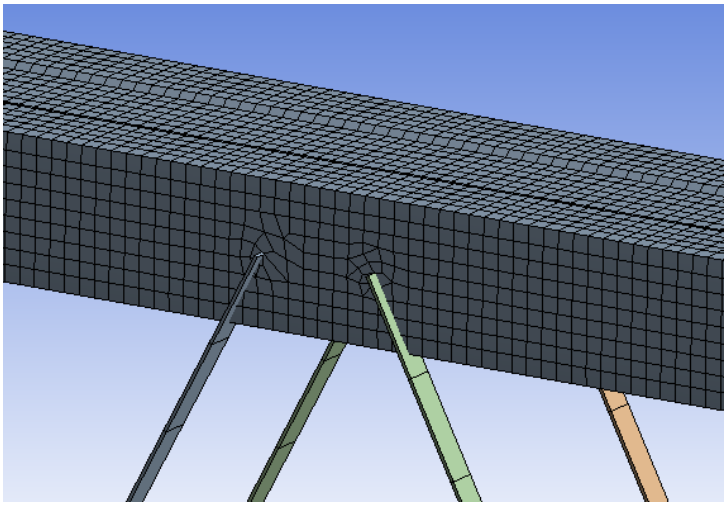

Figure 95. Connection Modeling

Pin and roller boundary conditions were defined at two ends of truss model by restraining the corresponding translational degrees of freedom of the related nodes. Loading was applied in the form of monotonically increasing vertical displacement defined at web nodes located in the middle of the top chord member.

Node paths were defined along chord members in order to obtain the analysis results systematically. Location of nodes used to define paths on the cross section of truss chord members is shown in Fig. 96. These paths were named as shown in the top left corner of the figure to indicate their locations on the chord member cross section. All paths had 6 meters length from start to end. Vertical deformations and normal strain results were obtained from the model along these node paths for different loading magnitudes.

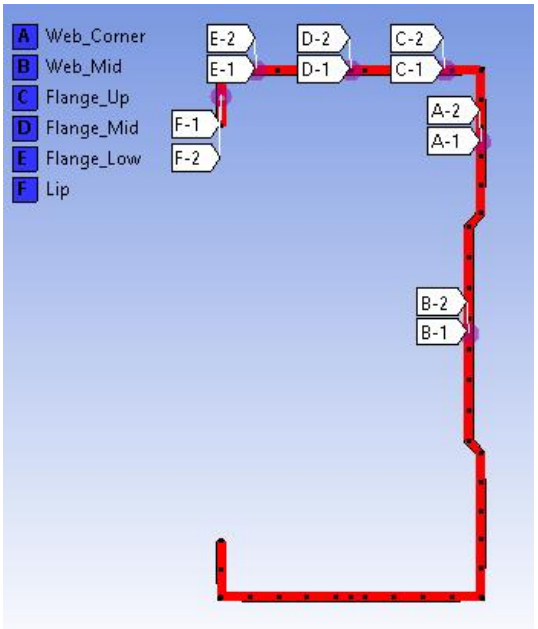

Figure 96. Paths on Truss chords

5.1.2 Finite Element Analysis Results

Results of model of 1.5-0.8_1+3_N_SG, which represents a hybrid truss with 1.5 mm thick compression chord member and 0.8 mm thick tension chord and diagonal members, are presented in Fig. 97 and 98. The figures include plots of normal strains along the compression and tension chord members at different locations in cross section. Locations of the paths along which the strain distributions are plotted are shown in Fig. 96. Positive values in the plots indicate tensile strains and negative values indicate compressive strains.

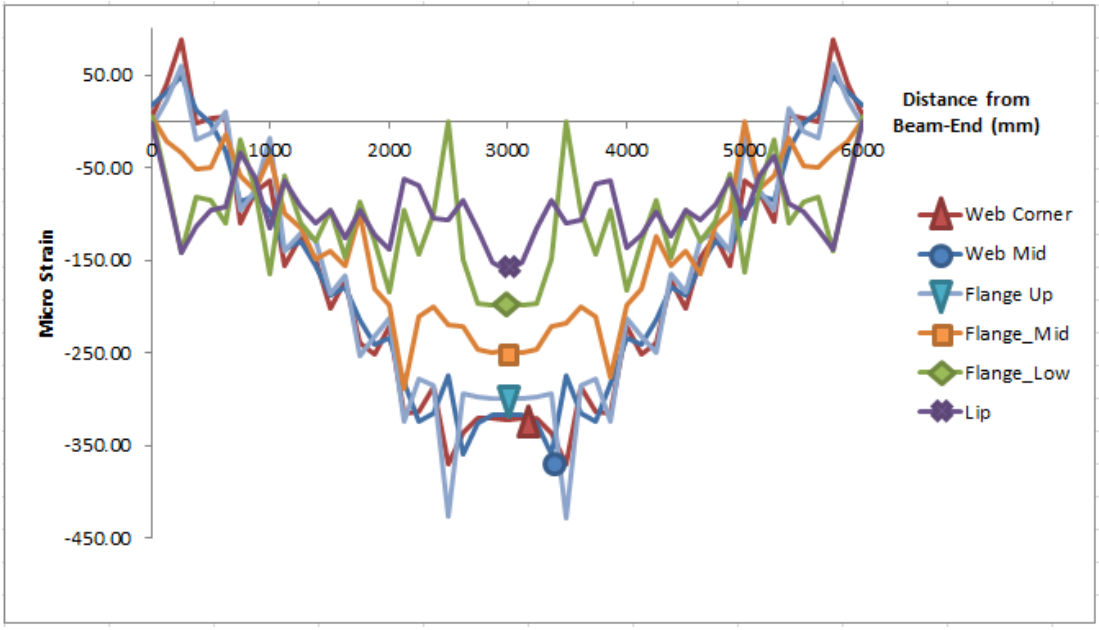

Figure 97. Strain Variation along Length of Compression Chord

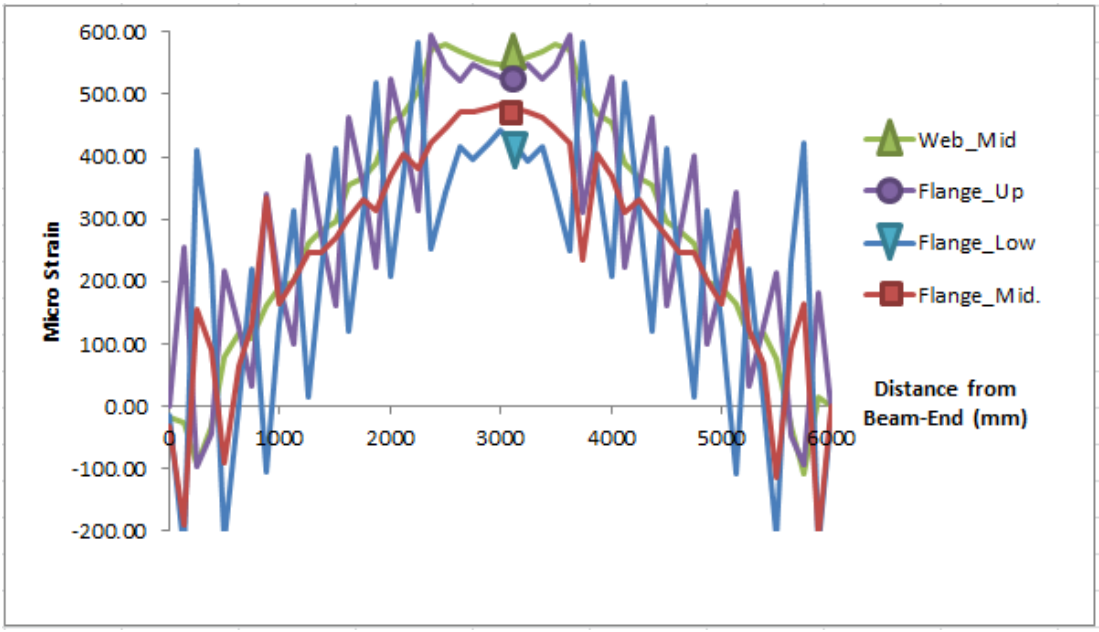

Figure 98. Strain Variation along Length of Tension Chord

The numerically obtained strain profiles indicate the presence of bending effect on both chord members. Such effect is evident from the difference in strain values obtained at different locations in chord member cross sections. Signs of strains due to normal force and bending expected to occur in top and bottom chord members are

illustrated in Table 17. In top chord member, larger compression is expected in the web part compared to the flange tips due to the presence of bending effect. In the bottom chord member, on the other hand, larger tension is expected in the web part compared to the flange tips. A close inspection of the strain plots shown in Figs. 97 and 98 indicates such a relation among the strain values obtained at different locations in cross sections of top and bottom chord members.

Table 17. Chord Member Strains due to Axial Force and Bending Moment

	Orientation of Cross Section	Strain due to Normal Force	Strain due to Bending	Resultant Strain
Top Chord		Compr. Compr.	Compr. Tens.	More compression Less compression
Bottom Chord		Tens. Tens.	Compr. Tens.	Less tension More tension

For verification of strain distributions obtained from the finite element model, the numerically predicted normal strain values were compared with the analytically calculated values. For this purpose, the normal force in truss chord members was determined by dividing the bending moment by the “effective truss depth”, which is taken as the distance between the centroids of the top and bottom chord members. The normal chord force determined this way was then converted into corresponding normal strains by using the cross-sectional area of chord members and elasticity modulus of steel. Comparison of the analytically and numerically determined normal strain variation along the half length of top and bottom chord members is provided respectively in Figs. 99 and 100. As evident, the two sets of values agrees well for both chord members.

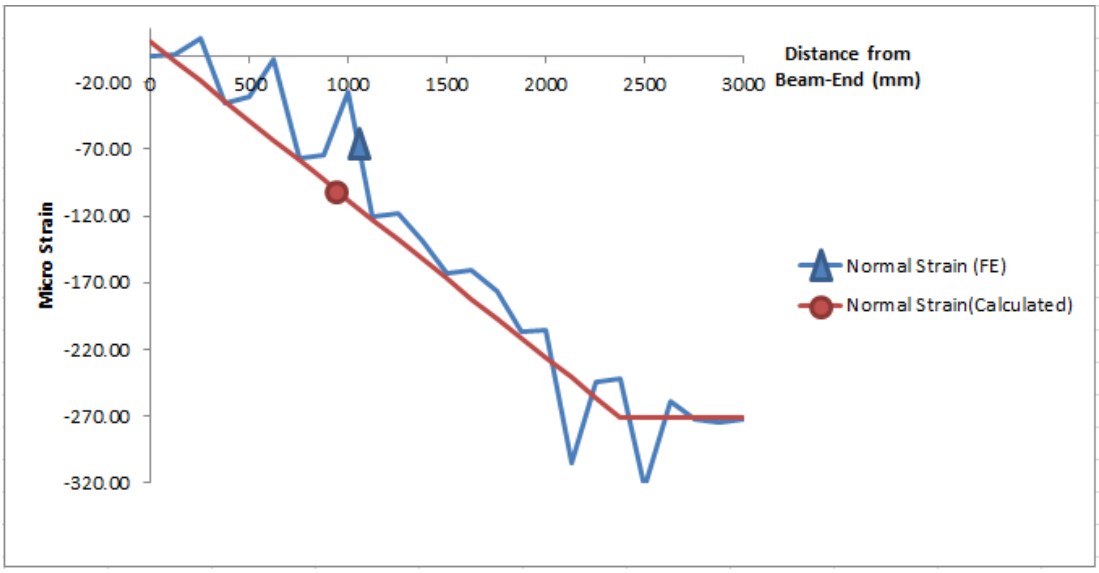

Figure 99. Normal Strain Values of Upper Chord

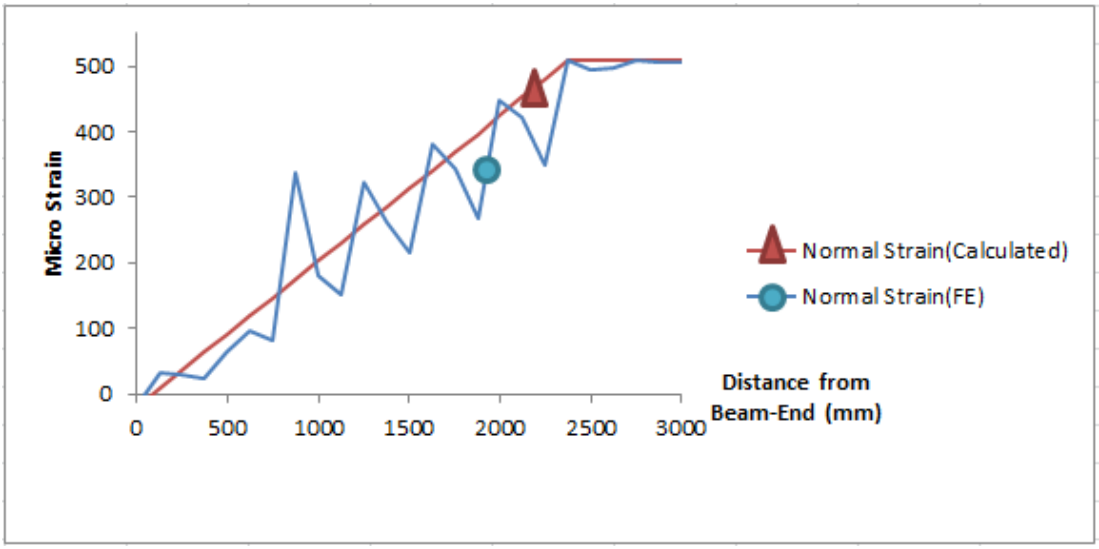

Figure 100. Normal Strain Values of Lower Chord

The observations explained above for model 1.5-0.8_1+3_N_SG are representative of those for models 0.8_1+1_N_SG and 0.8_1+3_N_SG. Therefore, results of the latter models are not reported.

5.1.3 Simple Approach to Determine the Magnitude of Chord Moment

Finite element analysis results clearly indicate the presence of bending effect on truss chord members. That phenomenon has crucial importance on determining ultimate resistance of trusses under flexural loading. However, finite element analysis is not a practical way of designing structural member because of its long-term effording process and computer requirements. To solve this problem a simpler approach was generated to obtain the moment effects on truss chords. In this approach, the truss chord members were assumed to undergo bending deformation as a simply-supported beam with a length equal to the total length of the truss under the effect of an imaginary vertical load. Under the effect of this imaginary loading the midspan vertical deflection of the chord members was assumed to be equal to the known value of the vertical deflection at truss midspan. Three different loading patterns of single-point, two-point and distributed loading, as shown in Fig. 101, were assumed for the imaginary loading on chord members. The vertical deflection profiles for chord members obtained for these three loading patterns are given in Fig. 102. The figure also includes the vertical deflection profile of the truss obtained from finite element analysis. The four plots shown in the figure have the same midspan deflection value. As evident, the choice of pattern for the imaginary loading assumed to act on chord members has no significant influence on the resulting deflection profile.

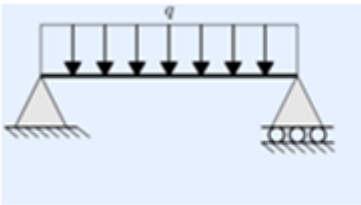

$$v = -\frac{qx}{24EI}(L^3 - 2Lx^2 + x^3)$$

$$\delta max = \frac{5qL^4}{384EI}$$

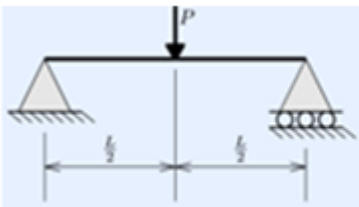

$$v = -\frac{Px}{48EI}(3L^2 - 4x^2)$$

$$\delta max = \frac{PL^3}{48EI}$$

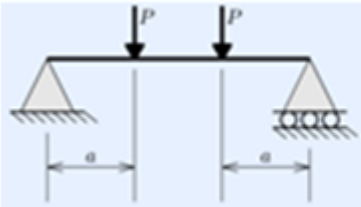

$$v = -\frac{Px}{48EI}(3aL - 3a^2 - x^2)$$

$$\delta max = \frac{Pa}{24EI}(3L^2 - 4a^2)$$

Figure 101. Beam Deflection Formulas

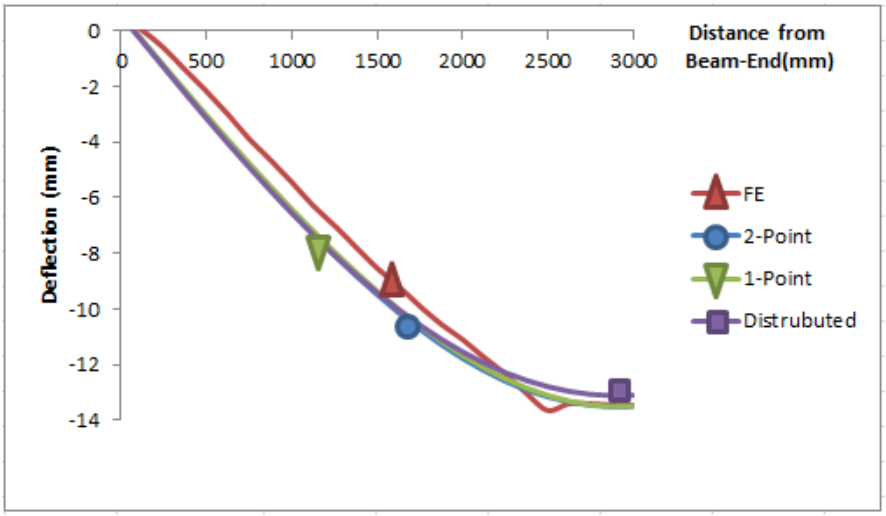

Figure 102. Comparison of Deflection Methods

After determining the imaginary loading on compression chord member, bending moment along chord length was determined and from these moment values curvature profile was extracted as *M/EI*, where *I* is the minor axis moment of inertia of chord section, *E* is elastic modulus and *M* is the bending moment. Flexural strains at several locations in chord cross section were then calculated by multiplying the curvature values with the corresponding distances from the section centroid. Normal strain due to axial force in chord, which was determined according to the procedure explained in the previous section, was added to the flexural strains to determine the total cross-sectional strain. Variation of such cross-sectional strain along compression chord member is provided in Fig. 103 for the three imaginary loading patterns studied. The strain profiles determined using the imaginary loading assumption agrees well with those predicted by finite element analysis.

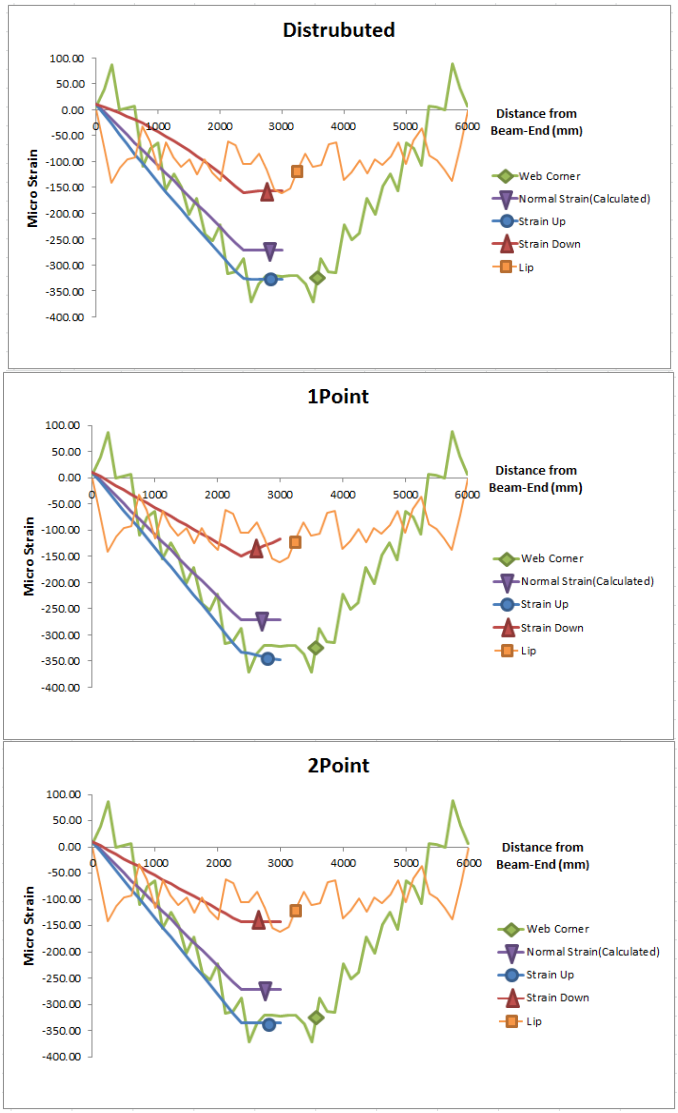

Figure 103. Strain Prediction Graphs

5.2 Experimental Study

In order to verify the numerical findings regarding the bending effect on truss chord members, three additional truss specimens, namely 0.8_1+1_N_SG, 0.8_1+3_N_SG, and 1.5-0.8_1+3_N_SG, were subjected to load tests. Prior to the load tests, chord members in these specimens were instrumented with strain gauges as shown in Fig. 104 in an attempt to obtain the cross-sectional strain distribution in chords. The strain gauges used for this purpose were of TML FLA-5-11-3L type. These specimens were subjected to several elastic loading-unloading cycles in order to verify the readings

of strain gauges and make sure that consistent strain readings are obtained in all loading cycles. During these loading cycles, special attention was paid not to load the specimens beyond half of their expected load capacities. Results of these load tests are presented for each specimen in the following sections.

Figure 104. Strain Gauges Applied on Compression Chord Member

5.2.1 Specimen 0.8_1+3_N_SG

Specimen 0.8_1+3_N_SG was made of 0.8 mm thick Group 2 material and had one rivet and three screws at each diagonal-chord connection. Strain gauges were placed only on the upper chord member at the midspan section in this specimen. Locations of the seven gauges attached on the top chord member are specified in Table 18. Midspan strain values obtained from these gauges at 3.9 kN vertical loading and 17.8 mm displacement are also tabulated in the same table.

The curvature of upper chord member was calculated with imaginary single point load following the relationships given below.

$$\frac{48EI}{L^3} * \delta = P \,; M = \frac{PL}{4} \,; \phi = \frac{M}{EI} = \frac{12\delta}{L^2}$$

For a vertical deflection of 17.8 mm, the upper chord curvature was obtained as 5.94×10^{-6} mm^{-1}. Bending strain at each strain gauge location was calculated using this curvature value and was added to the normal strain. Table 18 compares the sectional strains determined this way with those measured with the strain gauges. Graphical representation of measured and predicted midspan sectional strain profile is provided in Fig. 105. Except for the two strain gauges located near the web-flange corner, a remarkable agreement between the measured and predicted strains is evident in the figure. Error rate specified by dividing the difference between measured and calculated strains to measured strain.

Table 18. Upper Chord Strain Values for 3.9 kN Vertical Loading of Specimen 0.8_1+3_N_SG

Distance From Bottom (mm)	Measured Strain (με)	Calculated Strain (με)	Error Rate (%)
45	770.6	604.6	21.5
42	588.1	586.7	0.2
38.5	711.1	565.9	20.4
15.3	400.4	428.1	6.9
13	409.6	414.4	1.2
7	322.8	378.7	17.3
0	354.7	337.1	5.0
		Error Average :	10.4

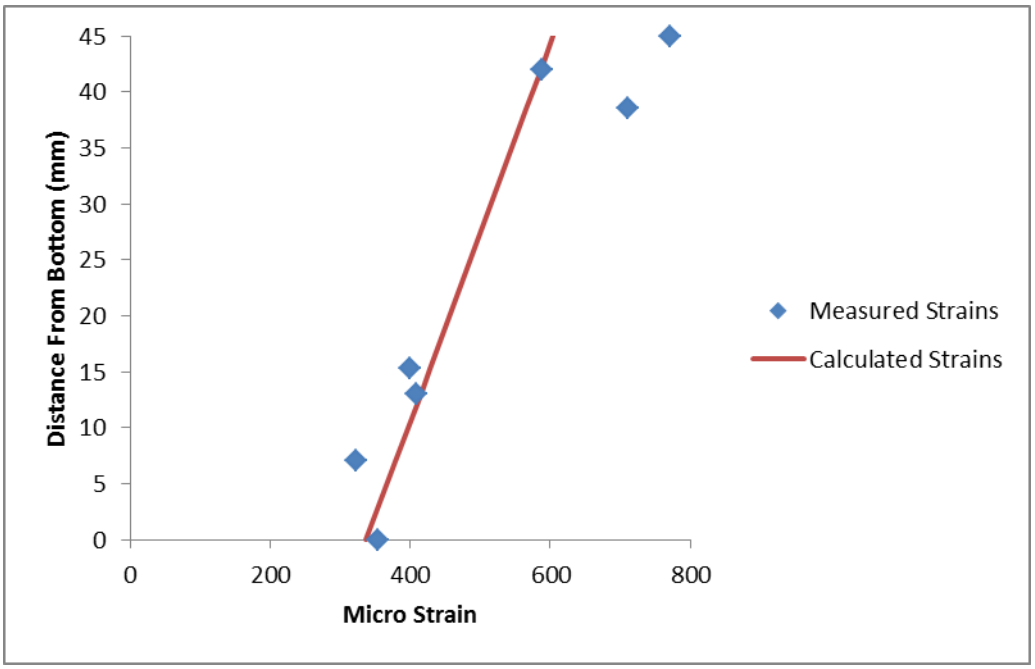

Figure 105. Upper Chord Strain Profile for 3.9 kN Vertical Loading of Specimen 0.8_1+3_N_SG

Strain profile within the compression chord member was also evaluated at the collapse point, which corresponds to 5.3 kN vertical loading. Vertical displacement of the truss was recorded as 24.7 mm at this loading value. Curvature of the upper chord member was calculated to be 8.23 $x10^{-6}$ mm^{-1}. Measured and calculated strain values and graphical representation of the strain profiles are given in Table 19 and Fig. 106. Deviation in measured strains from gauges located close to the web-flange corner is still valid, similar to the case with the strain profiles shown in Fig. 105.

Table 19. Upper Chord Strain Values for 5.3 kN Vertical Loading of Specimen 0.8_1+3_N_SG

Distance From Bottom (mm)	Measured Strain (με)	Calculated Strain (με)	Error Rate (%)
45	1183.9	798.1	32.6
42	799.3	780.3	2.4
38.5	1072.1	759.5	29.2
15.3	500.2	621.6	24.3
13	490.4	607.9	24.0
7	316.9	572.3	80.6
0	505.1	530.7	5.0
		Error Average :	28.3

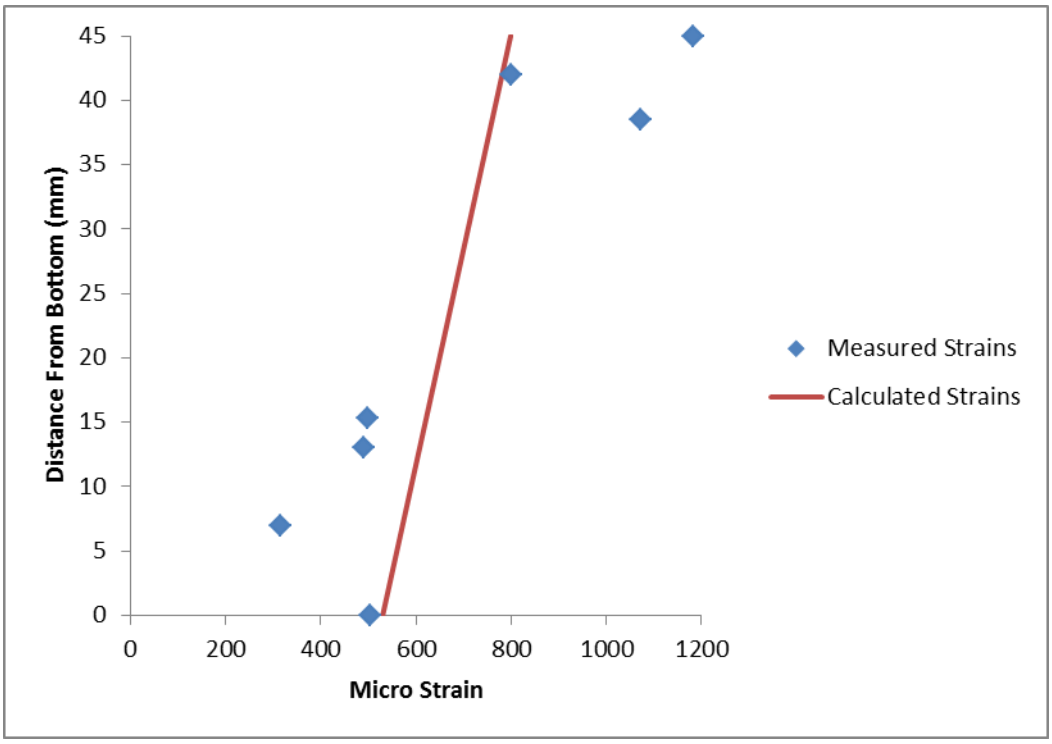

Figure 106. Upper Chord Strain Profile for 5.3 kN Vertical Loading of Specimen 0.8_1+3_N_SG

5.2.2 Specimen 1.5-0.8_1+3_N_SG

Specimen 1.5-0.8_1+3_N_SG was a hybrid specimen made of 1.5 mm thick compression chord and 0.8 mm thick tension chord and diagonal members. All members belonged to Group 2 materials and each diagonal-chord connection was achieved through one rivet and three screws. Strain gauges were placed on both the upper and the lower chords in this specimen. Six gauges were attached on the upper

chord and two gauges were attached on the lower chord member at the locations indicated in Tables 20 and 21.

First investigation was made on midspan strain values under 4 kN vertical loading and 13.7 mm displacement. Curvature was determined for the related displacement which is 4.56 x10^{-6} mm^{-1}. Measured and calculated strain values and graphical representation for the upper chord are given in Table 20 and Fig. 107. Lower chord under tensile effects again are given in Table 21 and Fig. 108. Good agreement exists between the measured and predicted section strains for both chord members.

Table 20. Upper Chord Strain Values for 4kN Vertical Loading of Specimen 1.5-0.8_1+3_N_SG

Dist. From Bottom (mm)	Measured Strain (με)	Calculated Strain (με)	Error Rate (%)
45	323.1	360.7	11.6
42	355.7	347.0	2.4
39	318.6	333.4	4.6
23	276.0	260.4	5.6
6	239.3	182.9	23.6
0	106.0	155.6	46.8
		Error Average :	15.8

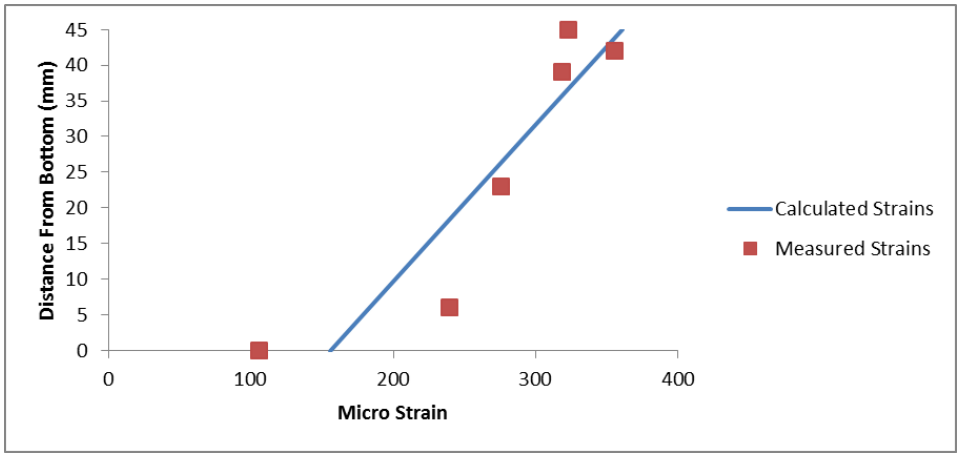

Figure 107. Upper Chord Strain Profile for 4 kN Vertical Loading of Specimen 1.5-0.8_1+3_N_SG

Table 21. Lower Chord Strain Values for 4kN Vertical Loading of Specimen 1.5-0.8_1+3_N_SG

Dist. From Bottom(mm)	Measured Strain (με)	Calculated Strain (με)	Error Rate (%)
39	496.7	505.0	1.7
6	620.1	655.3	5.7
		Error Average :	3.7

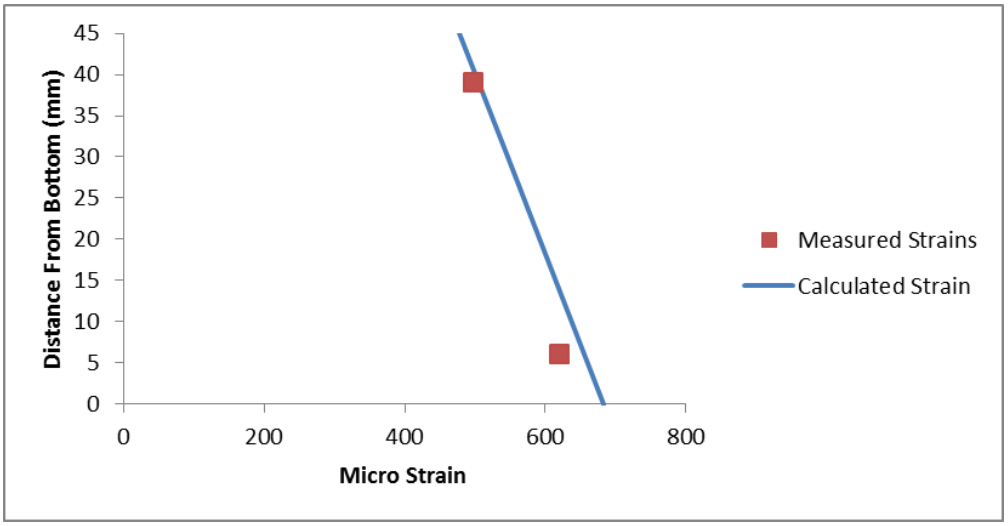

Figure 108. Lower Chord Strain Profile for 4 kN Vertical Loading of Specimen 1.5-0.8_1+3_N_SG

Second investigation for specimen 1.5-0.8_1+3_N_SG was made on cross-sectional strains at mid-span under 12.8 kN vertical loading and 80.4 mm displacement. Curvature determined for the related displacement is 26.8 x10^{-6} mm^{-1}. Measured and calculated strain values and graphical representation for upper chord are given in Table 22 and Fig. 109. Again, excellent agreement is valid between the measured and predicted strains. Strains at lower chord under tensile effects are given in Table 23 and Fig. 110. As evident, the measured lower chord strains are much larger than the predicted values. The reason for such discrepancy is due to yielding of the lower chord member at this stage of loading in the test specimen. The overall load-deflection response of this specimen is shown in Fig. 111. The lower chord strain profiles in Fig. 110 represent the values at a vertical deflection of 80.4 mm, and as evident in Fig. 111 inelastic response in the test truss has started long before this deflection value.

Table 22. Upper Chord Strain Values for 12.8 kN Vertical Loading of Specimen 1.5-0.8_1+3_N_SG

Dist. From Bottom (mm)	Measured Strain (με)	Calculated Strain (με)	Error Rate (%)
45	1202.0	1300.4	8.2
42	1242.4	1220.1	1.8
39	1105.1	1139.7	3.1
23	730.5	711.2	2.6
6	358.9	255.9	28.7
0	35.3	95.2	169.4
		Error Average :	35.7

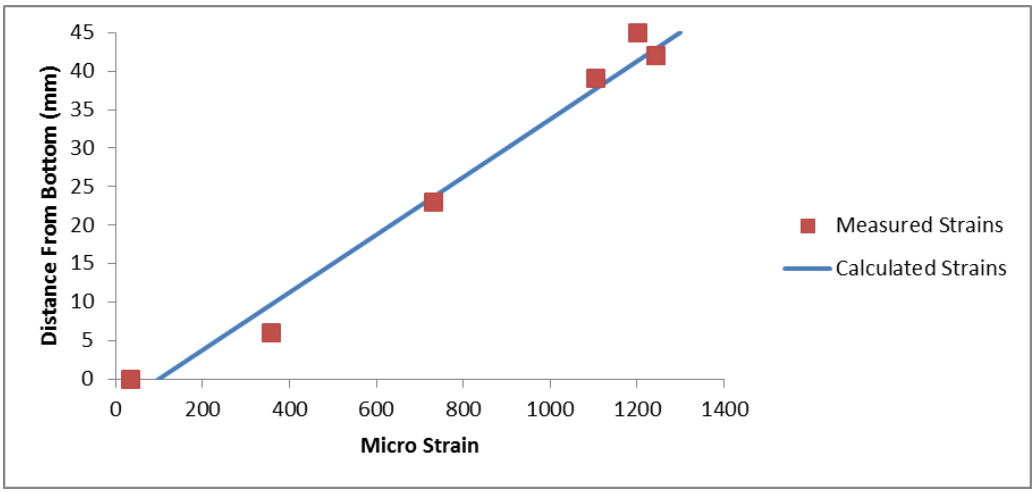

Figure 109. Upper Chord Strain Profile for 12.8 kN Vertical Loading of Specimen 1.5-0.8_1+3_N_SG

Table 23. Lower Chord Strain Values for 12.8 kN Vertical Loading of Specimen 1.5-0.8_1+3_N_SG

Dist. From Bottom(mm)	Measured Strain (με)	Calculated Strain (με)	Error Rate (%)
39	4404.997	1365.4	-
6	4389.99	2247.6	-

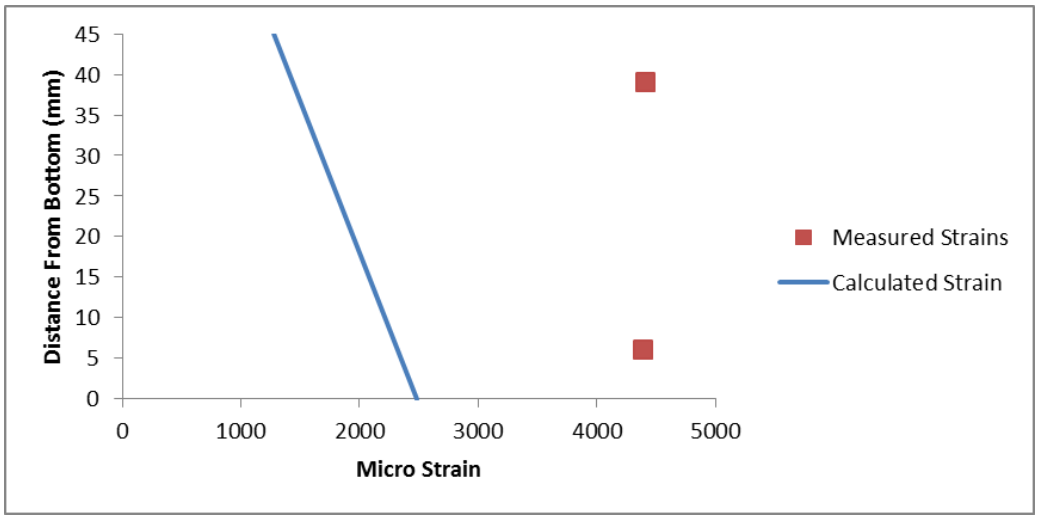

Figure 110. Lower Chord Strain Profile for 12.8 kN Vertical Loading of Specimen 1.5-0.8_1+3_N_SG

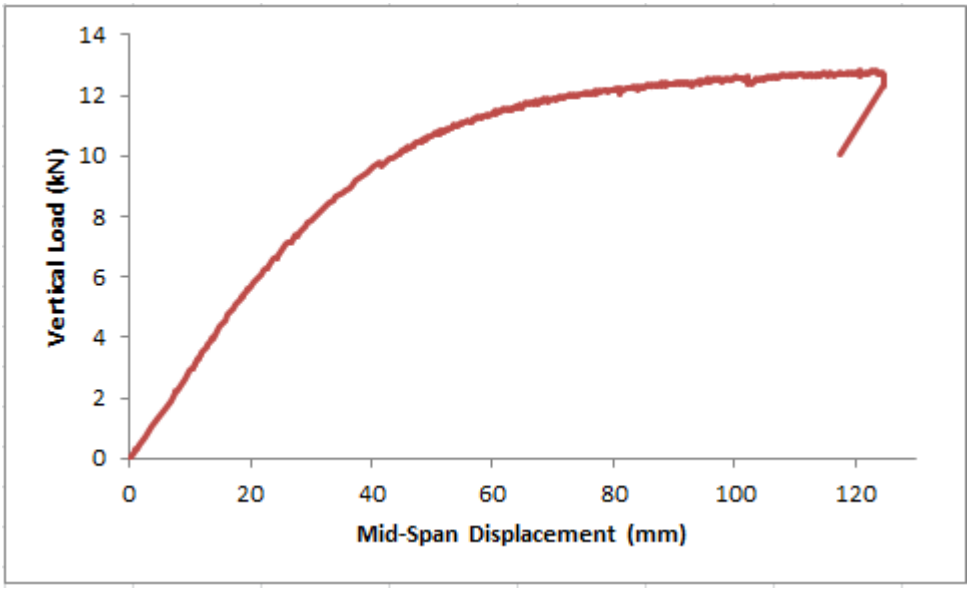

Figure 111. Vertical Load – Displacement Graph of Specimen 1.5-0.8_1+3_N_SG

5.2.3 Specimen 0.8_1+1_N_SG

Specimen 0.8_1+1_N_SG was made of 0.8 mm thick Group 2 material and had one rivet and one screw for each diagonal-chord connection. Strain gauges were placed on both the upper and the lower chords in this specimen. Six gauges were attached on the upper chord and only one gauge was attached on the lower chord.

Truss failure was observed at a vertical load 5.1 kN due to local buckling of upper chord member. At the time of failure 30.1 mm vertical midspan displacement was observed on the truss. Curvature of chord members was calculated to be 9.63 x10^{-6} mm^{-1}. Measured and calculated strains of upper chord are presented in Table 24 and Fig. 112. Strain profile for the lower chord is given in Fig. 113. Similar to the previous two specimens, the predicted strain profiles agree well with the measured strains for both the upper and lower chord members.

Table 24. Upper Chord Strain Values for 5.1 kN Vertical Loading of Specimen 0.8_1+1_N_SG

Dist. From Bottom (mm)	Measured Strain (με)	Calculated Strain (με)	Error Rate (%)
45	857.9	872.7	1.7
42	721.7	683.2	5.3
39	1036.9	654.3	36.9
23	616.7	500.3	18.9
6	254.1	336.7	32.5
0	388.1	439.5	13.2
		Error Average :	18.1

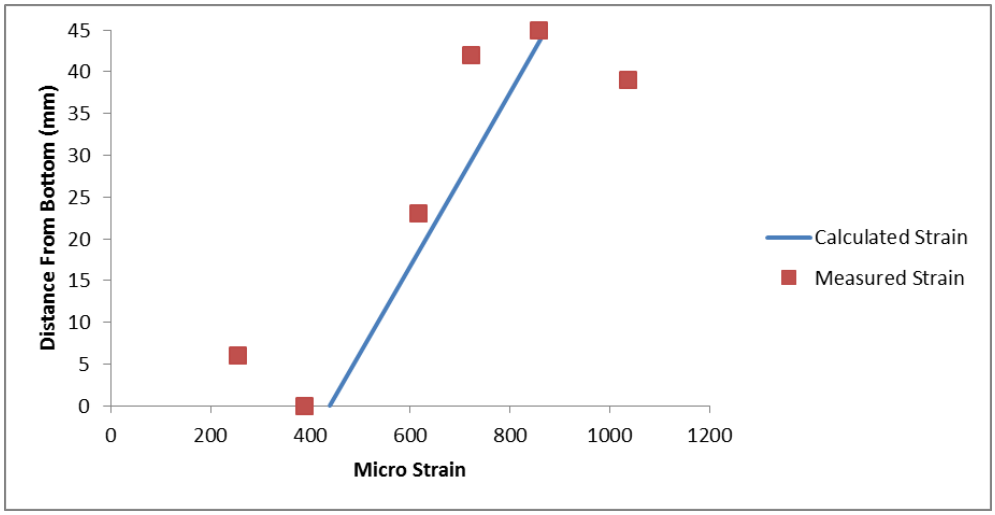

Figure 112. Upper Chord Strain Profile for 5.1 kN Vertical Loading of Specimen 0.8_1+1_N_SG

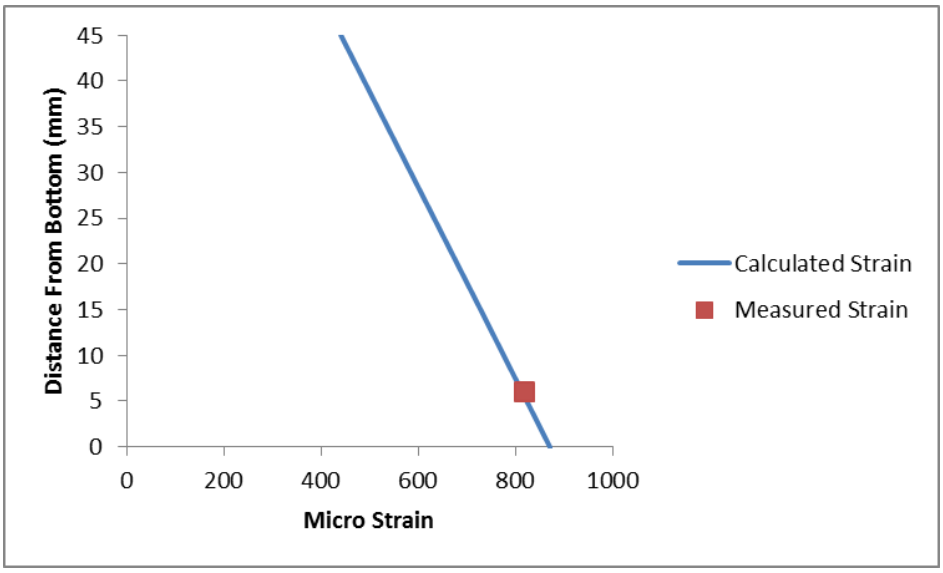

Figure 113. Lower Chord Strain Profile for 5.1 kN Vertical Loading of Specimen 0.8_1+1_N_SG

The good correlation between the predicted strain profiles for the truss chord members with the measured strain values indicates that the proposed analytical procedure to determine the bending and normal chord strains can be used for assessment of truss load capacity. As already reported above, tensile chords gave more accurate results with the analytical data. Compression chords gave more irregular strain distributions along the section. This fact was caused by local buckling, which is a common deformation mode in thin walled sections. In such sections, the effectiveness of the cross sections decreases with the amount of compression existing in the section. Beside this phenomenon, the finite element and analytical studies, as well as the experimental results, clearly indicate that bending effect occurs on chord members has a major influence on cross-sectional strain distribution in these members.

5.2.4 Strength Prediction with the Effect of Chord Moments

Additional calculations were performed to reflect the presence of bending of chord members on overall load capacity of truss specimens. Summary of these calculations is provided in Table 25. Maximum bending moment occurred on truss compression chord member was calculated using imaginary loading, which was determined based

on the measured midspan deflection of trusses. Chord normal force was calculated using the maximum value of the vertical load applied on truss specimen during load testing. The bending moment and normal force acting on chord member were then divided, respectively by the moment capacity and compressive axial force capacity of the member. The member capacities were determined based on the corresponding sections of AISI Specification [5]. The compressive axial force capacity of 1.2 mm thick members were taken as their yield capacities while the capacity of 0.8 mm thick members were taken as distortional buckling capacities under specified eccentricity levels. Moment capacity of sections with both thicknesses were calculated with the direct strength method available in the AISI Specification [1,17]. Capacity calculations are provided in Appendix.

Table 25. P/M Interaction Chart of Valid Truss Specimens

Specimen #	Thickness (mm)	Property	Strut Force (kN)	Max Disp (mm)	Moment (kNmm)	P/Pno	Mx/Mnx	PM
1.2_1+1_N	1.2	Rivet + 1 Screw	50.2	62.8	276.9	0.63	0.32	0.96
1.2_1+2_N	1.2	Rivet + 2 Screw	59.2	57.4	253.1	0.75	0.30	1.04
1.2_0+1_N	1.2	Single #12 Screw	51.8	113.9	502.3	0.65	0.59	1.24
1.2_0.8_1+2_N	1.2 - 0.8	Rivet + 2 Screw	46.6	75.3	332.1	0.59	0.39	0.98
1.2_1+3_N	1.2	Rivet + 3 Screw	55.0	49.2	217.0	0.69	0.25	0.95
1.2_PL_N	1.2	Plate	57.2	45.3	199.8	0.72	0.23	0.96
1.2_1+1_N_NDL	1.2	Rivet + 1 Screw	51.8	70.4	310.5	0.60	0.33	0.93
1.2_1+3_N_NDL	1.2	Rivet + 3 Screw	54.8	52.5	231.5	0.64	0.25	0.88
1.2_1+3_N_SS	1.2	Short Span	59.1	31.9	353.9	0.69	0.38	1.06
0.8_1+1_N	0.8	Rivet + 3 Screw	25.5	35.4	104.1	0.72	0.18	0.90
0.8_1+3_N	0.8	Rivet + 1 Screw	25.0	40.4	118.8	0.70	0.21	0.91
0.8_PL_N	0.8	Plate	30.7	36.3	106.7	0.86	0.19	1.05

Table 25 presents a successful prediction rate on experimental results, moreover it indicates that strength prediction of trusses relies on moment effect in important amount. PM interaction equations consist of approximately 66 % of compression and 33% of bending effect. According to presented method, a correct strength prediction strictly requires a correct deflection prediction in order to determine moment effect on strut. Furthermore, moment is directly correlates with the compression limit of cross-section which is caused by the inconsistent stability modes of thin-walled members under different eccentricities. This phenomenon was investigated in Chapter 4 as eccentric loading. Besides, the last but not least the cross-section's compression and moment capacities must be calculated correctly.

CHAPTER 6

CONCLUSIONS

Recent interest of construction market on Cold-Formed Steel structures is increasing day by day since its economical and short-term construction advantages. Floor trusses are definitely one of the essential parts of building type structures. However a gap has been noticed in literature with related emphasis. Therefore a comprehensive study was generated to observe CFS floor truss behavior under flexural loading. The study included experiments of full-scale trusses and was followed by a series of analytical studies.

Twenty-four full scale trusses with different properties were tested in the experimental study. Midspan deflection and loading magnitude are recorded during the tests. The main test parameters were section thickness, connection type, and presence of OSB sheathing plate. Response of trusses in terms of load capacity and stiffness were obtained from these tests. Additionally, it is worth to note that initially expected failure mode of lateral buckling was not observed in any of the truss tests.

The measured stiffness of truss specimens were determined to differ significantly from the values obtained from a linear structural analysis based on axially rigid connection assumption. Flexibility of diagonal-chord connections was the major factor for such discrepancy since the trusses with different connection types exhibited large variation in the stiffness values. Within an experimental approach, stiffness of connections were measured independently and a new structural model was created by incorporating connection springs with axial stiffness values extracted from the experimental results. Incorporating the connection axial flexibility resulted in a good agreement between the predicted and measured truss response.

Strength of trusses was investigated by correlating them with pure compression capacities of chords since the observed failure mode was buckling of compression chord in majority of trusses. CFS sections representing chord member of trusses in different lengths and with different lip conditions were tested under pure compression. Compression capacity of these sections were also predicted analytically and numerically using Direct Strength Method procedure and Finite Element Analyses. Analytical and experimental results gave satisfactory results however the measured truss load capacities did not correlate well with the obtained results. Therefore, additional eccentricity effect was investigated with Elastic Finite Strip Analyses. The CFS sections were observed to undergo two different failure modes of yielding and local buckling depending on the eccentricity of axial compressive force.

Presence of significant bending effect on truss chord members was demonstrated both numerically and experimentally. A simple procedure was established in order to quantify this effect and determine the value of chord bending moment. In the proposed procedure maximum bending moment occurred on truss chord members was calculated using imaginary loading, which was determined based on truss midspan deflection. The normal force and bending moment effects on chord members were considered together with the corresponding capacities determined based on the code provisions. Truss load capacities obtained through this procedure were observed to accurately represent the measured capacities.

REFERENCES

[1] AISI American Iron and Steel Institute (2012), “Commentary on Specification for the Design of Cold Formed Steel Structural members”, Washington DC.

[2] North American Standard for Cold-Formed Steel Framing: Truss Design. Commentary on the North American standard for cold-formed steel framing: truss design. (2007). Washington, D.C.: American Iron and Steel Institute.

[3] Eurocode 3: Design of Steel Structures. (2005). Brussels: European Committee for Standardization.

[4] Schafer, B.W. (2002a), “Local, Distortional, and Euler Buckling of Thin-Walled Columns”, ASCE Journal of Structural Engineering, 128(3), 289-299.

[5] AISI American Iron and Steel Institute (2016), “Specification for the Design of Cold Formed Steel Structural members”, Washington DC

[6] Schafer, B., Peköz, T. (1998). Computational Modeling of Cold-Formed Steel: Characterizing Geometric Imperfections and Residual Stresses. Journal of Constructional Steel Research, 47(3).

[7] Kumar, M. V., Kalyanaraman, V. (2014). Distortional Buckling of CFS Stiffened Lipped Channel Compression Members. Journal of Structural Engineering, 140(12)

[8] Yu, C., & Schafer, B. W. (2006). Distortional Buckling Tests on Cold-Formed Steel Beams. Journal of Structural Engineering, 132(4), 515-528.

[9] Mathieson, C., Clifton, G. C., & Lim, J. B. (2016). Novel pin-jointed connection for cold-formed steel trusses. Journal of Constructional Steel Research, 116, 173-182.

[10] Wood, J. V., Dawe, J. L. (2006). Full-Scale Test Behavior of Cold-Formed Steel Roof Trusses. Journal of Structural Engineering, 132(4), 616-623.

[11] Pedreschi, R., Sinha, B. (2008). An experimental study of cold formed steel trusses using mechanical clinching. Construction and Building Materials, 22(5), 921-931.

[12] Mohammad, S., Tahir, M. M., Tan, C. S., Shek, P. N. (2012). Experimental Investigation on Wide-Span Cold-Formed Steel Roof Truss System. Applied Mechanics and Materials, 166-169.

[13] Lakkavalli, B. S., Liu, Y. (2006). Experimental study of composite cold-formed steel C-section floor joists. Journal of Constructional Steel Research, 62(10), 995-1006.

[14] Xu, L., Tangorra, F. (2007). Experimental investigation of lightweight residential floors supported by cold-formed steel C-shape joists. Journal of Constructional Steel Research, 63(3), 422-435.

[15] SAP2000: integrated software for structural analysis and design user manual. (2006). Berkeley California: CSI.

[16] Zeynalian, M., Shelley, A., Ronagh, H. (2016). An experimental study into the capacity of cold-formed steel truss connections. Journal of Constructional Steel Research, 127, 176-186.

[17] Li, Z., Schafer, B.W. (2010) "Buckling analysis of cold-formed steel members with general boundary conditions using CUFSM: conventional and constrained finite strip methods." Proceedings of the 20th Int;l. Spec. Conf. on Cold-Formed Steel Structures, St. Louis, MO. November, 2010.

[18] ANSYS / WORKBENCH release 16.1. (2002). Canonsburg, PA: Ansys.

[19] Aghoury, M. E., Hanna, M., Amoush, E. (2017). Experimental and theoretical investigation of cold-formed single lipped sigma columns. Thin-Walled Structures, 111, 80-92.

[20] Schafer, B., Li, Z., Moen, C. (2010). Computational modeling of cold-formed steel. Thin-Walled Structures, 48(10-11).

[21] Beer, F. P., Johnston, E. R., DeWolf, J. T. (2002). Mechanics of materials. New York: McGraw-Hill.

[22] Yu, W. (1985). Cold-formed steel design. New York: Wiley.

APPENDIX

CALCULATIONS OF CFS SECTION COMPRESSION AND MOMENT CAPACITIES

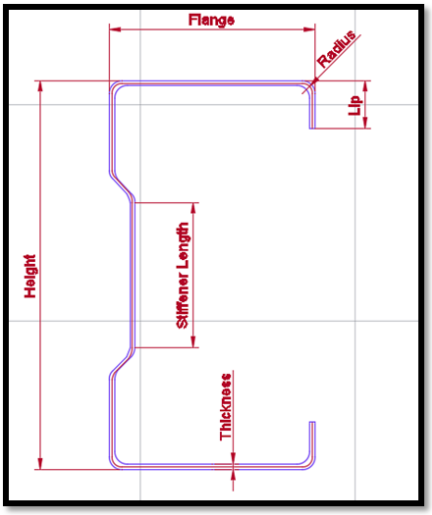

Figure 114. Representation of Dimensions were Used in Calculations

Calculation of Compression Yield Capacity of 1.2 mm Thick Section

Effective Area of Section according to AISI 12 Section B.Elements

AISI 12 Section 2. Members						
Geometric Input				Material Input		
Flanges	45	mm		Elasticity Modulus	210000	MPa
Web	90	mm		Fy	410	MPa
Thickness	1.2	mm		G (Shear Modulus)	78	MPa
Radius	3	mm		μ (poisson's ratio)	0.3	
Lip	10	mm				
Stiffener	36	mm				
Axial Loading Properties				Unreduced Geometric Properties		
Flanges		k=	1.9	Area	226.8234	mm2
w	36.6	mm		I3-3	330000	mm4
w/t	30.5			I2-2	51585.41	mm4
λ	1.02854	> 0.673		r3-3	38.14284	mm
ρ	0.764292			r2-2	15.08063	mm
b	27.97308	mm		r0	41.01588	mm
Δ	8.626918			x0	35	mm
Web		k=	16.4	y0	0	mm
w	45.6	mm		Cw	51700000	mm6
w/t	38			J	115.2	mm4
λ	0.436174	< 0.673				
ρ	1			Reduced Areas/Inertias		
b	45.6			Axial Loading	193.28	mm2
Δ	0			M(Major)	210.21	mm2
Web Stiffener				M(minor)	183.64	mm2
w	27.6	mm				
w/t	23					
λ	0.534559	< 0.673				
ρ	1					
b	27.6	mm				
Δ	0					
Lips						
w	5.8	mm				
ρ	0.078		R1			
b	0.4524	mm				
Δ	5.3476	mm				

Figure 115. Calculations for Material Group with Yield Limit of 410 MPa

Compression Yield Capacity AISI Section C4.1 :

$A_{eff} = 193.2\ mm^2$

$f_y = 410$ MPa

$P_{no} = 410 * 193.2 * 10^{-3} = 79.2$ kN ;

AISI 12 Section 2. Members						
Geometric Input				Material Input		
Flanges	45	mm		Elasticity Modulus	210000	MPa
Web	90	mm		Fy	450	MPa
Thickness	1.2	mm		G (Shear Modulus)	78	MPa
Radius	3	mm		μ (poisson's ratio)	0.3	
Lip	10	mm				
Stiffener	36	mm				
Axial Loading Properties				Unreduced Geometric Properties		
Flanges		k=	1.9	Area	226.8234	mm2
w	36.6	mm		I3-3	330000	mm4
w/t	30.5			I2-2	52650.91	mm4
λ	1.077545	> 0.673		r3-3	38.14284	mm
ρ	0.738561			r2-2	15.23558	mm
b	27.03132	mm		r0	41.0731	mm
Δ	9.568684			x0	35	mm
Web		k=	16.4	y0	0	mm
w	45.6	mm		Cw	51700000	mm6
w/t	38			J	115.2	mm4
λ	0.456956	< 0.673				
ρ	1			Reduced Areas		
b	45.6			Axial Loading	191.02	mm2
Δ	0			M(Major)	209.08	mm2
Web Stiffener				M(minor)	187.48	mm2
w	27.6	mm				
w/t	23					
λ	0.560029	< 0.673				
ρ	1					
b	27.6	mm				
Δ	0					
Lips						
w	5.8	mm				
ρ	0.078		R1			
b	0.4524	mm				
Δ	5.3476	mm				

Figure 116. Calculations for Material Group with Yield Limit of 450 MPa

Compression Yield Capacity AISI Section C4.1 :

$A_{eff} = 191.0\ mm^2$

$f_y = 450$ MPa

$P_{no} = 450 * 191.0 * 10^{-3} = 85.9$ kN ;

Calculation of Moment Capacity of 1.2 mm Thickness Section According to AISI

Appendix 1 DSM – Section 1.2.2

Elastic Buckling Capacities of Section (Mcre, Mcrd, Mcrl) determined with Finite Strip Analysis in accordance with Section 1.1.2 of AISI S-214 Appendix 1.

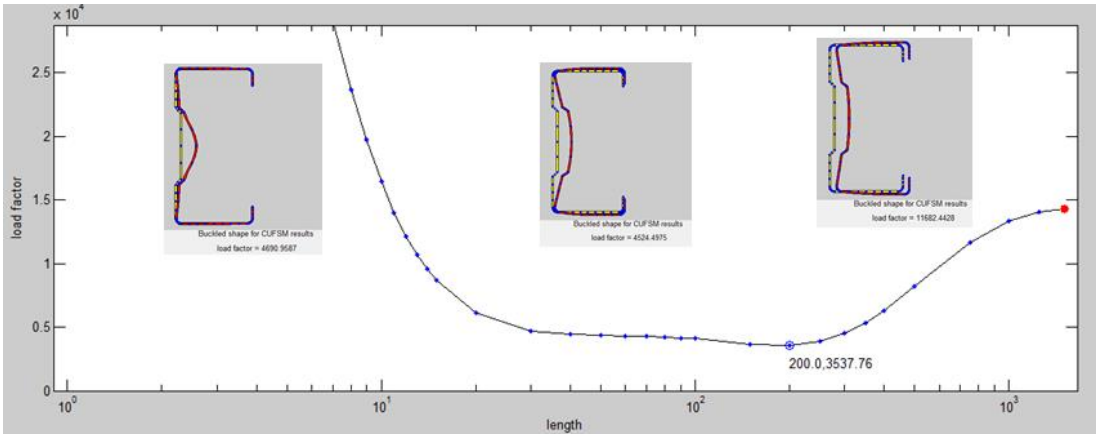

Figure 117. Elastic Signature Curve of 1.2 mm Thick Member

1.2.2.1.1.1.1 Lateral Torsional Buckling Strength

(c) For M_{cre}>2.78M_y

$M_{ne} = M_y$ (Eq. 1.2.2-3)

Where

M_{cre} =Critical elastic LTB moment (section 1.1.2)

M_y = Member yield moment

1.2.2.1.2.1.1 Local Buckling Strength

(a) For $\lambda_l < 0.776$

$M_{nl} = M_{ne}$ (Eq. 1.2.2-7)

Where

M_{crl} =Critical elastic LB moment (section 1.1.2)

$\lambda_l = \sqrt{Mne/Mcrl}$ (Eq. 1.2.2-9)

1.2.2.1.3.1.1 Distortional Buckling Strength

(a) For $\lambda_d < 0.673$

$M_{nd} = M_y$ (Eq. 1.2.2-17)

Where

M_{crd} =Critical elastic DB moment (section 1.1.2)

$\lambda_d = \sqrt{My/Mcrd}$ (Eq. 1.2.2-9)

MATERIAL GROUP 1		
Iz-z :	62940	mm4
W :	2090.20	mm3
fy :	410	MPa
My :	856.98	kNmm
Mcre :	4524.5	kNmm
Mcrl :	4690.9	kNmm
Mcrd :	4524.5	kNmm
Mcre	> 2.78 My	
Mne :	856.98	kNmm
λl :	0.43	< 0.78
Mnl :	856.98	kNmm
λd :	0.44	< 0.67
Mcrd :	856.98	kNmm
Mcap :	856.98	kNmm

MATERIAL GROUP 2		
Iz-z :	62940	mm4
W :	2090.20	mm3
fy :	450	MPa
My :	940.59	kNmm
Mcre :	4524.5	kNmm
Mcrl :	4690.9	kNmm
Mcrd :	4524.5	kNmm
Mcre	> 2.78 My	
Mne :	940.59	kNmm
λl :	0.45	< 0.78
Mnl :	940.59	kNmm
λd :	0.46	< 0.67
Mcrd :	940.59	kNmm
Mcap :	940.59	kNmm

Calculation of Moment Capacity of 0.8 mm Thickness Section According to AISI Appendix 1 DSM – Section 1.2.2

Elastic Buckling Capacities of Section (Mcre, Mcrd, Mcrl) determined with Finite Strip Analysis in accordance with Section 1.1.2 of AISI S-214 Appendix 1.

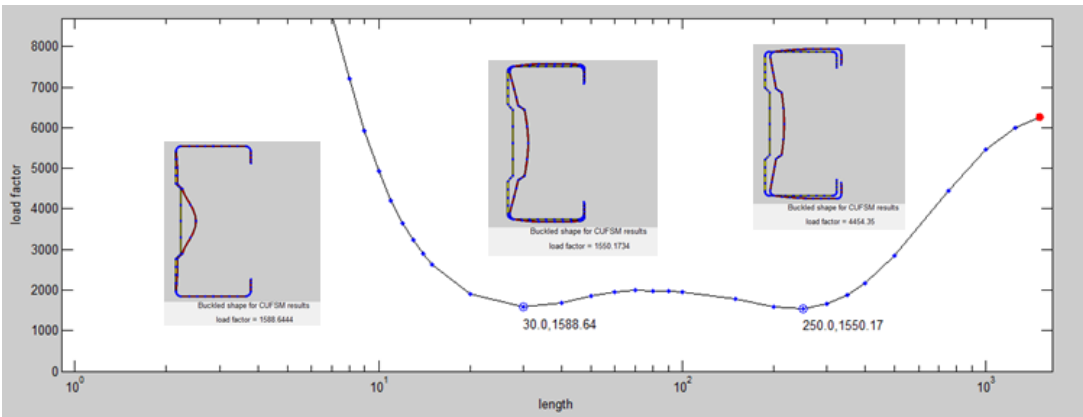

Figure 118. Elastic Signature Curve of 0.8 mm Thick Member

1.2.2.1.1.1.1 Lateral Torsional Buckling Strength

(c) For M_{cre}>2.78M_y

$M_{ne} = M_y$ (Eq. 1.2.2-3)

Where

M_{cre} =Critical elastic LTB moment (section 1.1.2)

M_y = Member yield moment

1.2.2.1.2.1.1 Local Buckling Strength

(a) For $\lambda_l < 0.776$

$M_{nl} = M_{ne}$ (Eq. 1.2.2-7)

Where

M_{crl} =Critical elastic LB moment (section 1.1.2)

$\lambda_l = \sqrt{Mne/Mcrl}$ (Eq. 1.2.2-9)

1.2.2.1.3.1.1 Distortional Buckling Strength

(a) For $\lambda_d < 0.673$

$M_{nd} = M_y$ (Eq. 1.2.2-17)

Where

M_{crd} =Critical elastic DB moment (section 1.1.2)

$\lambda_d = \sqrt{My/Mcrd}$ (Eq. 1.2.2-9)

MATERIAL GROUP 1		
Iz-z :	42960	mm4
W :	1426.67	mm3
fy :	395	MPa
My :	563.54	kNmm
Mcre :	4454.4	kNmm
Mcrl :	1588.6	kNmm
Mcrd :	1550.2	kNmm
Mcre	> 2.78 My	
Mne :	563.54	kNmm
λl :	0.60	< 0.78
Mnl :	563.54	kNmm
λd :	0.36	< 0.67
Mcrd :	563.54	kNmm
Mcap :	563.54	kNmm

MATERIAL GROUP 2		
Iz-z :	42960	mm4
W :	1426.67	mm3
fy :	350	MPa
My :	499.34	kNmm
Mcre :	4454.4	kNmm
Mcrl :	1588.6	kNmm
Mcrd :	1550.2	kNmm
Mcre	> 2.78 My	
Mne :	499.34	kNmm
λl :	0.56	< 0.78
Mnl :	499.34	kNmm
λd :	0.33	< 0.67
Mcrd :	499.34	kNmm
Mcap :	499.34	kNmm

Calculation of Compression Capacity of 0.8 mm Thickness Section According to AISI Appendix 1 DSM – Section 1.2.1

Elastic Buckling Capacity of Section (Pcrd) determined with Finite Strip Analysis in accordance with Section 1.1.2 of AISI S-214 Appendix 1.

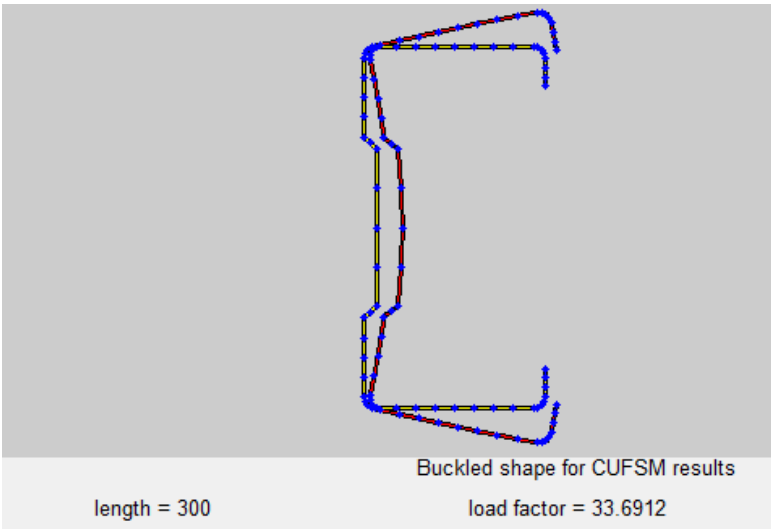

1.2.1.3. Distortional Buckling

(b) For $\lambda_d < 0.561$

$$P_{nd} = \left(1 - 0.25\left(\frac{Pcrd}{Py}\right)^{0.6}\right)\left(\frac{Pcrd}{Py}\right)^{0.6} * Py \qquad \text{(Eq. 1.2.1-11)}$$

Where

P_y = Members yield strength

P_{crd} =Critical elastic column DB load (section 1.1.2)

$$\lambda_d = \sqrt{Py/Pcrd} \qquad \text{(Eq. 1.2.1-12)}$$

MATERIAL GROUP 1		
A=	157.77	mm2
Fy=	395	MPa
E=	210000	MPa
Py=	62.32	kN
Pcrd=	33.69	kN
Lamda=	1.36	> 0.561
Pnd=	35.64	kN

MATERIAL GROUP 2		
A=	157.77	mm2
Fy=	350	MPa
E=	210000	MPa
Py=	55.22	kN
Pcrd=	33.69	kN
Lamda=	1.28	> 0.561
Pnd=	33.42	kN